

**Development and applications of
Quasi-Variational Coupled-Cluster theory**

Joshua A. Black

A thesis presented for the degree of
Doctor of Philosophy

School of Chemistry
Cardiff University

June 2017

Abstract

The Quasi-Variational (QV) family of methods are a set of single-reference algorithms that can be used to investigate multireference systems with large non-dynamic correlation effects. Within this current work, the Quasi-Variational Coupled Cluster Doubles (QVCCD) equations are derived and implemented into Molpro’s Integrated Tensor Framework (ITF), to produce fast and efficient code. This code, coupled with a new orbital optimisation implementation, is used to calculate potential energy curves for third-row diatomic molecules. In contrast to Traditional Coupled-Cluster methods, the QV methods are able to correctly describe the dissociation of these molecules.

QV and several other single-reference methods are also applied to 5 chemical databases comprising of 88 unique reactions. From this, the activation and reaction energies are determined and contrasted. The QV methods produce larger activation energies that may correct the shortcomings of the perturbative triples correction. These results also include a new QV method with an ‘asymmetric-renormalised’ triples correction. The numerical results show there is little difference between this procedure and ‘symmetric-renormalised’ triples.

Currently, only closed-shell QVCCD programs exist. Unrestricted QVCCD equations are derived and presented in the hope that this will facilitate the realisation of an open-shell QVCCD program.

Finally, calculating the rate of a chemical reaction is of fundamental importance to chemistry. Knowledge of how quickly a reaction proceeds allows for an understanding of macroscopic chemical change. Rate constants are calculated with the *on-the-fly* Instanton method. In contrast to semi-classical Transition State Theory, the Instanton method incorporates quantum effects like atomic tunnelling into its rate constants. The effects of hydrogen tunnelling are examined for a reaction involving a Criegee intermediate. It is discovered that tunnelling does play a role in the reaction rate and may increase it by a factor of 1000. Combination of the Instanton calculations with the QV methods are discussed.

Acknowledgements

First and foremost, I would like to thank my supervisor, Peter Knowles, for all the help and guidance he has given me. I would also like to thank Jeremy Richardson for inviting me to ETH Zürich and giving me the opportunity to work with the Instanton method. Finally, a big to thank you all my friends and family for their support, both in and out of Cardiff; a special thanks goes to Olga.

I also gratefully acknowledge the Engineering and Physical Sciences Research Council for providing funding.

Declaration

- This work has not been submitted in substance for any other degree or award at this or any other university or place of learning, nor is it being submitted concurrently in candidature for any other degree or award.
- This thesis is being submitted in partial fulfilment of the requirements for the degree of Doctor of Philosophy (PhD).
- This thesis is the result of my own independent work/investigation, except where otherwise stated, and the thesis has not been edited by a third party beyond what is permitted by Cardiff University's Policy on the Use of Third Party Editors by Research Degree Students. Other sources are acknowledged by explicit references. The views expressed are my own.
- I hereby give consent for my thesis, if accepted, to be available online in the University's Open Access repository, for inter-library loan and for the title and summary to be made available to outside organisations.

Candidate Signature:

Joshua A. Black

What are electrons really doing in molecules?

- attributed to R. S. Mulliken

Contents

1	Introduction	1
1.1	Quantum mechanics and quantum chemistry	1
1.2	The many-body wavefunction	2
1.3	Current work	4
1.4	Conventions and notations	5
2	Electronic Structure Theory	7
2.1	Postulates of Quantum Mechanics	7
2.2	Numerical solutions to the Schrödinger equation	8
2.2.1	The Born-Oppenheimer approximation	9
2.2.2	Spin orbitals and Slater Determinants	10
2.2.3	Basis sets	12
2.3	Hartree-Fock and Self-Consistent Field theory	13
2.3.1	The Hartree-Fock equations	14
2.3.2	Roothaan equations	15
2.3.3	Deficiencies of the SCF method: dynamic and non-dynamic correlation	16
2.4	Properties of a computational method	19
2.5	Many-Body Perturbation Theory	24
2.6	Configuration Interaction	26
2.7	Coupled Electron Pair Approximations	28
2.8	Coupled-Cluster theory	29
2.8.1	Variational Coupled-Cluster	31
2.8.2	Triple excitations	33
2.9	Second quantisation	33
2.10	Multireference methods	37

2.10.1	MCSCF and CASSCF	37
2.10.2	MRCI, MRCC and CASPT2	38
2.11	Contemporary single reference methods	39
2.11.1	Spin-flip	39
2.11.2	Term excluding methods	40
2.12	A remark on density based methods	44
3	Quasi-Variational Coupled-Cluster: Theory	47
3.1	The Linked Pair Functional	47
3.1.1	Approximating VCCD	47
3.1.2	Mathematics of LPDF	50
3.1.3	Comparisons to CID	52
3.1.4	Properties and limitations	55
3.2	Quasi-Variational Coupled-Cluster Doubles	56
3.3	Existence of the \mathbf{U}^p tensors	59
3.4	Single excitations	60
3.4.1	Projective Brueckner orbitals	61
3.4.2	Variational Brueckner orbitals	62
3.5	Triple excitations	62
3.5.1	The (T) correction	62
3.5.2	Triples correction for OQVCCD	63
3.5.3	Renormalised triples	64
4	Quasi-Variational Coupled-Cluster: Implementation	69
4.1	Programmable equations	69
4.1.1	Indices	70
4.1.2	Spin-orbital equations	70
4.1.3	Spatial-orbital equations	72
4.1.4	Contravariant configurations	77
4.2	Implementation	78
4.2.1	Integrated Tensor Framework	78
4.2.2	Auxiliary code	82
5	Benchmarking and applications	87
5.1	PECs and diatomic constants	87

5.1.1	Computational details	88
5.1.2	Singly bonded molecules	89
5.1.3	Multiply bonded molecules	93
5.1.4	Conclusions	97
5.2	Determination of activation and reaction energies	97
5.2.1	Computational details	98
5.2.2	Results and discussion	100
5.2.3	Conclusions	106
5.3	Asymmetric-renormalised triples correction	107
5.3.1	Potential energy curves	107
5.3.2	Spectroscopic constants	112
5.3.3	Harmonic frequencies	113
5.3.4	Computational time	113
5.3.5	Discussion and conclusions	114
5.4	Scaling and timings	114
5.4.1	Comparisons with the old code	115
5.4.2	Comparisons with the CC program	117
5.4.3	Scaling factors	119
5.4.4	Parallel timings	120
6	Calculating reaction rates with Instanton theory	123
6.1	Reaction rates and rate constants	123
6.1.1	Criegee intermediates	125
6.2	Theory	125
6.2.1	Ring-polymer potential	126
6.2.2	Rate constants	127
6.3	Methodology and instanton scripts	128
6.4	Instanton calculations	129
6.5	Conclusion	135
7	Unrestricted Quasi-Variational Coupled Cluster theory	137
7.1	UQVCCD theory	137
7.1.1	Restricted and unrestricted formalisms	137
7.2	UQVCCD equations	139

7.2.1	Density matrices	139
7.2.2	Transformed amplitudes	140
7.2.3	Residuals	141
8	Conclusions	145

Chapter 1

Introduction

1.1 Quantum mechanics and quantum chemistry

In the first half of the 20th century, physics undertook a methodological revolution. Since the middle of the 19th century, Newtonian mechanics had been under attack; no longer could it describe the new phenomena that was being observed at the atomic and sub-atomic levels. [1] Several phenomenological theories were constructed to overcome the discrepancies between current theory and observation; these would be grouped under the name of *Quantum Mechanics*.

As the century marched on, new ideas would be added to the new body of theory, one of the most successful being the wave mechanics model, articulated by Erwin Schrödinger, [2] which forms the foundations of the work carried out in this thesis. In essence, this describes particle positions and trajectories with *wavefunctions* that are solutions to the Schrödinger equation.

At the onset, quantum mechanics was used to investigate physical-chemical phenomena such as the spectroscopic structure of atoms (and later molecules), but it was also used to understand the nature of the bonding within molecular structures and thereby give a rational basis for the empirical rules that dominated experimental practice. [3]

However, there were two immediate problems with this enterprise: reductionism [4] and finding a many-body wavefunction which satisfies the Schrödinger equation. Whether chemical phenomena can be totally explained by quantum mechanics is too large a question to be discussed here, or anywhere in this work. Suffice for this thesis, the answer to this will be: quantum chemistry, a theory of

chemistry based on quantum mechanics,¹ can help to explain relevant chemical phenomena.

The second problem poses a direct relevance to this thesis; how to solve the equations of quantum mechanics given the seemingly impossible task of devising a many-body wavefunction to describe the states of the protons, neutrons and electrons within a molecular system. Approximations must be introduced to produce answers to chemical questions. The task of developing approximations and carrying out calculations has occupied many scientists from the pioneering work of Walter Heitler and Fritz London, [6] to the modern Coupled-Cluster theories of today. [7]

1.2 The many-body wavefunction

An approach to finding a many-body wavefunction usually begins by simplifying the problem at hand. As discussed in Chapter 2, the nuclei and electronic states that describe a system can be approximately decoupled, thereby reducing the problem to finding a wavefunction that describes the electronic states. Knowledge of just these states can be used to explain and explore many areas of chemistry including bonding, reactivity and spectroscopy.

A problem that must be addressed is how to systematically produce and compute these electronic wavefunctions for a wide range of molecular systems. The accurate prediction of the electronic structure of molecules not only allows the prediction of various physical properties that can be used to guide and inform experimental practice, but offers an understanding of chemical phenomena which can complement experimental results.

Many approximations have been devised to solve this problem. One of the first and most enduring methods for calculating electronic structure is the Hartree-Fock (HF) approximation. [8] Within this theory the two-body interactions between individual electrons are replaced by a sum of one-body interactions. This method is capable of producing impressive answers when compared to exper-

¹Theoretical chemistry as a term has been used synonymously with both quantum and computational chemistry. Theoretical chemistry has existed as long as chemistry; for example, we are not concerned with the old Caloric and Phlogiston theories. Therefore the term quantum chemistry will be used. [5]

imental data, however, for many chemical processes, knowledge of the correct two-body interaction is important for physically correct results.

Introducing correlations between electrons is often important in calculating accurate molecular properties like the energy of a system. These correlating effects can be broken down into two categories: dynamic and non-dynamic. Dynamic correlation describes the correct two-body electron interactions that are absent from the mean field HF method. Non-dynamic correlation is concerned with representing the many-body wavefunction in a complete basis of functions. Advanced methods like Configuration Interaction and Coupled-Cluster theory have been developed to circumvent the problem of dynamic correlation, [9, 10] however, they often fail to produce even qualitatively correct results for systems where non-dynamic correlation is important.

Configuration Interaction and Coupled-Cluster theory both rely on choosing a single electronic state, usually the HF state, to embody the electronic wavefunction. For certain systems, a better description would be to use a linear sum of electronic states. Constructing a wavefunction like this becomes important when investigating photochemistry, excited states, radicals, breaking and forming chemical bonds and predicting spectroscopic data. [11] In other words, a large amount of potentially interesting chemistry must take into account several electronic states to predict accurate results.

Traditionally, methods like Complete Active Space Self-Consistent Field theory and Multireference Configuration Interaction have been used to investigate these systems. [12] There are several problems associated with these methods; firstly, the user must manually choose which electronic states to include in the construction of the wavefunction, and secondly, the time required to run these calculations grows rapidly with increasing system size.

Choosing the correct electronic states can often be a difficult and error prone task. In recent years, methods have been developed which do not rely on the choice of multiple electronic states to generate accurate answers, yet manage to scale well with system size. One such family of methods are based on Quasi-Variational Coupled-Cluster Doubles theory (QVCCD). [13] These methods form the basis of this thesis.

1.3 Current work

Currently we are concerned with the development, extension and application of the QVCCD method. In Chapter 3, the previous work of developing QVCCD will be re-examined. This initially led to the method being programmed into the Molpro computational package. [14] However, this code has been determined to be too slow to use in practical quantum chemical calculations and so part of this project has been to derive and re-write the QVCCD and orbital optimisation programs so that it is faster and of more utility to the chemical community. This process is set out in Chapter 4.

Certain schemes to improve the QVCCD method have previously been devised, under the name *Renormalised Triples*. Several approximations were made in the construction this correction to make it as computationally cheap as possible. [15] One of the key approximations, hereafter denoted as the ‘asymmetric-renormalised’ triples, is coded and numerical tests carried out to determine if the original scheme was justified (Chapter 5).

Also within Chapter 5, the benchmarking of QVCCD is carried out against both single- and multireference methods. These are all used to determine how well QVCCD performs in dissociating third-row diatomic molecules and predicting their respective harmonic vibrational constants. QVCCD is also used to predict the activation and reaction energies of many different reactions and thereby ascertain if QVCCD can be applied to kinetic and thermodynamic investigations. The statistics of quantities are calculated and compared to other single-reference methods.

Quantum chemistry should be used to address chemical problems and predict results to confirm or guide experiment. With this in mind, the kinetics and dynamics for the Criegee [16] reaction are investigated in Chapter 6. Briefly, matter appears to display certain characteristics of waves, especially at the atomic level. This wavelike behaviour of atoms allows them to tunnel through certain potential energy barriers and therefore increase the rate of a reaction. [17] The effect of a hydrogen atom tunnelling through the energy barrier that defines a Criegee intermediate is investigated with four different computational methods. These are compared to determine the effects each method has on the result and also to determine whether a computationally cheaper method can be used in

future calculations.

Finally, to date, only a closed-shell QVCCD code exists within Molpro. In Chapter 7, the open-shell, spin adapted, QVCCD equations are derived and presented. It is the hope of the author that the presentation made here will help facilitate the implementation of an *Unrestricted* QVCCD program that can be used to investigate the numerous examples of open-shell chemistry.

1.4 Conventions and notations

Throughout this work, atomic, or Hartree, units have been used: The elementary charge (e), electron mass (m_e), reduced Plank's constant ($\hbar = \frac{h}{2\pi}$) and Coulomb's constant ($\frac{1}{4\pi\epsilon_0}$) are set to unity. [18] These constants will therefore be omitted from all equations and their dimensionality implied.

The exact many-body wavefunction will be denoted by Ψ , while ψ denotes the exact *electronic* wavefunction. Φ will represent an approximate electronic wavefunction. Spatial-orbitals and spin-orbitals will be represented by ϕ and χ respectively.

All operators will be written in non-italicised Latin script and topped with a caret (\hat{H} , \hat{T} , \hat{V} , \hat{a} , \hat{h} , *etc.*)

Excitation levels

The following letters at the end of CI, CC, QVCC, LPF, pCC and DC will denote the excitation level of the method:

S	Singles
D	Doubles
T	Triples
Q	Quadruples
P	Pentuples
H	Hexuples

Chapter 2

Electronic Structure Theory

2.1 Postulates of Quantum Mechanics

Any scientific theory must start from a set of postulates. Quantum mechanics is no exception, and so the description of these postulates are necessary to understand the theory. Different authors tend to choose different postulates, though by examination they are found to be related to the four presented here: [1,19]

1. The state and information of a system is fully described by a vector $|\Psi(\mathbf{r}, t)\rangle$ in a Hilbert Space,¹ where r represents the positions of particles and t is the time. The probability *amplitude* associated with it, $\Psi(\mathbf{r}, t)$, is commonly called the wavefunction.

The systems examined in this thesis consist of indistinguishable particles called fermions. This indistinguishability is expressed by imposing symmetry conditions on the wavefunction. For fermions, such as electrons, the wavefunction must be anti-symmetric and so must change sign when two particles exchange positions. Less rigorously, this condition is stated as the Pauli exclusion principle: No two fermions can occupy the same state within a system.

2. The probability of a particle in a specific state will be proportional to the probability density, $|\Psi(\mathbf{r}, t)|^2$. This postulate is sometimes referred to as the ‘Born interpretation’, after Max Born.
3. Physical observables are represented as Hermitian operators in the Hilbert

¹For our case, a Hilbert space is best described as a complex inner product space and also a complete metric space [20]

space. These operators are chosen to satisfy certain commutation relations and are invariant to the interchange of two identical particle coordinates in the wavefunction. If they admit eigenvectors, then the eigenvalues of these operators are the possible values that the state may take.

The eigenvalues of these operators correspond to possible values of measurement, which are proportional to $|\langle n|\Psi(\mathbf{r}, t)\rangle|^2$, *i.e.* the projection of the quantum state onto an eigenstate of the operator. In the Copenhagen interpretation, a quantum state is a superposition of different states, each with an associated probability amplitude. When a measurement is performed upon it, the wavefunction is said to ‘collapse’ into one of the states.

4. The wavefunction evolves in time according to the Schrödinger equation,

$$i\hbar \frac{\partial}{\partial t} |\Psi(\mathbf{r}, t)\rangle = \hat{H} |\Psi(\mathbf{r}, t)\rangle , \quad (2.1)$$

where $|\Psi(\mathbf{r}, t)\rangle$ is an eigenstate of the Hamiltonian operator, \hat{H} , that characterizes the total energy of the system. This is a second-order differentiation equation and so analytical solutions are not (in general) available for more than a two particle system.

The time dependent part of Eq.2.1 can often be separated, leaving the time-independent Schrödinger equation,

$$\hat{H} |\Psi(\mathbf{r})\rangle = \left[-\frac{\hbar^2}{2m} \nabla^2 + V(\mathbf{r}) \right] |\Psi(\mathbf{r})\rangle = E |\Psi(\mathbf{r})\rangle , \quad (2.2)$$

where E is the energy of the system and $V(\mathbf{r})$ is a potential function.

This project is not concerned with how a state will evolve with time, so only the time independent equation will be considered from here on.

2.2 Numerical solutions to the Schrödinger equation

Presently, there are no exact analytical solutions to the Schrödinger equation for many electron systems.² A course of action is to make approximations to the physical model and develop numerical methods which can be easily carried out on a computer. By doing this, approximate solutions to Eq. 2.2 can be developed.

²Exact analytical solutions do exist for the Hydrogen atom (one electron, one proton)

2.2.1 The Born-Oppenheimer approximation

The starting point for many electronic structure calculations is the Born-Oppenheimer (BO) approximation, which involves an approximate decoupling of equations involving the electron and nuclear eigenstates. [1]

The non-relativistic molecular Hamiltonian can be written succinctly as:

$$\hat{H} = \hat{T}_e + \hat{T}_N + (\hat{V}_{N,e} + \hat{V}_{e,e} + \hat{V}_{N,N}) = \hat{T}_e + \hat{T}_N + \hat{V}, \quad (2.3)$$

where \hat{T} and \hat{V} are the differential kinetic and potential energy operators labelled by e (electrons) or N (nuclei).

If the electron and nuclei coordinates are assumed to be approximately separable, then a trial eigenfunction to the above Hamiltonian can be constructed:

$$|\Psi(\mathbf{r}, \mathbf{R})\rangle = \psi(\mathbf{r}; \mathbf{R})\gamma(\mathbf{R}), \quad (2.4)$$

where $\psi(\mathbf{r}; \mathbf{R})$ is the electronic wavefunction that depends explicitly on the electron coordinates and parametrically on the nuclear coordinates, and $\chi(\mathbf{R})$ is the nuclear wavefunction.

This can be inserted into the Schrödinger equation,

$$\hat{H}(\psi\gamma) = \gamma\hat{T}_e\psi + \psi\hat{T}_N\gamma + \hat{V}\psi\gamma + U(\mathbf{r}, \mathbf{R}) = E(\psi\gamma), \quad (2.5)$$

$$\hat{T}_N(\psi\gamma) = \psi\hat{T}_N\gamma + U(\mathbf{r}, \mathbf{R}), \quad (2.6)$$

where $U(\mathbf{r}, \mathbf{R})$ represents the electronic and nuclear coupling terms that arise when \hat{T}_N is applied to the trial wavefunction. The inverse nuclear mass appears in $U(\mathbf{r}, \mathbf{R})$, so it is expected to be small and can be neglected. The remaining terms can be rearranged,

$$\psi\hat{T}_N\gamma + (\hat{T}_e\psi + \hat{V}\psi)\gamma = E(\psi\gamma). \quad (2.7)$$

The set of equations in the parenthesis depend only on the electronic coordinates and fixed nuclear positions; this is called the electronic Schrödinger equation. The nuclear potential term, $\hat{V}_{N,N}$, can be added into the Hamiltonian after ψ has been determined. It is a constant that depends on fixed nuclear positions and so only shifts the eigenvalues in energy.

The mathematics of the approximation can be justified thus: Nuclei are considerably more massive than electrons (an electron is 0.0545% less massive than

a proton) and therefore move at slower speeds. Relative to an electron's frame of reference, the nuclei appear fixed in space and do not seem to move at all.³

It should be noted that this approximation is only reliable for calculating ground state properties, *i.e.* the lowest energy eigenstate of a system. For excited states, or where one nuclear state correlates to several near-degenerate electronic states, this approximation breaks down and Eq. 2.4 no longer becomes valid. For this project, this is not an issue as we are only concerned with ground state properties.

By invoking the BO approximation, the number of dimensions has been reduced, so our problem now becomes one of finding the electronic wavefunction for fixed nuclear positions. Unfortunately, the only system that can be treated exactly with this approximation is H_2^+ , [23] however the BO approximation will form the point of departure for all successive approximations.

2.2.2 Spin orbitals and Slater Determinants

An electron can be described by a function of its three spatial coordinates, $\phi(\mathbf{r})$, and a spin function, $\alpha(\omega)$ or $\beta(\omega)$, which correspond to the spin up ($m_s = +\frac{1}{2}$) and spin down ($m_s = -\frac{1}{2}$) states respectively. This product is called a spin orbital which is a function of the combined spin and spatial coordinates \mathbf{x} ,

$$\chi(\mathbf{x}) = \begin{cases} \phi(\mathbf{r})\alpha(\omega) \\ \phi(\mathbf{r})\beta(\omega) \end{cases} . \quad (2.8)$$

From these basic building blocks, a wavefunction for a many electron system can be constructed. A naive approach would be to place N electrons into a product of N orbitals. This type of wavefunction is called the Hartree product, and apart from its deficiencies in describing inter-electron repulsion, it fails to take into account the indistinguishability of electrons and thereby the anti-symmetric principle. [8]

A true anti-symmetric wavefunction can be formed if a linear combination of several Hartree products are used. For a simple two-electron system a wavefunc-

³This simplistic interpretation has been challenged by Essén, who states that the structure of the Coulombic interaction term leads to the separation of the internal and relative degrees of freedom, and not the ratio of electron to nuclei masses. [21,22]

tion can be constructed where electron 1 is in $\chi_1(\mathbf{x}_1)$ and electron 2 in $\chi_2(\mathbf{x}_2)$,

$$|\Phi(\mathbf{x}_1, \mathbf{x}_2)\rangle' = \chi_1(\mathbf{x}_1)\chi_2(\mathbf{x}_2). \quad (2.9)$$

A linear combination can be constructed from these two functions such that the indistinguishability is maintained and the wavefunction is anti-symmetric, thereby fulfilling the Pauli exclusion principle:

$$|\Phi(\mathbf{x}_1, \mathbf{x}_2)\rangle = \chi_1(\mathbf{x}_1)\chi_2(\mathbf{x}_2) - \chi_1(\mathbf{x}_2)\chi_2(\mathbf{x}_1), \quad (2.10)$$

$$|\Phi(\mathbf{x}_1, \mathbf{x}_2)\rangle = -|\Phi(\mathbf{x}_2, \mathbf{x}_1)\rangle. \quad (2.11)$$

This type of wavefunction, named after John C. Slater, can be compactly written as a determinant,

$$|\Phi(\mathbf{x}_1, \mathbf{x}_2)\rangle = \frac{1}{\sqrt{2!}} \begin{vmatrix} \chi_1(\mathbf{x}_1) & \chi_2(\mathbf{x}_1) \\ \chi_1(\mathbf{x}_2) & \chi_2(\mathbf{x}_2) \end{vmatrix}. \quad (2.12)$$

and generalised to N -electrons:

$$|\Phi(\mathbf{x})\rangle = \frac{1}{\sqrt{N!}} \begin{vmatrix} \chi_p(\mathbf{x}_1) & \chi_q(\mathbf{x}_1) & \dots & \chi_r(\mathbf{x}_1) \\ \chi_p(\mathbf{x}_2) & \chi_q(\mathbf{x}_2) & \dots & \chi_r(\mathbf{x}_2) \\ \vdots & \vdots & \ddots & \vdots \\ \chi_p(\mathbf{x}_N) & \chi_q(\mathbf{x}_N) & \dots & \chi_r(\mathbf{x}_N) \end{vmatrix} = |\chi_p(\mathbf{x}_1)\chi_q(\mathbf{x}_1)\dots\chi_r(\mathbf{x}_1)\rangle. \quad (2.13)$$

It was no accident that a determinant was chosen to represent a wavefunction, as its mathematical properties are a good model for fermionic particles. For example, when two rows (two electrons) are interchanged, the sign changes, while having two columns the same (two electrons in the same orbital) makes the determinant vanish.

A Slater Determinant (SD) is not a perfect representation of the electronic wavefunction. Formally, it is an uncorrelated wavefunction because the probability of finding an electron is independent of the probability of finding another electron of opposite spin in a given volume of space. Nevertheless, a SD will correlate electrons of parallel spins. [24] This expresses itself through the exchange correlation effect: two electrons of parallel spin in the same volume of space will produce a zero determinant.

Though there are many specific cases where an analytical function can be derived for a wavefunction, in theoretical chemistry, single SDs or linear combina-

tions of SDs are usually used due to their general applicability to any N -electron system.

2.2.3 Basis sets

If there were an infinite set of functions that formed a complete basis (*i.e.* a basis that spans the whole function space), then any N -electron molecular wavefunction could be constructed from this set.

Computationally, an infinite sum of an infinite set of functions can not be calculated, therefore it is necessary to restrict the basis to a finite subset which spans a subspace of the complete space. As mentioned in the previous section, SDs are usually chosen as a basis for a molecular wavefunction. Often, one SD dominates this expansion, so as a further simplifying step, this single SD is chosen to represent the molecular wavefunction. [25]

These SDs are in turn constructed from a set of orbitals: the one-electron wavefunctions of Eq. 2.8. These orbitals are themselves expanded in a finite set of known functions⁴. Formally, this method is named Linear Combination of Atomic Orbitals (LCAO) and it forms the cornerstone of the Molecular Orbital (MO) picture of bonding. [1]

MOs are constructed from the combination of the one-electron orbitals and describe the electronic states in a molecule. This theory does away with any assumptions about the form the MOs can take and as a result, usually provides an accurate and unbiased description of the electronic structure. This should be contrasted with Valence Bond (VB) theory, which evolved from empirical chemical experience. [3, 26] This theory contends that the wavefunction can be modelled by using the overlap of bonding atomic orbitals; though this adherence to the atomic orbitals is usually at the expense of an accurate wavefunction. Historically, VB was the first theory used to examine chemical systems, however MO theory became more popular in the mid 20th century and is now the dominant picture in electronic structure calculation. This project is based in the LCAO/MO picture and so VB theory, though an important tool, will not be considered again.

There are several 'known functions' from which the one-electron orbitals may

⁴By convention, this set of functions are referred to as *the* basis set, as opposed to the basis of SDs or one-electron orbitals. All occurrences of an unqualified *basis set* will be taken to refer to the set of functions that the one-electron orbitals are constructed from.

be constructed. For example, Slater-type functions could be used; these can be generically written as, [8]

$$\theta(\mathbf{r}) = A r^l e^{-\alpha r}, \quad (2.14)$$

where A is a normalisation constant, r is the distance of the electron from the nucleus, l is the angular momentum quantum number and α is a constant related to the charge on the nucleus.

Slater-type functions can approximate the exact Schrödinger solutions to the hydrogen atom very well. Nevertheless, it is computationally more practical to use Gaussian functions of the form,

$$\theta(\mathbf{r}) = A r^l e^{-\alpha r^2}, \quad (2.15)$$

to approximate the Slater functions. Integrals over four basis functions are common in computational chemistry and a product of Gaussians is simply another Gaussian function. Therefore these integrals can be reduced to products of just two Gaussians. Most basis sets are constructed by using linear combinations of these Gaussian functions to approximate more complicated forms.

Some of the most commonly used basis sets are those designed by Dunning and co-workers. [27] These basis functions were fitted using highly accurate quantum chemical methods and were designed to converge quickly to the limit of infinite basis functions. Because of these properties, the *correlation consistent* basis sets, cc-pVXZ, where $X = \{D, T, Q, 5, 6, 7, \dots\}$, can be applied to various chemical problems with confidence. This family of basis sets have been used throughout this project.

2.3 Hartree-Fock and Self-Consistent Field theory

The Hartree-Fock (HF) method was one of the first methods developed to find numerical solutions to the Schrödinger equation for a many-body system. It is computationally inexpensive and can account for 99% of the total energy of a molecule. [8] It achieves this by invoking the BO approximation and the LCAO method to construct the HF wavefunction. These properties make the HF solu-

tion a good zeroth-order approximation to the wavefunction and a starting point for many subsequent improvements.

2.3.1 The Hartree-Fock equations

HF theory states that a single SD is an adequate approximation to the electronic wavefunction,

$$|\Phi_0\rangle = |\chi_1(\mathbf{x}_1)\chi_2(\mathbf{x}_2)\dots\chi_i(\mathbf{x}_N)\rangle . \quad (2.16)$$

The Hamiltonian in atomic units,

$$\hat{H} = \left(-\frac{1}{2} \sum_i \nabla_i^2 - \sum_{i,A} \frac{Z_A}{|r_i - R_A|} \right) + \sum_{i,j} \frac{1}{|r_i - r_j|} = \hat{h}(i) + \hat{v}(i, j) , \quad (2.17)$$

where the potential term is now a sum of the nuclei-electron and electron-electron electrostatic potentials (Z_A is the charge on nuclei A ; R_A and r_i are the nuclei and electron position vectors respectively), can be split into a sum of one-body and two-body terms. The task is then to find a set of spin orbitals that minimise the electronic energy *via* the variational theorem,

$$\min_{\chi_i} E_0 = \langle \Phi_0 | \hat{H} | \Phi_0 \rangle = \langle i | \hat{h} | i \rangle + \frac{1}{2} \langle ij | ij \rangle , \quad (2.18)$$

$$\langle i | \hat{h} | i \rangle = \int \chi_i^*(\mathbf{x}_1) h(\mathbf{r}_1) \chi_i(\mathbf{x}_1) d\mathbf{x}_1 , \quad (2.19)$$

$$\langle ij | ij \rangle = \langle ij | ij \rangle - \langle ij | ji \rangle , \quad (2.20)$$

$$\langle ij | ji \rangle = \int \chi_i^*(\mathbf{x}_1) \chi_j^*(\mathbf{x}_2) r_{12}^{-1} \chi_i(\mathbf{x}_1) \chi_j(\mathbf{x}_2) d\mathbf{x}_1 d\mathbf{x}_2 . \quad (2.21)$$

In the equations above, the Einstein summation convention has been used, where repeated indices are summed over. This convention will be used in all equations to follow, unless the sum needs to be explicitly stated for clarity.

The energy can be minimised by restricting the orbitals to be orthonormal (which in practice means introducing a set of Lagrangian multipliers) and varying the spin orbitals. In this fashion, the HF integro-differential equations can be derived, [8]

$$\begin{aligned} \hat{f} |i\rangle &= \sum_j \epsilon_{ij} |i\rangle , \\ \left[\hat{h} + \sum_{j \neq i}^N \hat{J}_j - \hat{K}_j \right] |i\rangle &= \sum_j \epsilon_{ij} |i\rangle , \end{aligned} \quad (2.22)$$

where \hat{f} is called the Fock operator.

This formulation removes the two-electron terms in Eq. 2.18, and constructs the kinetic and potential interactions as the sum of three one-electron operators:

- \hat{h} represents the kinetic energy of the electrons and the Coulombic attraction between electrons and the nuclei.
- \hat{J} is the Coulomb operator which represents the average potential that an electron in χ_i experiences from the other $N - 1$ electrons in the system.
- \hat{K} is the exchange operator that cannot be given a classical interpretation like the Coulomb operator. It is defined for each unique pair of same spin electrons, thereby correlating their motions (the same is not true for electrons of opposite spin).

The use of these one-electron operators means the electronic coordinates (\mathbf{x}_i) can be separated in the Schrödinger equation, making possible the use of a SD constructed from one-electron orbitals. [24]

2.3.2 Roothaan equations

The HF equations can not be solved analytically for systems larger than single atoms. Instead, the numerical procedure introduced by Roothaan must be used to find a set of spin orbitals that satisfy Eq. 2.22. [28] This is called the Self-Consistent Field (SCF) approach, in which the HF wavefunction is the limiting result. [7]

For a closed-shell molecule, the spatial orbitals defined in the previous section may be used instead of the spin orbitals. [8] A set of known basis functions must be introduced in which these spatial orbitals can be expanded and given form,

$$|i\rangle = C_{\mu i} |\mu\rangle . \quad (2.23)$$

If this set is complete, *i.e.* infinite, then the exact HF orbitals could be obtained. This cannot be achieved, so a finite set is chosen so that the error in the expansion can be reduced by systematically increasing the size of the basis set. Increasing the basis set to a large number of functions will converge the molecular energy to a limit known as the HF limit.

The problem can now be stated: Find the set of expansion coefficients (\mathbf{C}) that minimize the energy functional.

To do this, the integro-differential equations can be rewritten in matrix form. The new definition of the spatial orbitals are inserted into Eq. 2.22, and the resulting equations post-multiplied by $\langle\mu|$,

$$\sum_{\mu} \langle\mu|\hat{f}|\nu\rangle C_{\nu i} = \sum_{\mu} \langle\mu|\nu\rangle C_{\nu i} \epsilon_i. \quad (2.24)$$

Two $K \times K$ Hermitian matrices can be defined; the overlap matrix,

$$S_{\mu\nu} = \langle\mu|\nu\rangle, \quad (2.25)$$

and the Fock matrix,

$$F_{\mu\nu} = \langle\mu|\hat{f}|\nu\rangle, \quad (2.26)$$

which is simply the Fock operator in the $|\mu\rangle$ basis representation. Eq. 2.24 can be written compactly as,

$$\mathbf{FC} = \mathbf{SC}\epsilon, \quad (2.27)$$

where ϵ is a diagonal matrix of orbital energies. The MOs are usually chosen to be orthonormal, so \mathbf{S} becomes the identity matrix ($S_{\mu\nu} = \delta_{\mu\nu}$ ⁵) and Eq. 2.27 reduces to a standard eigen equation.

At the end of a SCF calculation, two sets of orbitals are produced. The set of orbitals which are doubly occupied in the ground state are called the occupied orbitals, while the remainder are called the virtual orbitals. These virtual orbitals hold the key to further improvements of the SCF method.

An infinite number of different orbitals can be generated, which are related to each other *via* a unitary transformation. It is convenient to work with the set of orbitals that diagonalize the Fock matrix called the *canonical* orbitals.

2.3.3 Deficiencies of the SCF method: dynamic and non-dynamic correlation

As the basis set is increased, the SCF energy will converge to a limit (the *HF limit*). A quantity called the ‘correlation energy’ [24] can be theoretically defined

⁵ δ_{ij} is the Dirac delta function. Simply put: $\delta_{ij} = \begin{cases} 1, & i = j \\ 0, & i \neq j \end{cases}$.

as,

$$E_{\text{exact}} = E_{\text{HF}} + E_{\text{corr}}, \quad (2.28)$$

where E_{corr} , E_{exact} and E_{HF} are the correlation energy, the exact Schrödinger energy and the reference energy respectively. The correlation energy represents the energy effects that HF does not take into account. [29] This can be investigated with a qualitative analysis of the approximations the HF method makes.

Dynamic correlation

HF theory is a mean field theory, where the two-body interactions have been replaced by a sum of one-body operators. Each electron, instead of experiencing the electrostatic repulsion of each individual electron, only experiences an average repulsion from all other electrons.

The anti-symmetrised SD state can effectively correlate electrons of parallel spin, as two identical columns will make a determinant vanish (this effect is called the Fermi hole). The major error comes from the uncorrelated electrons of opposite spin; the failure to take these interactions into account can lead to qualitative failures in the wavefunction.

For a two-electron system the r_{12} term from the Hamiltonian in Eq. 2.17 introduces a condition upon the wavefunction called the cusp condition, [29]

$$\left(\frac{\partial \Phi}{\partial r_{12}} \right)_{r_{12}=0} = \frac{1}{2} \Phi(r_{12} = 0) \quad (2.29)$$

The failure of the HF wavefunction to capture this cusp can be illustrated by comparing a HF and an explicitly correlated (Hylleraas-type) wavefunction for He. [30]

Fig. 2.1 displays both wavefunctions where one electron is fixed in position and the other is allowed to move towards it in a straight line.⁶ As the second electron moves towards the first, the Hylleraas-type wavefunction forms a cusp (the Coulomb hole). The electron avoids this region due to the presence of the other electron and the Coulomb repulsion between the two. The HF wavefunction does not reproduce this and in general, tends to overestimate the interelectronic repulsion. For this case, the Hylleraas-type wavefunction is able to model the correlated motions of the electrons, called dynamic correlation. The HF answer fails to capture this interaction and produces a qualitatively incorrect wavefunction.

⁶This is the Molpro logo. Plotting was carried out in Mathematica [31]

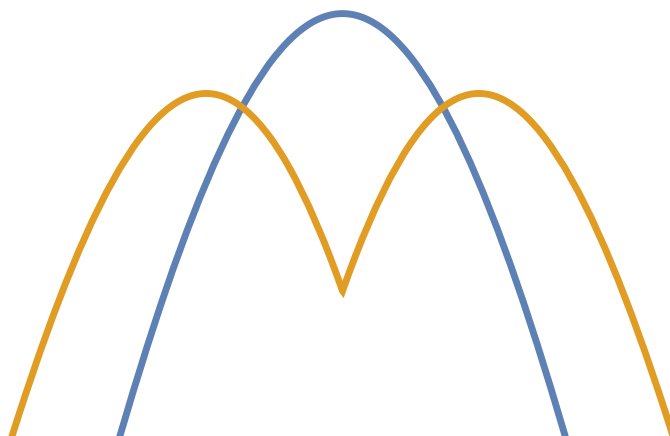


Figure 2.1: HF (blue) and Hylleraas-type (orange) wavefunctions for He, where one electron is fixed at 0.94 Bohr (the orange cusp) and the other electron is moved in a straight line towards it.

Non-dynamic correlation

An error occurs when a single SD is used to represent the wavefunction. In many cases, such as ground state closed-shell organic molecules, this error is minimal and can be ignored. For other cases, such as transition states, molecular dissociations, radicals, photo-excitations etc., [11] more than one electronic state dominates the SD expansion and this approximation is no longer valid.

This is illustrated with a simple example involving H_2 . [32,33] If two spherical Gaussian functions, θ_A and θ_B , are centred on each hydrogen atom A and B , then two MOs can be formed,

$$\sigma_g = \frac{1}{\sqrt{2(1+S)}} [\theta_A(\mathbf{r}) + \theta_B(\mathbf{r})], \quad (2.30)$$

$$\sigma_u = \frac{1}{\sqrt{2(1+S)}} [\theta_A(\mathbf{r}) - \theta_B(\mathbf{r})]. \quad (2.31)$$

In a SCF calculation, the ground state wavefunction (ignoring spin) can be formed by placing the two electrons into σ_g .

$$\Phi = \sigma_g(1)\sigma_g(2), \quad (2.32)$$

$$\begin{aligned} \sigma_g(1)\sigma_g(2) = \frac{1}{2(1+S)} & [\theta_A(\mathbf{1})\theta_A(\mathbf{2}) + \theta_A(\mathbf{1})\theta_B(\mathbf{2}) \\ & + \theta_B(\mathbf{1})\theta_A(\mathbf{2}) + \theta_B(\mathbf{1})\theta_B(\mathbf{2})]. \end{aligned} \quad (2.33)$$

This wavefunction contains a mixture of ionic ($\theta_A(\mathbf{1})\theta_A(\mathbf{2})$) and covalent ($\theta_A(\mathbf{1})\theta_B(\mathbf{2})$) terms.

As H_2 dissociates, the ionic terms remain, thus describing the unphysical situation where both electrons are situated on one hydrogen atom. To remedy this, the σ_u MO needs to be included into the wavefunction expansion with a varying parameter,

$$\Phi = \sigma_g(1)\sigma_g(2) + \lambda\sigma_u(1)\sigma_u(2). \quad (2.34)$$

The energy can then be minimised with respect to λ . In this way, as H_2 dissociates, the ionic terms cancel ($\lambda = -1$) and a physically correct wavefunction is obtained.

The inability of a single SD to describe the molecular wavefunction is called *non-dynamic* correlation and is important to the present project. Capturing non-dynamic correlation is hard to automate, leaving the user to guess which configurations to include in the wavefunction expansion. For a general N -electron case with several nuclei, the choice of configurations is no longer as simple as the H_2 example. Instead of a rigorous mathematical justification, the user must use their experience and inductive chemical knowledge to judge which configurations to choose, thereby introducing possible errors.

The failure of HF theory to account for these correlation effects has led to a series of methods termed *Post-HF*. Methods like Configuration Interaction and Coupled-Cluster have been successful in dealing with dynamic correlation. For non-dynamic correlation, the issue of choosing the active space still remains a barrier to wider use. This difficulty has motivated a series of approximations that maintain the single determinant postulate, but try to capture the non-dynamic correlation effects. Most importantly for this project, the Quasi-Variational Coupled-Cluster method was developed to address this problem and will be the topic of subsequent chapters.

2.4 Properties of a computational method

Before proceeding to discuss the Post-HF methods, it will be useful to set out a number of criteria in which they can be judged. [34, 35] Ultimately it is a subjective choice of which standards a method should satisfy, nevertheless there are objective reasons for each of the properties presented here which will go some way to justifying the ones chosen. [36] Satisfaction of these properties will

usually guarantee that the method can be widely and reliably applied to different chemical systems and achieve accurate answers. In general, a method will not be able to satisfy them all.

- **Chemical accuracy**

A fundamental requirement of a method is that can produce accurate results. We are interested in chemical problems, so this requirement can be quantified by specifying that the calculated energies must match chemical experiments that are within an error of 4 kJ mol⁻¹.⁷ [25] Larger errors in energy can totally change the reactive and kinetic predictions of the method. For the cases where there is no experimental data, there must be confidence that the method can be systematically improved to calculate chemically accurate results.

- **Computational scaling and implementation**

A straight forward parametrisation of the wavefunction can generate results that are within chemical accuracy, but the result will be of little use if it takes years of computational time to run.

There are two issues to consider; the computational complexity, or time, and the total memory used. The computational complexity represents the number of operations that a computer must complete to run the method, while the memory represents how much storage is needed and accessed at one point. Both of these algorithmic properties can be described by a prefactor multiplied by a scaling factor, which can be represented using big-*O* notation.⁸

What complexity one finds acceptable depends upon the system size, type of calculation, time and memory constraints. Therefore it is difficult to suggest which scaling is best for the general situation.

CCSD and CCSD(T) are two of the most widely used *ab initio*⁹ methods for investigating small to medium sized systems (around 1 to 50 atoms).¹⁰ It seems

⁷This number has changed throughout the years, for example, Ruedenberg called an energy error on the magnitude of 1 mhartree ‘chemically accurate’ [37]

⁸ $f(\epsilon) = O(\epsilon^p)$ means, for a sufficiently small ϵ , there exists a positive constant, K , such that $|f(\epsilon)| = K|\epsilon|^p$. In our cases it means that our approximation to $f(\epsilon)$ grows no faster than ϵ^p for $O(\epsilon^p)$. [38]

⁹Latin for *from the beginning*. Methods that are derived solely from quantum mechanical arguments and do not use parameters or experimental data are described as *ab initio*.

¹⁰Using Web of Science, a search for the terms ‘CCSD’ and ‘CCSD(T)’ in the literature published in 2016 returns 515 results.

possible that for a many scientists, the scaling of CCSD and CCSD(T) is reasonable for their research purposes. Therefore, for this project, a computationally practical method is an iterative method that scales no more than $O(o^2v^4)$ (where o and v denote occupied and virtual orbitals respectively), or a non-iterative method that scales no more than $O(o^3v^4)$. Storage should then scale as $O(o^2v^2)$.

Notwithstanding, it is no longer sufficient that the algorithm scale acceptably, but the implementation be efficient; for a practical method it is also required that the code be can run in parallel. This means that several jobs can be deconstructed into independent tasks and evaluated at the same time on different CPUs. Though the scaling factors remain the same, the prefactors can be dramatically reduced and produce significant time savings.

- **Extensivity and size-consistency**

Extensivity and intensivity are concepts that originate in thermodynamics. [23] An extensive property is one that scales with system size, while an intensive property is invariant. These same principles apply to electronic structure theory: the energy of a system must scale linearly in the limit of a large number of electrons, N , [39]

$$\lim_{N \rightarrow \infty} \frac{E_{\text{corr}}(N)}{N} = \text{const} > 0. \quad (2.35)$$

If a method does not obey this, then it cannot produce accurate results for systems of increasing N as the correlation energy will deviate. [40]

A similar, but less general concept is size-consistency. [41] This states that the energy of two identical non-interacting molecules should be twice the energy of the of the single molecule. This is important is calculating thermodynamic properties such as enthalpy changes. Extensivity implies size-consistency, however size-consistency does not imply extensivity.

It is trivial to test for size-consistency, but extensivity is harder to prove. Brueckner showed for perturbation theory, that terms with the incorrect dependence on N will cancel out, leaving behind an extensive method. [8] However, using the techniques of second quantisation, introduced in Section 2.9, extensivity can be rigorously determined for a given method.

- **Invariance of orbitals under a unitary transformation**

The energy of a system is a scalar and therefore should be invariant to a unitary rotation of the orbital basis. If this principle is not obeyed the method in question will not give a unique energy for a set of non-degenerate orbitals and will in practice produce different energies for the same calculation. [8] The HF method obeys this principle as the energy stays the same even if rotations occur in the occupied and virtual subspaces (though rotations across the whole space will change the state and hence the energy).

The importance of this property has become apparent in recent years with the development of local correlation methods. [42] Invariance of the orbitals means that a localized basis can be constructed that can be used in a correlation calculation with significantly reduced computational cost. A method must satisfy this property if a local treatment is to be applied to it.

- **Exact treatment of limiting systems**

The use of a finite (one electron) basis means that exact solutions to the Schrödinger equation can never be found, however exact solutions within such a finite basis can be calculated. This answer is usually called the Full Configuration Interaction (FCI) solution. Solutions are constructed from a basis of SDs which ultimately span the entire space. Such a treatment leads to an impractical method that is too expensive for anything but small systems and so a subset of this SD expansion is usually chosen instead.

A more achievable property for a method is to produce the same (exact) answer as FCI for some limiting system. This benchmark is usually chosen to be a two-electron system, as this will guarantee the correct treatment of two-body correlation terms which represent the major contribution to the total correlation energy. [7]

- **Variational minimisation of a functional**

In most cases we want to find extrema of an energy functional, as the state that corresponds to the minimum will be the ground state [43]. By using the variational method, not only can stationary states be found, but the approximations to the state can be improved in a controlled way.

A functional, called the Rayleigh ratio, can be defined by rearranging the Schrödinger equation and dividing by the norm,

$$E_{\text{trial}} = \frac{\langle \Phi | \hat{H} | \Phi \rangle}{\langle \Phi | \Phi \rangle}. \quad (2.36)$$

The variation theorem posits that that $E_{\text{trial}} \geq E_{\text{exact}}$.

The trial state that produces the lowest energy is therefore the best approximation to the actual ground state. The energy of the state is also bounded from below by E_{exact} , therefore guaranteeing that the energy will never fall below the exact Schrödinger equation energy.

- **Generalised Hellmann-Feynman theorem**

Various molecular properties can be calculated from the energy functional by expanding its derivative with respect to a perturbation as a Taylor series. The derivatives of the functional then represent the molecular properties of interest. To simplify this procedure, a method must satisfy the Generalised Hellmann-Feynman theorem (GHF). [34] This states that the derivative of the energy with respect to some perturbation can be related to the expectation value of the derivative of the Hamiltonian, [43]

$$\frac{dE}{d\lambda} = \left\langle \Phi \left| \frac{d\hat{H}}{d\lambda} \right| \Phi \right\rangle. \quad (2.37)$$

This equation is obeyed exactly by variational methods that determine the exact wavefunction. As the quality of this wavefunction declines, Eq. 2.37 becomes less reliable. For non-variational methods, like coupled-cluster theory, the energy functional can always be cast into a variational form by using Lagrangian multipliers. [25]

For example, if the perturbation represented an external electromagnetic field, the derivatives of the energy functional would then represent polarizabilities and magnetizabilities. [44] Satisfaction of the GHF theorem is a benefit to calculating these properties because it means the first-order analytical derivatives can be derived without the knowledge of the derivatives of the perturbed wavefunction.

- **Black box methodology**

Finally, a computational method should be easy to use for general members of the chemical community. In other words, it would be beneficial for the method to be a ‘black box’.

There has been debate in the literature as to what constitutes a ‘black box’ method. [11] A general definition for computational chemistry could be:

A method that requires minimum input to obtain an accurate output.

For example, the method would only require the geometry and basis set for inputs (possibly the number of electrons, charge and multiplicity). The main reason for including this definition is to discriminate against various multireference methods. As Bartlett *et al.* have shown, it is possible to construct a definition that could class multireference methods as a ‘black box’, [11] however it seems disingenuous to do so. There is a large difference between a single reference calculation and a multireference one where various electronic states need to be chosen *a priori*. Such a choice of states is by no means straightforward and in a lot of cases can be very difficult. A method that can be easily used and therefore widely used, should not be dismissed.

2.5 Many-Body Perturbation Theory

With the properties of an ideal method in mind, attention will now be turned towards improving the SCF solution. A straightforward way to capture the effects of dynamic correlation is to use Many-Body Perturbation Theory (MBPT). [45]

MBPT proposes that the exact problem to be solved differs by a small amount from a solvable problem. If this is the case, then the exact Hamiltonian (\hat{H}) can be decomposed into a sum of a reference, the zeroth-order problem already solved (\hat{H}_0), and a (perturbative) correction (\hat{V}),

$$\hat{H} = \hat{H}_0 + \lambda\hat{V}, \quad (2.38)$$

where λ is a parameter that determines the strength of the perturbation. For \hat{H}_0 it is convenient to use the sum of the Fock operators, so the perturbation becomes the difference between the exact and average electron-electron potential,

$$\hat{V} = \sum_{i < j}^N r_{ij}^{-1} - \sum_i^N v_i^{\text{HF}}, \quad (2.39)$$

This describes the Møller-Plesset (MP n , $n=\{2,3,4,5..\}$) method.

As λ is continuously varied to 1, the energy and wavefunction change. These

can be expanded as a Taylor series, [8, 25]

$$E = \lambda^0 E^{(0)} + \lambda^1 E^{(1)} + \lambda^2 E^{(2)} + \dots, \quad (2.40)$$

$$|\psi_i\rangle = \lambda^0 |\Phi_i^{(0)}\rangle + \lambda^1 |\Phi_i^{(1)}\rangle + \lambda^2 |\Phi_i^{(2)}\rangle + \dots, \quad (2.41)$$

and inserted into the Schrödinger equation. Intermediate normalisation is usually chosen for the perturbed and unperturbed states,

$$\langle \Phi_i^{(0)} | \Phi_i^{(0)} \rangle = 1, \quad (2.42)$$

$$\langle \Phi_i^{(0)} | \psi_i \rangle = 1, \quad (2.43)$$

so that,

$$\langle \Phi_i^{(0)} | \Phi_i^{(n)} \rangle = 0. \quad (2.44)$$

Finally, the fundamental theorem of perturbation theory can be invoked and the powers of λ collected together to form a system of equations, [38]

$$\begin{aligned} \hat{H}_0 |\Phi_i^{(0)}\rangle &= E^{(0)} |\Phi_i^{(0)}\rangle, \\ \hat{H}_0 |\Phi_i^{(1)}\rangle + \hat{V} |\Phi_i^{(0)}\rangle &= E^{(0)} |\Phi_i^{(1)}\rangle + E^{(1)} |\Phi_i^{(0)}\rangle, \\ \hat{H}_0 |\Phi_i^{(2)}\rangle + \hat{V} |\Phi_i^{(1)}\rangle &= E^{(0)} |\Phi_i^{(2)}\rangle + E^{(1)} |\Phi_i^{(1)}\rangle + E^{(2)} |\Phi_i^{(0)}\rangle. \end{aligned} \quad (2.45)$$

The perturbed state, $|\Phi_i^{(n)}\rangle$, can be expanded in the one-electron basis which was generated in SCF calculation. This new set of states, $|\Phi_n\rangle$, are known and are eigenfunctions of \hat{H}_0 with energy $E_n^{(0)}$. With these, Eq. 2.45 can be solved and the n^{th} -order corrections to both the energy and the wavefunction can be determined.

As an example, the second-order correction to the energy is:

$$E_i^{(2)} = \sum_{n \neq 0} \frac{\langle \Phi_i^{(0)} | \hat{V} | \Phi_n \rangle^2}{E_i^{(0)} - E_n^{(0)}}, \quad (2.46)$$

which is just the matrix elements of the perturbation operator over a set of unperturbed functions and energies.

If \hat{H}_0 was chosen as described above, the n^{th} -order energy corrections described the hierarchy of MP n methods. The first-order correction (MP1) is simply the SCF energy, so it necessary to go to the MP2 level to improve the SCF wavefunction and include dynamic correlation effects.

MP2 typically accounts for 80-90% of the correlation energy and only scales as $O(M^5)$, where M is the number of basis functions, so is relatively cheap compared to the other Post-HF methods. The energy is not variationally determined, meaning that it is not an upper bound of the exact energy, though it is extensive. [7]

There are several drawbacks to the MP_n methods. The main problem being that various molecular properties, in general, do not converge as the method goes to higher orders. In most cases, the values of the properties will oscillate and slowly converge. [46,47] The Møller-Plesset postulate that the SCF wavefunction is a good zeroth-order approximation is also not necessarily true; if it is a poor description of the system, then higher order terms are needed to produce a reliable answer. Though in some cases, the answers may diverge as higher orders are used.

It has also been shown that higher order MP_n methods depend strongly on choice of basis. Using routine basis sets with diffuse functions can make the series diverge for even simple single reference cases. [48] Therefore, increasing the order and basis set may not lead to improvements.

2.6 Configuration Interaction

The exact wavefunction for a given basis set can be constructed if a complete (and finite) basis of SDs are used,

$$|\psi\rangle = c_i |\Phi_i\rangle . \quad (2.47)$$

The energy can then be minimised with respect to the expansion coefficients, c_i .

The linear expansion of SDs needs to be chosen so that it forms a complete basis. To do this, the set of virtual orbitals (by-products from the SCF procedure) are used. By forming products of these orbitals, electron motions can be correlated. In practice these correlating determinants look like ‘excited’ SDs when compared to the SCF reference state. For example, to correlate the motion of every pair of electrons, all the states are chosen where electrons i and j have

been *excited* into virtual orbitals a and b :¹¹

$$|\psi\rangle = c_{ij}^{ab} |\Phi_{ab}^{ij}\rangle, \quad (2.48)$$

$$c_{ij}^{ab} = -c_{ij}^{ba}. \quad (2.49)$$

The set of mixing coefficients, \mathbf{c} , are often referred to as the *amplitudes* and satisfy fermion symmetry requirements.

This procedure can be repeated for single, double, triple, *etc.* groups of electrons, until N -electrons are placed into N -virtual orbitals. Including all these states into the linear CI expansion produces the Full Configuration Interaction (FCI) wavefunction, [7]

$$|\psi_{\text{FCI}}\rangle = c_0 |\Phi_0\rangle + c_i^a |\Phi_a^i\rangle + \frac{1}{4} c_{ij}^{ab} |\Phi_{ab}^{ij}\rangle + \frac{1}{36} c_{ijk}^{abc} |\Phi_{abc}^{ijk}\rangle + \dots, \quad (2.50)$$

where the implied summation has not been restricted to $i < j < k$ and $a < b < c$, *etc.*, so a factor has been introduced to account for the double counting of spin orbitals. With a suitably chosen excitation operator, \hat{C} , this expansion can be written more compactly as:

$$|\psi_{\text{FCI}}\rangle = (1 + \hat{C}) |\Phi\rangle, \quad (2.51)$$

$$\hat{C} = \hat{C}_1 + \hat{C}_2 + \hat{C}_3 + \dots \quad (2.52)$$

Here, \hat{C} is a sum of excitation operators, \hat{C}_n , that generate the n -excited SDs.

Unlike MBPT which needs to go to infinite order to capture all the correlation energy, the FCI parametrisation can generate a closed form expression,

$$E_{\text{FCI}} = \langle \Phi_0 | \hat{H} | \psi_{\text{FCI}} \rangle. \quad (2.53)$$

Generating all possible excitations for a given basis set is theoretically possible, but is often practically impossible for everything but atoms and very small molecules. An approximation can be easily formed for FCI which can dramatically reduce the number of configurations in the CI expansion. If only single and double excitations are included, a reasonable amount of dynamic correlation can be captured while remaining computationally practical. This describes the CISD method,

$$E_{\text{corr}} = \langle \Phi_0 | \hat{H} | \psi_{\text{CISD}} \rangle = \frac{1}{4} c_{ij}^{ab} \langle \Phi_0 | \hat{H} | \Phi_{ij}^{ab} \rangle. \quad (2.54)$$

¹¹Throughout this thesis, the indices in the set $\{i, j, k, l, m, n, o, p\}$, $\{a, b, c, d, e, f\}$ and $\{r, s\}$ will respectively refer to occupied, unoccupied (virtual) and generic orbitals in the reference state.

CISD has not been popular in recent years, because it is not extensive; it can be shown that the correlation energy scales as \sqrt{N} . [8] So as N goes to infinity, the correlation energy per monomer will go towards zero.

CISD can be modified by the Davidson correction *ex post facto*, [49]

$$E_{\text{corr}} = \frac{1}{4} c_{ij}^{ab} \langle \Phi_0 | \hat{H} | \Phi_{ij}^{ab} \rangle + \Delta E_{\text{Davidson}},$$

$$\Delta E_{\text{Davidson}} = (1 - c_0^2) \left(\frac{1}{4} c_{ij}^{ab} \langle \Phi_0 | \hat{H} | \Phi_{ij}^{ab} \rangle \right). \quad (2.55)$$

This uses the SCF wavefunction coefficient to make the energy approximately size consistent, but at a loss of exactness for two-electrons and the variational principle.

Other attempts have been made to correct for the lack of extensivity, including Quadratic Configuration Interaction (QCI), which removes (in an *ad hoc* way [50]) certain powers of the amplitudes from the energy and amplitude equations. As a result, all the terms that scale incorrectly are cancelled and the energy becomes extensive. Coupled-cluster theory, that accounts for more (higher-order) terms while scaling the same as QCI, has been shown to be more reliable in general calculations and therefore the use of QCI has generally decreased. [51, 52]

Even though truncated approximations of CI are not extensive and FCI is computationally impractical, the CI method gives us a systematic method to approach an exact answer. The rest of the approximations considered in this chapter will be compared to FCI and how well they can be systematically extended to produce the FCI answer for limiting cases.

2.7 Coupled Electron Pair Approximations

A family of methods related to CI are the Coupled Electron Pair Approximation (CEPA), and the Coupled Pair Functional (CPF), both of which were developed to remedy the lack of extensivity in CISD. The main idea behind both is to include the effects of higher order terms into the energy expression, in an approximate way. [53]

CEPA begins with the CISD amplitude equations, but replaces E_{corr} with $\langle \Phi_0 | \hat{H} | \Phi_0 \rangle$, the unperturbed SCF energy, and removes all the terms quadratic in

c , [54]

$$c_{ab}^{ij} W = \langle \Phi_{ab}^{ij} | \hat{H} | \Phi_0 \rangle + c_{cd}^{kl} \langle \Phi_{ab}^{ij} | \hat{H} | \Phi_{cd}^{kl} \rangle, \quad (2.56)$$

$$W = \langle \Phi_0 | \hat{H} | \Phi_0 \rangle + \Delta W. \quad (2.57)$$

By introducing different energy shifts, ΔW , various CEPA(n) methods can be defined, where $n = \{0, 1, 2, 3, 4, 5\}$. For example, $\Delta W = 0$ in CEPA(0).

CEPA can restore extensivity to CISD, however, CEPA(n) are generally not exact for the two-electron case, no longer variational and are not invariant to a rotation of orbitals (apart from CEPA(1)) [54]; a heavy price to pay that shows the value of an extensive method. Traditionally, there has been no systematic hierarchy of CEPA(n) methods because they have been developed by experimenting with different variations on a theme, *i.e.* including different energy shifts to find which ones are best for certain test cases. As a result, “this introduces empiricism”. [55]

Coupled-cluster theory has been more popular as it captures dynamic correlation energy in a more rigorous way than CEPA. Nevertheless, in recent years there has been a renewed interest in rewriting a CEPA-*type* functional in terms of the variational principle (while maintaining the other problems). [56]

Another modification of the CISD energy functional, *via* a partial normalization denominator, gives an extensive method called the Coupled Pair Functional (CPF). [57] Divided by a so called ‘topological factor’ that has the effect of cancelling out localised terms in the CI numerator, CPF is an approximately extensive functional. CPF is related to the present work as interesting parallels can be drawn between it and Linked Pair Functional theory, which forms the basis of QVCCD theory.

2.8 Coupled-Cluster theory

So far, an approach to improving the SCF wavefunction was to find an operator that could reproduce the exact wavefunction within a given basis set,

$$|\psi\rangle = \hat{X} |\Phi_0\rangle. \quad (2.58)$$

For CI, \hat{X} was chosen as $(1 + \hat{C})$. Another parametrisation involves choosing \hat{X} to be an exponential operator, [58]

$$|\psi_{\text{CC}}\rangle = e^{\hat{T}} |\Phi_0\rangle = (1 + \hat{C}) |\Phi_0\rangle, \quad (2.59)$$

where \hat{T} is a sum of excitation operators,

$$\hat{T} = \sum_i^N \hat{T}_i. \quad (2.60)$$

This is often referred to as the *exponential ansatz* and defines the Coupled-Cluster (CC) wavefunction. [59]

To obtain an expression for the energy and amplitude coefficients, the CC wavefunction is inserted into the Schrödinger equation and pre-multiplied by $\langle \Phi | e^{-\hat{T}}$, where Φ is either the SCF reference state or the set of n -excited states:

$$\langle \Phi_0 | e^{-\hat{T}} \hat{H} e^{\hat{T}} | \Phi_0 \rangle = E_{\text{TCC}}, \quad (2.61)$$

$$\langle \Phi_i^a | e^{-\hat{T}} \hat{H} e^{\hat{T}} | \Phi_0 \rangle = 0, \quad (2.62)$$

$$\langle \Phi_{ij}^{ab} | e^{-\hat{T}} \hat{H} e^{\hat{T}} | \Phi_0 \rangle = 0. \quad (2.63)$$

Determining the energy and amplitude equations *via* projection onto a manifold of states has been termed Traditional Coupled-Cluster (TCC). [60]

It is worthwhile comparing how this parametrisation differs from CI, as both are equal to each other when the excitation operators are not truncated. To see the differences, the exponential operator for only single and double excitations, can be expanded as a Taylor series,

$$e^{(\hat{T}_1 + \hat{T}_2)} \Phi_0 = \left(1 + \hat{T}_1 + \frac{1}{2!} \hat{T}_1^2 + \hat{T}_2 + \frac{1}{2!} \hat{T}_2^2 + \hat{T}_2 \hat{T}_1 + \frac{1}{2!} \hat{T}_2 \hat{T}_1^2 \right) \Phi_0. \quad (2.64)$$

In this form it is easy to see that, unlike CI, this ansatz contains products of excitation operators called ‘disconnected clusters’. These effectively cancel out terms with an incorrect dependence on N and lead to an extensive method, even if \hat{T} is truncated. [10] They also account for the effects of higher excitations. For example, \hat{T}_2^2 represents the quadruple excitation of two sets of independently correlated electrons. In a general case, the \hat{T}_2^2 contributions will be more important than \hat{T}_4 . [7]

To generate a set of working equations, $e^{-\hat{T}} \hat{H} e^{\hat{T}}$ (also called the similarity transformed Hamiltonian) can be expanded as a series of nested commutators using

the Baker-Campbell-Hausdorff (BCH) expansion, [43]

$$e^{-\hat{T}}\hat{H}e^{\hat{T}} = \hat{H} + [\hat{H}, \hat{T}] + \frac{1}{2!}[[\hat{H}, \hat{T}], \hat{T}] + \frac{1}{3!}[[[\hat{H}, \hat{T}], \hat{T}], \hat{T}] + \frac{1}{4!}[[[[\hat{H}, \hat{T}], \hat{T}], \hat{T}], \hat{T}] + \dots \quad (2.65)$$

where,

$$[\hat{H}, \hat{T}] = \hat{H}\hat{T} - \hat{T}\hat{H}. \quad (2.66)$$

The Hamiltonian does not commute with the excitation operators, however, because it is at most a two-body operator, it will only interact with at most four excitation operators before it can commute and make the term equal to zero,

$$[[[[\hat{H}, \hat{T}], \hat{T}], \hat{T}], \hat{T}] = 0. \quad (2.67)$$

As a result, the BCH expansion terminates at the fourth nested commutator, leading to a finite expression that can be implemented exactly on a computer.

Unfortunately, using the similarity transformed Hamiltonian comes at a price: it is no longer Hermitian,

$$(e^{-\hat{T}}\hat{H}e^{\hat{T}})^\dagger = e^{-\hat{T}^\dagger}\hat{H}e^{\hat{T}^\dagger} \neq e^{-\hat{T}}\hat{H}e^{\hat{T}}. \quad (2.68)$$

This coupled with the fact that the energy and amplitude equations are determined by projection means that the TCC energy can not be variationally determined and therefore is no longer bounded by the exact energy. [10]

2.8.1 Variational Coupled-Cluster

The CC ansatz can be cast in a variational form, namely Variational Coupled-Cluster (VCC). Instead of using the similarity transformed Hamiltonian, the expectation value of a Hermitian operator is constructed and minimised with respect to the set of amplitudes,

$$E_{\text{VCC}} = \frac{\langle \Phi_0 | e^{\hat{T}^\dagger} \hat{H} e^{\hat{T}} | \Phi_0 \rangle}{\langle \Phi_0 | e^{\hat{T}^\dagger} e^{\hat{T}} | \Phi_0 \rangle}. \quad (2.69)$$

VCC is both rigorously extensive and variational, however a major problem arises with the use of the Hermitian Hamiltonian. The BCH expansion does not exist for such an operator and so it must be expanded as an infinite sum. As a

result, the method scales as a factorial of the number of particles in the system and therefore fails to be computationally practical.

Several methods have been developed that attempt to approximate VCC. Firstly, there is Unitary Coupled Cluster (UCC), which defines an anti-Hermitian operator,¹²

$$|\psi\rangle = e^{\hat{\sigma}} |\Phi_0\rangle, \quad (2.70)$$

$$\hat{\sigma} = \hat{T} - \hat{T}^\dagger. \quad (2.71)$$

This operator is then used to construct the energy expression,

$$E_{\text{UCC}} = \frac{\langle \Phi_0 | e^{-\hat{\sigma}} \hat{H} e^{\hat{\sigma}} | \Phi_0 \rangle}{\langle \Phi_0 | e^{-\hat{\sigma}} e^{\hat{\sigma}} | \Phi_0 \rangle}. \quad (2.72)$$

Eq. 2.72 still remains an infinite expression, though it converges quickly at low orders of T (the UCC equations correspond to the VCC equations for all orders of T [61]). However, higher order UCC terms quickly become very complex compared to the corresponding VCC terms, [62] leading to no immediate gain from the re-parametrisation.

In Extended Coupled-Cluster (ECC), a different state is projected onto the similarity transformed Hamiltonian, [63]

$$E_{\text{ECC}} = \frac{\langle \Phi_0 | e^{\hat{T}^\dagger} \hat{H} e^{\hat{T}} | \Phi_0 \rangle}{\langle \Phi_0 | e^{\hat{T}^\dagger} e^{\hat{T}} | \Phi_0 \rangle} = \langle \Phi_0 | e^{\hat{S}^\dagger} e^{-\hat{T}} \hat{H} e^{\hat{T}} | \Phi_0 \rangle. \quad (2.73)$$

where \hat{S} is an effective de-excitation operator. The energy is then varied with respect to both \hat{T} and \hat{S} to find a minimum. The de-excitation operator can be truncated at second order to give, [64]

$$E_{\text{QCC}} = \langle \Phi_0 | (1 + \hat{S}^\dagger + \frac{1}{2} \hat{S}^{\dagger 2}) e^{-\hat{T}} \hat{H} e^{\hat{T}} | \Phi_0 \rangle, \quad (2.74)$$

which defines Quadratic Coupled-Cluster (QCC).

All of these methods have been shown to perform better than TCC for systems with strong non-dynamic correlation (for systems without non-dynamic correlation effects, the results are effectively the same). The problem remains that these approximations to VCC are still computationally expensive.

¹²The exponential of an anti-Hermitian operator is always unitary. [43]

2.8.2 Triple excitations

CC theory provides a robust framework for capturing dynamic correlation, that remains extensive and, when truncated to single and double excitations (CCSD), is computationally practical for many chemical systems. However, to produce chemically accurate answers, the inclusion of triple excitations are often required. [65] A more detailed discussion of the triples corrections will be left for Chapter 3. The key points are briefly discussed here.

CCSD is equivalent to MP theory through to third-order. It can be corrected up to forth-order and thereby include some of the effects of triple excitations, while avoiding the full triples amplitude equations which are computationally expensive to evaluate. This can be further improved by including certain fifth-order terms. [66] The correction takes the form of a non-iterative step which is carried out with an optimised set of CCSD cluster amplitudes. This defines the (T) correction and the CCSD(T) method which scales as $O(o^3v^4)$. Its success in computational chemistry has lead to the often parroted (either ironically or not) phrase that CCSD(T) is *the gold standard* of computational chemistry. [67]

While CCSD(T) produces impressive results for many systems, the method breaks down when it encounters non-dynamic correlation due to its single reference nature. This is especially apparent in the cases of molecular dissociations where it produces unphysical results; instead of the energy approaching an asymptotic limit, it forms a maximum before falling towards negative infinity.

2.9 Second quantisation

So far, all equations have been presented within the *first quantisation* framework. At this stage, it is appropriate to introduce a new formulaism: *second quantisation*. Within this framework, concrete sets of working equations can be developed for computational implementation; as a result, it makes equations easier to evaluate at the expense of introducing new notation and concepts. It also provides a proof, by diagrammatic means, of whether a method can be extensive or not. A comprehensive review of second quantisation can be found in Ref. [43]

Second quantisation takes place in a linear vector space called the Fock space. SDs are represented by Occupation Number (ON) vectors and form a complete

basis:

$$|\mathbf{k}\rangle = |k_1, k_2, \dots, k_M\rangle, \quad (2.75)$$

$$k_p = \begin{cases} 1, & \text{if } \phi_p \text{ occupied} \\ 0, & \text{if } \phi_p \text{ unoccupied} \end{cases}. \quad (2.76)$$

Electronic states are represented by a string of annihilation and creation operators acting on an ON vector,

$$\text{creation} \begin{cases} \hat{a}_p^\dagger |k_1, k_2, \dots, 0_p, \dots, k_M\rangle = |k_1, k_2, \dots, 1_p, \dots, k_M\rangle \\ \hat{a}_p^\dagger |k_1, k_2, \dots, 1_p, \dots, k_M\rangle = 0 \end{cases}, \quad (2.77)$$

$$\text{annihilation} \begin{cases} \hat{a}_p |k_1, k_2, \dots, 1_p, \dots, k_M\rangle = |k_1, k_2, \dots, 0_p, \dots, k_M\rangle \\ \hat{a}_p |k_1, k_2, \dots, 0_p, \dots, k_M\rangle = 0 \end{cases}, \quad (2.78)$$

The \hat{T} excitation operators can be written in terms of these operators,

$$\hat{T}_1 = t_a^i \hat{a}_a^\dagger \hat{a}_i, \quad (2.79)$$

$$\hat{T}_2 = \frac{1}{4} t_{ab}^{ij} \hat{a}_a^\dagger \hat{a}_b^\dagger \hat{a}_i \hat{a}_j, \quad (2.80)$$

as well as the Hamiltonian

$$\hat{H} = h_{pq} a_p^\dagger a_q + \frac{1}{2} g_{pqrs} a_p^\dagger a_r^\dagger a_s a_q \quad (2.81)$$

$$= \hat{\mathcal{H}} + \hat{\mathcal{V}}. \quad (2.82)$$

Matrix elements of the Hamiltonian between different states can be reduced to evaluating strings of creation and annihilation operators, by using the concept of normal ordering and Wick's theorem. [68]

A string of operators are said to be in normal order when all the annihilation operators are permuted to the right of the creation operators,

$$\{\hat{a}_p \hat{a}_q^\dagger \hat{a}_r \hat{a}_s^\dagger\}_N |\mathbf{k}\rangle = \hat{a}_q^\dagger \hat{a}_s^\dagger \hat{a}_p \hat{a}_r |\mathbf{k}\rangle = 0, \quad (2.83)$$

thus producing a zero.

Wick's theorem states that a string of operators can be written as a normal ordered product and a sum of all normal ordered products with all possible contractions,

$$\hat{a}_p \hat{a}_q^\dagger \hat{a}_r \hat{a}_s^\dagger = \{\hat{a}_p \hat{a}_q^\dagger \hat{a}_r \hat{a}_s^\dagger\}_N + \{\hat{a}_p \hat{a}_q^\dagger \hat{a}_r \hat{a}_s^\dagger\}_N + \{\hat{a}_p \hat{a}_q^\dagger \hat{a}_r \hat{a}_s^\dagger\}_N \quad (2.84)$$

$$+ \{\hat{a}_p \hat{a}_q^\dagger \hat{a}_r \hat{a}_s^\dagger\}_N + \{\hat{a}_p \hat{a}_q^\dagger \hat{a}_r \hat{a}_s^\dagger\}_N, \quad (2.85)$$

where a non-vanishing contraction is defined as,

$$\hat{a}_p \hat{a}_q^\dagger \equiv \hat{a}_p \hat{a}_q^\dagger - \{\hat{a}_p \hat{a}_q^\dagger\}_N = \delta_{pq}. \quad (2.86)$$

When Wick's theorem is applied to matrix elements, the result is a sum of elements involving delta functions and normal ordered strings. The normal ordered parts vanish, leaving only the fully contracted elements. [10]

For example, the CCD energy expression is:

$$E_{\text{CCD}} = \langle \Phi_0 | e^{-\hat{T}_2} \hat{H} e^{\hat{T}_2} | \Phi_0 \rangle. \quad (2.87)$$

The Hamiltonian is at most a two-body operator, which means that only states that differ from each other by two spin orbitals can interact through the Hamiltonian (an analogue of the Slater-Condon rules [8]). This means that only one term from Eq. 2.87 will contribute:

$$\begin{aligned} E_{\text{CCD}} &= \langle \Phi_0 | (\hat{\mathcal{V}} \hat{T}_2) | \Phi_0 \rangle \\ &= \frac{1}{16} t_{ij}^{ab} \langle pq | rs \rangle \langle \Phi_0 | (a_p^\dagger a_q^\dagger a_s a_r) (a_a^\dagger a_b^\dagger a_j a_i) | \Phi_0 \rangle. \end{aligned} \quad (2.88)$$

Applying Wick's theorem to the string of operators leads to an expression involving only a sum of anti-symmetrised integrals and cluster amplitudes,

$$E_{\text{CCD}} = \frac{1}{4} t_{ij}^{ab} \langle ij | ab \rangle. \quad (2.89)$$

One of the most appealing features of working with second quantisation is the use of diagrams to generate algebraic expressions and eliminate the manipulation of annihilation and creation operators. Taking inspiration from the Feynmann diagrams of quantum electrodynamics, we can postulate a one to one correspondence to algebraic terms that appear in second quantisation and a set of specific diagrams. [10, 69]

Briefly, downwards-directed (hole) lines and upwards-directed (particle) lines correspond respectively to creation and annihilation operators. The excitation

operators can thus be drawn:

$$\hat{T}_1 = \begin{array}{c} \diagup \quad \diagdown \\ \downarrow \quad \uparrow \\ \text{---} \\ \uparrow \quad \downarrow \\ \diagdown \quad \diagup \end{array} \quad , \quad (2.90)$$

$$\hat{T}_2 = \begin{array}{c} \diagup \quad \diagdown \quad \diagup \quad \diagdown \\ \downarrow \quad \uparrow \quad \downarrow \quad \uparrow \\ \text{---} \\ \uparrow \quad \downarrow \quad \uparrow \quad \downarrow \\ \diagdown \quad \diagup \quad \diagdown \quad \diagup \end{array} \quad . \quad (2.91)$$

The one- and two-body operators of the Hamiltonian can be represented by a dashed horizontal interaction line. The task is to join up the excitation and interaction lines in every unique way, making sure that no lines are left unconnected. For example, there is only one possible diagram for Eq. 2.89, as only the two-body operator in the Hamiltonian can fully connect with the doubles excitation operator,

$$E_{\text{CCD}} = \begin{array}{c} \text{---} \\ \updownarrow \quad \updownarrow \\ \text{---} \end{array} \quad . \quad (2.92)$$

Using a series of rules (for a details see Ref. [10]), these *Goldstone anti-symmetrised spin orbital* diagrams, can be translated into algebraic expressions which can be implemented on a computer.

A result of deriving equations in this manner is the ability to invoke the *linked diagram theorem*. This states that if only linked diagrams are included in the energy expression, *i.e.* diagrams in which all the excitation operators are linked to the Hamiltonian (with no free hole or particle lines left unconnected), *then* the energy will be extensive. The CCD energy consists of only one linked diagram and so must be extensive. For a proof of this theorem, see Ref. [7]

Finally, another useful feature of the diagrammatic method is the ability to easily sum over a subset of diagrams to infinite order. For example, ‘ladder’ diagrams form a family, which can be obtained by inserting two-body operators into the middle of Eq. 2.92, thereby representing a growing ladder. [7] Instead

of evaluating these diagrams separately, to a finite order, a closed form equation can be derived which accounts for the complete sum. [69]. Such infinite order summations will become important in the discussion of QVCCD theory in Chapter 3.

2.10 Multireference methods

So far, only theories based around the single reference paradigm have been examined. This approximation is only valid when the wavefunction expansion is dominated by a single reference determinant. Barlett has defined this in terms of a set of electronic configurations, $|x\rangle$, the reference state, $|\Phi_0\rangle$, and the exact electronic state, $|\psi\rangle$: [11]

$$|\langle x|\psi\rangle| \leq \epsilon, \langle \Phi_0|\psi\rangle = 1. \quad (2.93)$$

A single reference wavefunction can be used when $\epsilon \in [0.1, 0.2]$.

Many systems in their equilibrium geometry and ground state can be adequately described by using a single SD. However, this approximation can break down when chemistry other than equilibrium geometries are investigated. For example, in transition states, when bonds stretch and break, radicals and metal-metal bonding. Quantitatively these problems can be expressed in terms of the above equation, when $\epsilon \geq 0.2$.

As a result, CCSD is no longer able to approximate the different configurations with excitations. To capture these effects, it is necessary to use CCSDT, CCSDTQ, CCSDTQP, *etc.* But these scale as $O(N^8)$, $O(N^{10})$ and $O(N^{12})$, so for practical purposes, these cannot be used.

2.10.1 MCSCF and CASSCF

The multireference analogue of the SCF method is Multi-Configurational Self-Consistent Field (MCSCF). The wavefunction is expanded into explicitly chosen states,

$$|\psi_{MCSCF}\rangle = C_I |\Phi_I\rangle, \quad (2.94)$$

where I labels the different electronic (configuration) states. The energy is minimised with respect to the orbitals and the mixing coefficients. [12, 70]

The choice of the configuration basis is left to the user and their ‘chemical intuition’. If such intuition is faulty or incomplete, the wrong configurations can easily be chosen.

The Complete Active Space (CASSCF) method can make the choice of the states more systematic. [71] The orbitals are partitioned into two subspaces: an active and an inactive (or closed) set of orbitals. The inactive orbitals remain doubly occupied in all configurations, while the active orbitals are free to change their occupation number. FCI is applied to all the active electrons and orbitals to generate a set of excited SDs and hence the configurational space.

The number of configurations generated by CASSCF scales factorially. As a result, calculations tend not to use more than 18 electrons arranged in 18 active orbitals due to restrictions of computational resources. [72] The number of states can be reduced by subdividing the active space again into three more subspaces (Restricted Active Space, RASSCF), where a limit is placed on the number of holes and electrons in two of the subspaces (RAS1 and RAS3), while no limits are placed on the occupation numbers in the remaining subspace (RAS2). [25]

2.10.2 MRCI, MRCC and CASPT2

CASSCF and RASSCF both suffer from the slow convergence of the dynamic correlation energy. Even for large active spaces, dynamic effects are not captured completely. [12] To account for this, combinations of the MCSCF procedure with MP2, CI and CC have been proposed.

Conceptually, the most straight forward ways to do this is to perform CISD on each configuration in the MR expansion (MRCI) [73, 74] or use second-order perturbation theory to evaluate the CI expansion coefficients (CASPT2). [75] Both these approaches give the wavefunction sufficient flexibility to model many difficult cases, however MRCI suffers from the usual non-extensivity of CISD (Davidson’s correction can again be applied to make the method approximately extensive), while the CASPT2 energy is no longer bounded from above. There are also added issues in choosing \hat{H}_0 for CASPT2; unlike MPn, the Fock operator can’t simply be used. [76, 77]

Multireference Coupled-Cluster (MRCC) theory is a large topic in of itself, where various different methods have attempted to combine the linear parametri-

sation of the MCSCF wavefunction with the exponential parametrisation of CC theory. Because of the large scope and depth of the subject, the interested reader is pointed towards this review article. [11] To date, many of the attempts contain problems like complexity of equations (icMRCC), or suffer from a lack of spin adaption (state-universal MRCC). So far, no particular method has come to dominate the rest, [78] with all of them having deficiencies in some areas.

The methods presented above seem like the ideal way to capture non-dynamic (and even dynamic) correlation. However, there are two major caveats: firstly, it quickly becomes very expensive to run these methods on systems with many configurations, secondly, none are black box methods and in a lot of cases it is hard to choose the active space for a particular region of the potential energy surface. As a result, these methods are not used by many people outside the computational chemistry community and will possibly never become the standard tool of experimental chemists.

This thesis follows on from the work of Robinson, Cooper and Knowles, in that it is postulated that both dynamic and non-dynamic correlation effects can be captured using a single reference method, instead of a multireference one. [13,79]

2.11 Contemporary single reference methods

Capturing dynamic and non-dynamic correlation with a single reference state has been the motivation behind the development of many computational methods. A quick review of more recent methods will be presented here.

2.11.1 Spin-flip

In certain cases, non-dynamic correlation effects are negligible in triplet ($S=+1$, $M_s=+1, 0, -1$) states compared to singlet ($S=0$) states. This suggests that the triplet state can be modelled well by just using a single reference determinant. In essence, this is what the Spin-Flip (SF) method attempts to do; it constructs a reference triplet state and generates an expansion of excited states by ‘flipping’ the spin of one electron and thereby generating the original singlet state of interest, [80]

$$|\Phi_{M_s=0}^s\rangle = \hat{R}_{M_s=-1} |\Phi_{M_s=+1}^t\rangle. \quad (2.95)$$

This method is analogous to the Equation Of Motion (EOM) approach in which the final state is expanded in a basis that conserves the total number of electrons, but not the number of α or β electrons. [81]

A hierarchy of SF methods can be described by using different reference states. The simplest uses the SCF wavefunction and diagonalises the Hamiltonian in the space of all single excitations (similar to CIS, but where only α to β excitations are allowed). CIS, CCSD and OO-CCD states can all be used without any increase in computational expense. All of these methods are size extensive up to the limit of including one single non-spin-flip excitation in the reference state (SF-CCSDT would not be size extensive, but 2SF-CIST would be)

The SF methodology has also been extended to the excitation of pairs of electrons (2SF). Instead, a quintet ($M_s=2$) reference state is chosen. 2SF Offers improvement over CCSD/CCSDT for double bond breaking, but little known about its performance. [82] In theory it is possible to extend this to triples etc, but to date, this has not been achieved.

The SF method has produced accurate energies for diradical separation states (due to single reference nature of the triplet states), while EOM-SF-CCSD has been shown to perform well when modelling the breaking of C-H and C-C bonds.

The main problem with SF is that it is restrictive of the systems that can be investigated with confidence. Single SF is restricted to systems where the non-dynamical correlation comes from small HOMO-LUMO gap (quasi-degenerate orbitals), *i.e.* single bond breaking, diradicals, triradicals. 2SF can model double bond breaking and tetraradicals, but is again limited in what systems it can examine with confidence.

The SF postulate that the triplet state is inherently single reference is not generally true. When this is the case, SF cannot hope to capture non-dynamic correlation any better than the TCC methods. In this respect, it has been named a *few-reference*, instead of multi-reference, method. [82]

2.11.2 Term excluding methods

It has been shown that the larger cluster effects (*eg.* CCSDTQ) are needed to correctly describe certain potential energy surfaces. [83] Apart from adding more terms that deal with the correlations of larger numbers of electrons, the higher

cluster operators may cancel out lower order terms in CCD/CCSD.

One of the first attempts at excluding terms in the cluster expansion was carried out by Paldus. [84] Since then, research continues into which terms in the amplitude equations can be removed and thereby simulate the effect of higher excitations and improve upon CCSD. Terms that these class of methods exclude usually contribute a negative energy in dissociation limits.

nCC

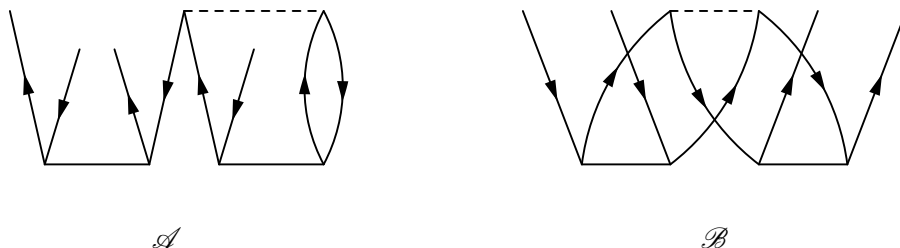
What are the minimal amount of terms that need to be retained in CCSD, CCSDT and CCSDTQ, that still give answers that are exact for 2, 3 and 4 electrons? This question defines the n Coupled-Cluster (nCC, where $n=\{2,3,4\}$) hierarchy of methods. [85]

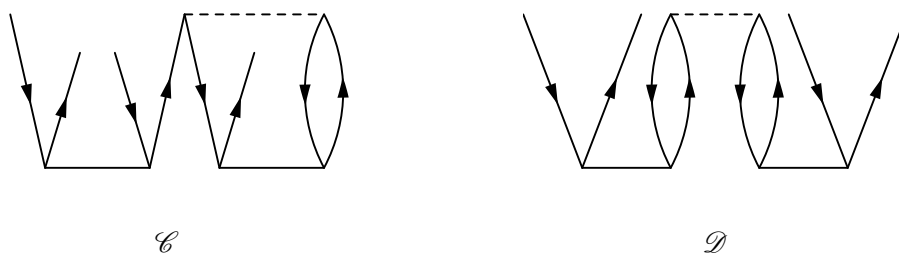
Exclusion principle violating (EPV) terms in the CC equations can be separated into two categories. [7] One set contains all the diagrams where one or two commonly labelled hole lines are crossed and are called hole-hole conjoint terms (HCJ). The second group consisted of the same diagrams as the HCJs, but the common label is a particle and also ‘disjoint’ terms where no common labelling is possible. These are collected together and called the non-HCJ. Retaining only the HCJ terms to n -order leads to exactness for n -electrons and a reduction of the number of terms that are evaluated compared to CCSD.

nCC is orbitally invariant and extensive, however it has been shown that it still reproduces the unphysical CCSD maximum when dissociating N_2 . [83]

pCCSD

The Parametrised Coupled-Cluster Singles Doubles (pCCSD) method introduces a bivariate parametrisation of the quadratic terms into the CCSD amplitude equations. Certain relationships exist between these quadratic terms,





and thus can be factorised and multiplied by two varying parameters, α and β , [55]

$$\mathcal{A} + \mathcal{B} + \mathcal{C} + \mathcal{D} = \mathcal{A}/2 + \alpha(\mathcal{A}/2 + \mathcal{B}) + \beta(\mathcal{C} + \mathcal{D}). \quad (2.96)$$

This defines the pCCSD(α, β) method, which for any values of α and β , retains all the desirable properties of CCSD (exactness for two electrons, extensive, orbitally invariant). For $\alpha = \beta = 1$, the CCSD equations are recovered. The questions are then posed: Is the CCSD choice of α/β parameters the optimal one? Is it possible to obtain answers in a systematic way by varying these parameters? For example, when $\alpha = 1$ and $\beta = 0$ the method is identical to 2CC.

pCCSD has been shown to decrease energies and equilibrium geometries errors compared with CCSD, when measured against CCSD(T) and experiment. For example, it has been shown to produce improved results when α ranges from $-3/2$ to -1 and β from 1 to $3/2$.

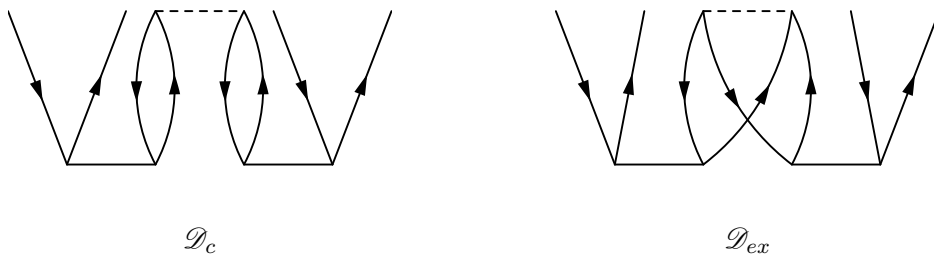
A problem immediately presents itself: what values should α and β take?. It has been shown that certain values produce better results for some cases, but this does not mean they will be the best choice for different cases; pCCSD is no longer an *ab initio* method in the strictest sense. In some cases (when $\alpha = \beta = 0$) pCCSD will have a reduced scaling prefactor compared to CCSD (due to the exclusion of terms that need to be evaluated), but as the authors admit, this does not produce the best results. [55] The only way to determine the best α and β values is to try many calculations with different values and then to compare the results to a more accurate multireference calculation, thereby defeating the point of using pCCSD in the first place!

Distinguished Cluster approximation

Inspired by a questioning of particle indistinguishability, the Distinguished Cluster (DC) approximation begins with an examination of exchange terms in the CCSD

equations. [86] The operators in second quantisation obey the anti-symmetric principle, this means (for FCI) that all exchange processes between molecular fragments will be included in the energy expression and there will be a mutual cancellation between them. In a truncated formalism, these terms don't cancel. DC postulates that this may be the reason for unphysical results of CCSD.

Starting with the same quadratic terms from pCCSD, the \mathcal{D} term is separated into a Coulomb (\mathcal{D}_c) and an exchange (\mathcal{D}_{ex}) part. These diagrams are no longer anti-symmetrised Goldstone diagrams; here the two-body interaction line represents the individual Coulomb and exchange integrals.



The DC equations are then parametrised with two parameters and set to 0, which has the effect of removing both the \mathcal{D}_{ex} and \mathcal{B} exchange terms while leaving the theory exact for two electrons, [83]

$$\begin{aligned} \mathcal{A} + \mathcal{B} + \mathcal{C} + \mathcal{D} &= \mathcal{A} + \mathcal{B} + \mathcal{C} + \mathcal{D}_c + \mathcal{D}_{ex} \\ &= \mathcal{A}/2 + \gamma(\mathcal{A}/2 + \mathcal{B}) + \delta(\mathcal{C}/2 + \mathcal{D}_{ex}) + \mathcal{C}/2 + \mathcal{D}_c. \end{aligned} \quad (2.97)$$

DCSD can produce qualitatively correct potential energy curves (PECs) for specific molecular dissociations (N_2 , CO). [86] More surprisingly, when compared to CCSD, it produces improved bond lengths and frequencies around the equilibrium geometry. However when the perturbative triples are added, DCSD(T) fails to produce even a qualitatively correct PEC for N_2 dissociation and H_2O bond angle stretch. [83, 87]

As a method, DC can produce impressive results, especially for the N_2 dissociation. Nevertheless, DCSD(T) does not reliably produce accurate results for multireference systems. The fact that DCSD generally produces better results than CCSD/CCSD(T) has spurred on several interesting analyses using physics not generally found in theoretical chemistry papers. [86, 87] In this respect, the DC approximation has great value.

2.12 A remark on density based methods

This thesis is focused on finding approximate solutions to the many-body wavefunction and thereby determining molecular properties from this. In this respect, all the methods discussed so far can be classed as *wavefunction* based methods. Nevertheless, there are other ways to determine molecular properties without constructing a wavefunction. The Hohenberg-Kohn theorem states that the ground state properties of a many-electron system can be determined uniquely by an electron density. This problem can be related to minimising an energy functional with respect to a density that depends on only three spatial (ignoring spin) coordinates, [88]

$$\begin{aligned} E[n] &= \langle \Phi[n] | \hat{H} | \Phi[n] \rangle \\ &= F[n] + V[n], \end{aligned} \tag{2.98}$$

where the energy and wavefunction have been written in terms of a functional that depends on the electron density, n . $F[n]$ is called a universal functional that describes the kinetic and electron-electron interactions, while $V[n]$ is an external potential that depends on the system (for example the nuclei of a molecule). If both these functionals are known, then the energy is uniquely and exactly determined.

$F[n]$ is currently unknown and so approximations must be introduced. A popular approach are the Kohn-Sham (KS) equations, that share similarities with the SCF procedure. [89] Here, $F[n]$ is replaced by three functionals:

$$F[n] = t[n] + v_H[n] + v_{xc}[n], \tag{2.99}$$

where $t[n]$ and $v_H[n]$ represent the kinetic and potential energy of a set of non-interacting electrons and $v_{xc}[n]$ is an unknown functional that describes the Coulomb and exchange correlation interactions.

The KS equations are formally exact, nevertheless $v_{xc}[n]$ is not known and must be given an approximate form. To date, there are hundreds of different exchange-correlation functionals that are designed for specific and general chemical situations. The interested reader is directed to Ref. [88] for more details.

The KS procedure posses many beneficial properties. For example, HF theory, describes the exchange interaction exactly, but completely ignores dynamic-

correlation. KS theory, captures both quantities, albeit in an approximate manner, and sometimes can perform better than HF. [90] The procedure also scales as $O(N^4)$ and is far cheaper to run than the post-HF methods.

There are several drawbacks to KS theory. Firstly, the approximate description of the exchange-correlation effects does not produce chemically accurate answers for general systems. One functional may be designed to perform well for certain systems, however a general functional that can describe a wide range of chemical phenomena to within chemical accuracy currently does not exist. [91]

Secondly, there exists no clear hierarchy of functionals that can be used to improve results. Many different functionals will produce many different answers and there is usually no way to gauge which functional produces the best answer. An approximate hierarchy, exaggeratedly called ‘Jacobs ladder’, has been developed where different families of approximations represent different rungs on a ladder. [92] This addresses the problem of a hierarchy between, but not amongst families.

Lastly, and importantly for the current work, KS theory offers no simple and consistent way of treating non-dynamic and dynamic correlation. [93] Describing both correlation effects with the use of a single determinant can not be achieved in a reliable way and so research is mainly focused around integrating multireference wavefunction based methods into DFT. [94] These methods lose the simplicity of KS theory and increase the computational cost.

Chapter 3

Quasi-Variational Coupled-Cluster: Theory

3.1 The Linked Pair Functional

This project is focused on developing and improving the QVCCD method and applying it to chemical systems. With this in mind, it is worth examining the precursor to QVCCD, Linked Pair Functional Doubles (LPFD), as there are many methodological similarities. [79, 95] Both methods form an approximation to VCCD, correct up to third-order, which is postulated will qualitatively match the VCCD energy. This is achieved by combining a subset of linked diagrams from VCCD into a modified CEPA(0) energy functional. As a result, the only difference between the two is the definition of a modified excitation operator: ${}_q\hat{T}_2$.

This section will introduce LPFD and discuss the benefits and limitations of the method. Because of the similarity, much of the following analysis can be applied to QVCCD.

3.1.1 Approximating VCCD

As discussed in the previous chapter, VCC has been shown to produce accurate results for systems with large dynamic and non-dynamic effects. [64] Nonetheless, it does not utilize a similarity transformed Hamiltonian, so the BCH expansion cannot be used to produce a finite expression for the energy functional. [43] It is postulated that if a suitable approximation can be made to VCC, then a

computationally simpler single reference formalism can be developed that could capture non-dynamic correlation effects.

A first attempt at the problem could be to truncate the excitation operator to only double excitations (VCCD). The energy functional can be written as:

$$E_{\text{VCCD}} = \frac{\langle \Phi_0 | e^{\hat{T}_2^\dagger} \hat{H} e^{\hat{T}_2} | \Phi_0 \rangle}{\langle \Phi_0 | e^{\hat{T}_2^\dagger} e^{\hat{T}_2} | \Phi_0 \rangle} = \langle \Phi_0 | e^{\hat{T}_2^\dagger} \hat{H} e^{\hat{T}_2} | \Phi_0 \rangle_L \equiv \langle e^{\hat{T}_2^\dagger} \hat{H} e^{\hat{T}_2} \rangle_L, \quad (3.1)$$

where shorthand notation for matrix elements between two reference states has been introduced. Here the subscript L stands for *Linked*, as the denominator exactly cancels with the unlinked terms in the numerator and so can be omitted.

The problem still remains; the exponential operator must be expanded as an infinite series. The next step could be to remove the exponential altogether and replace it with a linear operator, $(1 + \hat{T}_2)$.

$$E_{\text{CEPA}(0)} = \langle (1 + \hat{T}_2)^\dagger \hat{H} (1 + \hat{T}_2) \rangle_L. \quad (3.2)$$

This is simply the CEPA(0) approximation. [96]

CEPA(0) only contains linked diagrams, like VCCD, and so is strictly extensive. However, it is not exact for two electrons. Even if the operator was increased to include quadratic terms (\hat{T}_2^2), the method would still not be exact.

Using the Maclaurin series for an exponential, the VCCD and CEPA(0) functionals can be expanded and compared,

$$\begin{aligned} E_{\text{VCCD}} &= \langle (1 + \hat{T}_2^\dagger + \frac{(\hat{T}_2^\dagger)^2}{2!} + \dots) \hat{H} (1 + \hat{T}_2 + \frac{\hat{T}_2^2}{2!} + \dots) \rangle_L \\ &= \langle (\hat{H} + 2 \hat{H} \hat{T}_2 + \hat{T}_2^\dagger \hat{H} \hat{T}_2 + \hat{T}_2^\dagger \hat{H} \frac{\hat{T}_2^2}{2!} + \frac{(\hat{T}_2^\dagger)^2}{2!} \hat{H} \frac{\hat{T}_2^2}{2!} + \dots) \rangle_L, \\ E_{\text{CEPA}(0)} &= \langle (\hat{H} + 2 \hat{H} \hat{T}_2 + \hat{T}_2^\dagger \hat{H} \hat{T}_2) \rangle_L. \end{aligned} \quad (3.3)$$

By inspection, it appears that $\langle \hat{T}_2^\dagger \hat{H} \frac{\hat{T}_2^2}{2!} \rangle_L$ is the lowest order term that occurs in the VCCD energy, but not in CEPA(0). If this term is inserted into the CEPA(0) functional, a cubic order approximation ($O(t^3)$) of VCCD could be formed.

This $O(t^3)$ term can be evaluated using diagrammatic techniques which were introduced in Chapter 2. As a result, four linked diagrams can be constructed

and translated into a sum of four algebraic terms,

$$\begin{aligned}
\langle \hat{T}_2^\dagger \hat{H} \frac{\hat{T}_2^2}{2!} \rangle_L &= \text{Diagram 1} + \text{Diagram 2} \\
&+ \text{Diagram 3} + \text{Diagram 4} \\
&= \frac{1}{4} \langle ij || ab \rangle t_{ij}^{db} t_{cd}^{kl} t_{kl}^{ca} + \frac{1}{4} \langle ij || ab \rangle t_{lj}^{ab} t_{cd}^{kl} t_{ki}^{cd} \\
&+ \frac{1}{16} \langle ij || ab \rangle t_{kl}^{ab} t_{cd}^{kl} t_{ij}^{cd} + \frac{1}{2} \langle ij || ab \rangle t_{lj}^{db} t_{cd}^{kl} t_{ki}^{ca} \\
&= \mathcal{A} + \mathcal{B} + \mathcal{C} + \mathcal{D}. \tag{3.4}
\end{aligned}$$

The terms have been labelled by Latin letters as they appear in expression.

For convenience, these four terms can be written with respect to the one- and two-particle density matrices,

$$\begin{aligned}
\mathcal{A} + \mathcal{B} + \mathcal{C} + \mathcal{D} &= \frac{1}{2} \langle ij || ab \rangle t_{ij}^{db} \mathcal{A} \eta_d^a + \frac{1}{2} \langle ij || ab \rangle t_{lj}^{ab} \mathcal{B} \eta_i^l \\
&+ \frac{1}{8} \langle ij || ab \rangle t_{kl}^{ab} \mathcal{C} \eta_{ij}^{kl} + \frac{1}{2} \langle ij || ab \rangle t_{lj}^{db} \mathcal{D} \eta_{al}^{id}, \tag{3.5}
\end{aligned}$$

where,

$$\begin{aligned}
\mathcal{A} \eta_d^a &= \langle \hat{T}^\dagger a_a a_d^\dagger \hat{T} \rangle = \frac{1}{2} t_{cd}^{kl} t_{ki}^{ca}, \\
\mathcal{B} \eta_i^l &= \langle \hat{T}^\dagger a_i a_l^\dagger \hat{T} \rangle = \frac{1}{2} t_{cd}^{kl} t_{ki}^{cd}, \\
\mathcal{C} \eta_{kl}^{ij} &= \langle \hat{T}^\dagger a_k a_l a_j^\dagger a_i^\dagger \hat{T} \rangle = \frac{1}{2} t_{cd}^{kl} t_{ij}^{cd}, \\
\mathcal{D} \eta_{al}^{id} &= \langle \hat{T}^\dagger a_l a_d^\dagger a_a a_i^\dagger \hat{T} \rangle = t_{cd}^{kl} t_{ki}^{ca},
\end{aligned} \tag{3.6}$$

and each density matrix has been pre-labelled by the term it is responsible for generating.

For the limiting case of two electrons, a relationship between these terms becomes apparent,

$$\begin{aligned}
\mathcal{A} + \mathcal{B} + \mathcal{C} + \mathcal{D} &= \langle \tilde{e}\tilde{e} || ab \rangle (t_{\tilde{e}\tilde{e}}^{db} t_{cd}^{\tilde{e}\tilde{e}} t_{\tilde{e}\tilde{e}}^{ca} - t_{\tilde{e}\tilde{e}}^{ab} t_{cd}^{\tilde{e}\tilde{e}} t_{\tilde{e}\tilde{e}}^{ca}) \\
&+ \frac{1}{2} t_{\tilde{e}\tilde{e}}^{ab} t_{cd}^{\tilde{e}\tilde{e}} t_{\tilde{e}\tilde{e}}^{cd} - t_{\tilde{e}\tilde{e}}^{db} t_{cd}^{\tilde{e}\tilde{e}} t_{\tilde{e}\tilde{e}}^{ca}) \\
&= \mathcal{B} + \frac{1}{2} \mathcal{C}, \tag{3.7}
\end{aligned}$$

$$\mathcal{A} + \mathcal{D} = 0, \tag{3.8}$$

$$\mathcal{B} + 2\mathcal{C} = 0. \tag{3.9}$$

Here, the $m_s = +\frac{1}{2}$ and $m_s = -\frac{1}{2}$ electrons are labelled \tilde{e} and \bar{e} respectively. The Einstein summation convention is no longer implied over these indices.

The complete cubic term can therefore be parametrised with the \mathcal{B} and \mathcal{C} terms, yet still remain exact for two electrons,

$$\mathcal{A} + \mathcal{B} + \mathcal{C} + \mathcal{D} = \frac{1}{2}(1 - \lambda)\mathcal{B} - \lambda\mathcal{C}. \quad (3.10)$$

LPFD(λ) includes a subset of these cubic terms into a modified CEPA(0) functional, thereby producing a third-order approximation to VCCD.

3.1.2 Mathematics of LPDF

The $O(t^3)$ terms can't simply be added onto the energy functional, as this would not be exact for two electrons. Instead, the cluster amplitudes in CEPA(0) are modified *via* a matrix transformation that produces one or two of the terms in Eq. 3.10 according to the parametrisation. [95] This transformation takes the following form:

$$U_{kl}^{ij} = \delta_{kl}^{ij} + \Delta_{kl}^{ij}, \quad (3.11)$$

$$\Delta_{kl}^{ij} = \lambda\eta_{kl}^{ij} + \frac{1}{2}(1 - \lambda)(1 - \hat{\tau}_{ij})(1 - \hat{\tau}_{kl})\delta_k^i\eta_l^j, \quad (3.12)$$

where $\hat{\tau}_{pq}$ are permutational operators that swap the indices p and q .

Powers of this transformation act on the cluster amplitudes to produce a set of *transformed* cluster amplitudes, which are pre-labelled by the transformation power,¹

$$q^t_{ab}{}^{ij} = \frac{1}{2}(U^{-\frac{q}{2}})_{kl}^{ij} t_{ab}^{kl}. \quad (3.13)$$

This transformation also obeys the fermionic anti-symmetry requirements of the original cluster amplitudes,

$$q^t_{ab}{}^{ij} = -q^t_{ab}{}^{ji} = q^t_{ba}{}^{ji} = -q^t_{ba}{}^{ij}. \quad (3.14)$$

¹A power of this rank-4 tensor is defined in terms of a two dimensional matrix, where $i > j$ and $k > l$. This convention will be used throughout this thesis.

Eq. 3.13 defines the *transformed* excitation operator,

$$\hat{T}_2 = \frac{1}{4} t_{ab}^{ij} a_a^\dagger a_b^\dagger a_j a_i$$

$$= \text{Diagram}, \quad (3.15)$$

where the double line has been introduced to differentiate it from the standard excitation operator. This can be inserted into the CEPA(0) energy expression to produce the LPFD(λ) energy,

$$E_{\text{LPDF}(\lambda)} = \langle (1 + {}_q\hat{T}_2)^\dagger \hat{H} (1 + {}_q\hat{T}_2) \rangle_L$$

$$= \langle \hat{H} \rangle + 2\langle \hat{H} {}_2\hat{T}_2 \rangle + \langle {}_1\hat{T}_2^\dagger (\hat{H} - \langle \hat{H} \rangle) {}_1\hat{T}_2 \rangle. \quad (3.16)$$

The effect of using a power of the transformation matrix is to generate the subset of cubic terms, but to infinite order. This concept can be explored by constructing a binomial expansion of the powered U matrix:

$$\langle \hat{H} {}_2\hat{T}_2 \rangle = \text{Diagram}$$

$$= \frac{1}{4} \langle ij || ab \rangle {}_2t_{ij}^{ab}$$

$$= \frac{1}{8} \langle ij || ab \rangle (U^{-\frac{2}{2}})_{ij}^{kl} t_{kl}^{ab}$$

$$= \frac{1}{8} \langle ij || ab \rangle \left(t_{ij}^{ab} + \sum_{m=1}^{\infty} \binom{-1}{m} (\Delta^m)_{ij}^{kl} t_{kl}^{ab} \right) \quad (3.17)$$

This is simply a geometric series of VCCD terms based on the cubic terms in Δ . The effect of using the power of a \mathbf{U}^{-1} matrix is to sum this series to infinity and thereby capture the effects of higher odd order terms than just $O(t^3)$. For example the next term in the series would produce, $\langle ij || ab \rangle (\eta^2)_{ij}^{kl} t_{kl}^{ab}$, which is proportional to $O(t^5)$. A similar analysis can be carried out with $\mathbf{U}^{-\frac{1}{2}}$, which generates all the even ordered terms in the series. As a result of using the powered matrices, a closed form expression of an infinite sum can be constructed.

To show how LPDF(λ) is an approximation to VCCD, the definition of Δ can

be inserted into the first terms of the geometric series,

$$\begin{aligned}
\frac{1}{8} \langle ij || ab \rangle (t_{ij}^{ab} - \Delta_{ij}^{kl} t_{kl}^{ab}) &= \frac{1}{8} \langle ij || ab \rangle t_{ij}^{ab} \\
&\quad - \frac{1}{16} (1 - \lambda) \langle ij || ab \rangle (\delta_i^k \eta_j^l - \delta_j^k \eta_i^l - \delta_i^l \eta_j^k + \delta_j^l \eta_i^k) t_{kl}^{ab} \\
&\quad - \frac{1}{8} \lambda \langle ij || ab \rangle \eta_{ij}^{kl} t_{kl}^{ab} \\
&= \frac{1}{8} \langle ij || ab \rangle T_{ij}^{ab} \\
&\quad - \frac{1}{4} (1 - \lambda) \langle ij || ab \rangle \eta_j^k t_{ik}^{ab} - \frac{1}{8} \lambda \langle ij || ab \rangle \eta_{ij}^{kl} t_{kl}^{ab} \\
&= \frac{1}{8} \text{[Diagram: Two parallel vertical ovals with arrows pointing down, connected by a dashed horizontal line at the top and a solid horizontal line at the bottom.]} \\
&\quad + \frac{1}{4} (1 - \lambda) \text{[Diagram: A sequence of three vertical ovals with arrows pointing down, connected by curved lines. The first and second ovals are connected by a solid line, and the second and third by a dashed line.]} - \frac{1}{8} \lambda \text{[Diagram: A sequence of three vertical ovals with arrows pointing down, connected by curved lines. The first and second ovals are connected by a solid line, and the second and third by a dashed line.]} \\
&= O(t) + O(t^3). \tag{3.18}
\end{aligned}$$

This reproduces the leading contribution to VCCD of order $O(t)$, but also the two $O(t^3)$ terms that remain in the limit of two electrons. The $O(t^2)$ terms are recovered by the $\mathbf{U}^{-\frac{1}{2}}$ transformation matrix.

3.1.3 Comparisons to CID

To further understand the LPFD(λ) methodology and provide another perspective of its rationale, comparisons can be made with the CID energy functional, which shares similarities with CEPA(0) and hence the LPFD(λ) energy.

The CID energy can be expanded and partitioned into reference and correlation energy contributions:

$$\begin{aligned}
E_{\text{CID}} = E_{\text{corr}} + E_0 &= \frac{\langle \hat{H} \rangle + 2\langle \hat{H} \hat{T}_2 \rangle + \langle \hat{T}_2^\dagger \hat{H} \hat{T}_2 \rangle}{1 + \langle \hat{T}_2^\dagger \hat{T}_2 \rangle} \\
&= \frac{(1 + \langle \hat{T}_2^\dagger \hat{T}_2 \rangle) E_0 + \langle \hat{H} - E_0 \rangle + 2\langle (\hat{H} - E_0) \hat{T}_2 \rangle + \langle \hat{T}_2^\dagger (\hat{H} - E_0) \hat{T}_2 \rangle}{1 + \langle \hat{T}_2^\dagger \hat{T}_2 \rangle},
\end{aligned}$$

if $E_0 = \langle \hat{H} \rangle$,

$$E_{\text{CID}} = \langle \hat{H} \rangle + \frac{2\langle \hat{H} \hat{T}_2 \rangle + \langle \hat{T}_2^\dagger (\hat{H} - \langle \hat{H} \rangle) \hat{T}_2 \rangle}{1 + \langle \hat{T}_2^\dagger \hat{T}_2 \rangle}. \tag{3.19}$$

A similar procedure can be carried out for the CEPA(0) energy:

$$E_{\text{CEPA}(0)} = \langle \hat{H} \rangle + 2\langle \hat{H} \hat{T}_2 \rangle + \langle \hat{T}_2^\dagger \hat{H} \hat{T}_2 \rangle_L. \quad (3.20)$$

All the terms in the above equation contain only linked diagrams. The subscript L can be dropped from the last term if the reference state is explicitly removed from it, as this is the only generator of unlinked diagrams in this term:

$$\begin{aligned} \langle \hat{T}_2^\dagger \hat{H} \hat{T}_2 \rangle &= \langle \hat{T}_2^\dagger \hat{H} \hat{T}_2 \rangle_L + \langle \hat{H} \rangle \langle \hat{T}_2^\dagger \hat{T}_2 \rangle, \\ \langle \hat{T}_2^\dagger (\hat{H} - \langle \hat{H} \rangle) \hat{T}_2 \rangle &= \langle \hat{T}_2^\dagger \hat{H} \hat{T}_2 \rangle_L + (\langle \hat{H} \rangle - \langle \hat{H} \rangle) \langle \hat{T}_2^\dagger \hat{T}_2 \rangle \\ &= \langle \hat{T}_2^\dagger \hat{H} \hat{T}_2 \rangle_L \\ &= \text{[Diagram 1]} + \text{[Diagram 2]} \\ &+ \text{[Diagram 3]} + \text{[Diagram 4]} \\ &+ \text{[Diagram 5]}, \end{aligned} \quad (3.21)$$

$$E_{\text{CEPA}(0)} = \langle \hat{H} \rangle + 2\langle \hat{H} \hat{T}_2 \rangle + \langle \hat{T}_2^\dagger (\hat{H} - \langle \hat{H} \rangle) \hat{T}_2 \rangle. \quad (3.22)$$

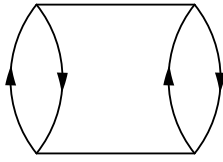
The dashed line capped with a dot represent the interactions with the one-body part of the Hamiltonian.

It immediately becomes apparent by inspection that Eq. 3.19 and Eq. 3.22 are very similar; the only difference being the CID correlation energy is divided by $1 + \langle \hat{T}_2^\dagger \hat{T}_2 \rangle$. If CEPA(0) only contains linked terms, then the same must be true for the CID numerator. This means that the unlinked terms, and therefore, the lack of extensivity comes from the CID denominator. This can be shown by using the binomial theorem to expand the denominator,

$$E_{\text{CID}} = \langle \hat{H} \rangle + (2\langle \hat{H} \hat{T}_2 \rangle + \langle \hat{T}_2^\dagger (\hat{H} - \langle \hat{H} \rangle) \hat{T}_2 \rangle) (1 + \langle \hat{T}_2^\dagger \hat{T}_2 \rangle + \langle \hat{T}_2^\dagger \hat{T}_2 \rangle^2 + \dots). \quad (3.23)$$

Only the first term in the right most parenthesis will generate linked terms, the

rest will introduce terms like,

$$\langle \hat{T}_2^\dagger \hat{T}_2 \rangle = \frac{1}{4} t_{ab}^{ij} t_{ij}^{ab} = \begin{array}{c} \text{---} \\ \text{---} \\ \text{---} \\ \text{---} \\ \text{---} \end{array} \quad (3.24)$$


which are not linked *via* the Hamiltonian and do not grow linearly with system size. If the excitation operator is complete, then the unlinked terms in the numerator and denominator cancel. However, if the excitation operator is truncated, this does not happen and the unlinked terms remain.

Conversely, it is this denominator that also makes CID exact for two electrons, where as CEPA(0) is not. LPFD(λ) introduces the effect of this denominator into CEPA(0) and in the limit of two electrons, reduces exactly to CID. This can be shown by inserting the definition of the transformed cluster amplitudes into the energy functional:

$$\begin{aligned} E_{\text{LPFD}(\lambda)} &= \langle \hat{H} \rangle + 2 \langle \Phi_0 | \hat{H} t_{ab}^{\tilde{e}\tilde{e}} | \Phi_{\tilde{e}\tilde{e}}^{ab} \rangle + \langle \Phi_0 | (t_{ab}^{\tilde{e}\tilde{e}})^\dagger (\hat{H} - \langle \hat{H} \rangle) t_{ab}^{\tilde{e}\tilde{e}} | \Phi_{\tilde{e}\tilde{e}}^{ab} \rangle \\ &= \langle \hat{H} \rangle + 2 \langle \Phi_0 | \hat{H} (U^{-\frac{1}{2}})^{\tilde{e}\tilde{e}} t_{ab}^{\tilde{e}\tilde{e}} | \Phi_{\tilde{e}\tilde{e}}^{ab} \rangle \\ &+ \langle \Phi_0 | (U^{-\frac{1}{2}})^{\tilde{e}\tilde{e}} (t_{ab}^{\tilde{e}\tilde{e}})^\dagger (\hat{H} - \langle \hat{H} \rangle) (U^{-\frac{1}{2}})^{\tilde{e}\tilde{e}} t_{ab}^{\tilde{e}\tilde{e}} | \Phi_{\tilde{e}\tilde{e}}^{ab} \rangle \\ &= \langle \hat{H} \rangle + 2 \frac{\langle \Phi_0 | \hat{H} t_{ab}^{\tilde{e}\tilde{e}} | \Phi_{\tilde{e}\tilde{e}}^{ab} \rangle}{U_{\tilde{e}\tilde{e}}^{\tilde{e}\tilde{e}}} + \frac{\langle \Phi_0 | (t_{ab}^{\tilde{e}\tilde{e}})^\dagger (\hat{H} - \langle \hat{H} \rangle) t_{ab}^{\tilde{e}\tilde{e}} | \Phi_{\tilde{e}\tilde{e}}^{ab} \rangle}{U_{\tilde{e}\tilde{e}}^{\tilde{e}\tilde{e}}}, \end{aligned} \quad (3.25)$$

$$\begin{aligned} U_{\tilde{e}\tilde{e}}^{\tilde{e}\tilde{e}} &= \delta_{\tilde{e}\tilde{e}}^{\tilde{e}\tilde{e}} + \lambda \eta_{\tilde{e}\tilde{e}}^{\tilde{e}\tilde{e}} + \frac{1}{2} (1 - \lambda) (\delta_{\tilde{e}}^{\tilde{e}} \eta_{\tilde{e}}^{\tilde{e}} + \delta_{\tilde{e}}^{\tilde{e}} \eta_{\tilde{e}}^{\tilde{e}} + \delta_{\tilde{e}}^{\tilde{e}} \eta_{\tilde{e}}^{\tilde{e}} + \delta_{\tilde{e}}^{\tilde{e}} \eta_{\tilde{e}}^{\tilde{e}}) \\ &= 1 + \lambda \langle \hat{T}_2^\dagger \hat{T}_2 \rangle + \frac{1}{2} (1 - \lambda) (\langle \hat{T}_2^\dagger \hat{T}_2 \rangle + \langle \hat{T}_2^\dagger \hat{T}_2 \rangle) \\ &= 1 + \lambda \langle \hat{T}_2^\dagger \hat{T}_2 \rangle + (1 - \lambda) (\langle \hat{T}_2^\dagger \hat{T}_2 \rangle + \langle \hat{T}_2^\dagger \hat{T}_2 \rangle) \\ &= 1 + \langle \hat{T}_2^\dagger \hat{T}_2 \rangle, \end{aligned} \quad (3.26)$$

$$\begin{aligned} E_{\text{LPFD}(\lambda)} &= \langle \hat{H} \rangle + 2 \frac{\langle \Phi_0 | \hat{H} t_{ab}^{\tilde{e}\tilde{e}} | \Phi_{\tilde{e}\tilde{e}}^{ab} \rangle}{1 + \langle \hat{T}_2^\dagger \hat{T}_2 \rangle} + \frac{\langle \Phi_0 | (t_{ab}^{\tilde{e}\tilde{e}})^\dagger (\hat{H} - \langle \hat{H} \rangle) t_{ab}^{\tilde{e}\tilde{e}} | \Phi_{\tilde{e}\tilde{e}}^{ab} \rangle}{1 + \langle \hat{T}_2^\dagger \hat{T}_2 \rangle} \\ &= E_{\text{CID}}. \end{aligned} \quad (3.27)$$

This is the same as FCI in the two-electron limit and so LPFD(λ) must also produce an exact answer.

For the many electron cases, the effect of the transformed cluster operators is to renormalise the CEPA(0) functional by a general CI denominator, but one that only includes linked terms and so remains extensive.

This simple case also illustrates how LPFD(λ) retains the extensivity of CEPA(0). In Eq. 3.26, U_{kl}^{ij} becomes a 1×1 matrix. For the case of N separated electron pairs, then U_{kl}^{ij} simply becomes a block diagonal matrix of 1×1 blocks and so no unphysical energy contributions are introduced *via* the off-diagonal blocks.

3.1.4 Properties and limitations

As well as being exact for the two-electron case and extensive, LPFD(λ) also possesses other desirable features. Like CCSD, the energy functional contains fully linked diagrams, which means that there are no free indices and so the energy must be a scalar and invariant to rotations in the occupied and virtual subspaces. The method does not obey the variational principle, however the energy is variationally minimized so as to satisfy the GHF theorem.

The most computationally expensive step in LPFD(λ) is the contraction of the transformed cluster amplitude with the two-electron integrals, *i.e.* constructing the \mathcal{C} term. However, this scales as $O(o^4v^2)$, which is the same as the most expensive step in CCSD. If its possible to use CCSD on a system, then it's also *theoretically* possible to use LPFD(λ).²

Nevertheless, LPFD(λ) is not a true *ab initio* theory. The λ parameter vanishes in the two-electron case (Eq. 3.26), but for the general N -electron case, λ must be chosen, thereby introducing unnecessary empiricism. The particular values of $\lambda = \{0, 1\}$, which correspond to including the $\frac{1}{2}\mathcal{B}$ and $-\mathcal{C}$ terms respectively, were chosen and have been previously investigated. [13]

Ultimately, even though LPFD(0) and LPFD(1) showed promising results for certain systems, both diverge from the VCCD result in many diatomic dissociations, thereby offering no real benefit over CCSD. The failure was predicted to be caused by the lack of a complete low order correspondence between LPFD(λ) and VCCD. This was rectified in the QVCCD method.

²Currently, in practice, an LPFD(λ) calculation within Molpro will take longer than the corresponding CCSD calculation.

3.2 Quasi-Variational Coupled-Cluster Doubles

The LPFD(λ) paradigm is based on the limiting case of two electrons. For this, the \mathcal{A} and \mathcal{D} terms cancel and are assumed to be unimportant for the N -electron case. In fact, LPFD(0) and LPFD(1) only reproduce one $O(t^3)$ term each and with the wrong prefactor compared to the full VCCD expansion.

Table 3.1 shows that all four terms are important in the general N -electron case. The energy contributions of the two relationships that justified LPFD(λ), $\mathcal{A} + \mathcal{B} = 0$ and $\mathcal{B} + 2\mathcal{C} = 0$, are examined. For He, these relationships hold, however, they are no longer equal when the number of electrons is greater than two.

Atom	$\mathcal{A} + \mathcal{D}$	$\mathcal{B} + 2\mathcal{C}$
He	0	0
Ne	-0.00220	0.00281
Ar	-0.00139	0.00428
Kr	-0.00036	0.00047
Xe	-0.00009	0.00026
Rn	0.00017	-0.00005

Table 3.1: Contributions of the $O(t^3)$ terms to the total energy / hartree.

It is clear that for a general N -electron system, all the cubic terms must be captured for a method to at least qualitatively match VCCD and thereby approximately correct CEPA(0) for non-dynamic correlation effects. QVCCD sets out to capture all these cubic terms by modifying the transformed excitation operator and introducing four distinct matrices to generate the four different terms:

$$\begin{aligned}
 q t_{ab}^{ij} = & + \alpha \left[\frac{1}{2} (1 - \hat{\tau}_{ab}) (\mathcal{A} U^\rho)_a^c t_{cb}^{ij} \right] \\
 & + \beta \left[\frac{1}{2} (1 - \hat{\tau}_{ij}) (\mathcal{B} U^\rho)_k^i t_{ab}^{kj} \right] \\
 & + \gamma \left[\frac{1}{2} (c U^\rho)_{kl}^{ij} t_{ab}^{kl} \right] \\
 & + \delta \left[\frac{1}{4} (1 - \hat{\tau}_{ij}) (1 - \hat{\tau}_{ab}) (\mathcal{D} U^\rho)_{ak}^{ic} t_{cb}^{kj} \right], \quad (3.28)
 \end{aligned}$$

where the permutation operators have been introduced to maintain the symmetry requirements of the original cluster amplitudes, and ${}_{\mathcal{X}}U^\rho$ are now labelled by the

terms they generate. These are in turn constructed from the four different density matrices which are taken directly from the definition of the cubic terms in Eq. 3.6:

$$\begin{aligned}
({}_{\mathcal{A}}\mathbf{U}^\rho)_b^a &= \delta_b^a + {}_{\mathcal{A}}\eta_b^a, \\
({}_{\mathcal{B}}\mathbf{U}^\rho)_j^i &= \delta_j^i + {}_{\mathcal{B}}\eta_j^i, \\
({}_{\mathcal{C}}\mathbf{U}^\rho)_{kl}^{ij} &= \delta_{kl}^{ij} + {}_{\mathcal{C}}\eta_{kl}^{ij}, \\
({}_{\mathcal{D}}\mathbf{U}^\rho)_{aj}^{ib} &= \delta_{aj}^{ib} + {}_{\mathcal{D}}\eta_{aj}^{ib}.
\end{aligned} \tag{3.29}$$

Several parameters, represented by Greek letters, have been introduced. These function to balance the cubic terms in the case of two electrons, but also two holes; a full derivation of these quantities can be found in Ref. [13]. The corrected transformed amplitude equations can be written:

$$\begin{aligned}
q t_{ab}^{ij} &= +2 \left[\frac{1}{2} (1 - \hat{\tau}_{ab}) ({}_{\mathcal{A}}\mathbf{U}^{-\frac{q}{2}})_a^c t_{cb}^{ij} \right] \\
&+ 2 \left[\frac{1}{2} (1 - \hat{\tau}_{ij}) ({}_{\mathcal{B}}\mathbf{U}^{-\frac{q}{2}})_k^i t_{ab}^{kj} \right] \\
&- 1 \left[\frac{1}{2} ({}_{\mathcal{C}}\mathbf{U}^{-\frac{q}{2}})_{kl}^{ij} t_{ab}^{kl} \right] \\
&- 2 \left[\frac{1}{4} (1 - \hat{\tau}_{ij}) (1 - \hat{\tau}_{ab}) ({}_{\mathcal{D}}\mathbf{U}^{-\frac{q}{2}})_{ak}^{ic} t_{cb}^{kj} \right].
\end{aligned} \tag{3.30}$$

With these new definitions, the QVCCD energy takes the same form as the LPFD(λ) energy,

$$E_{\text{QVCCD}} = \langle \hat{\mathbf{H}} \rangle + 2 \langle \hat{\mathbf{H}}_2 \hat{\mathbf{T}}_2 \rangle + \langle {}_1\hat{\mathbf{T}}_2^\dagger (\hat{\mathbf{H}} - \langle \hat{\mathbf{H}} \rangle) {}_1\hat{\mathbf{T}}_2 \rangle,$$

$$\begin{aligned}
&= \text{---} \bullet \text{---} \bigcirc \text{---} + \bigcirc \text{---} \text{---} \bigcirc \text{---} \\
&+ 2 \left(\text{---} \bigcirc \text{---} \bigcirc \text{---} + \text{---} \bigcirc \text{---} \bullet \right) \\
&+ \left(\text{---} \bigcirc \text{---} \bullet + \text{---} \bigcirc \text{---} \bigcirc \text{---} \right) \\
&+ \left(\text{---} \bigcirc \text{---} \bigcirc \text{---} + \text{---} \bigcirc \text{---} \bigcirc \text{---} \right) .
\end{aligned} \tag{3.31}$$

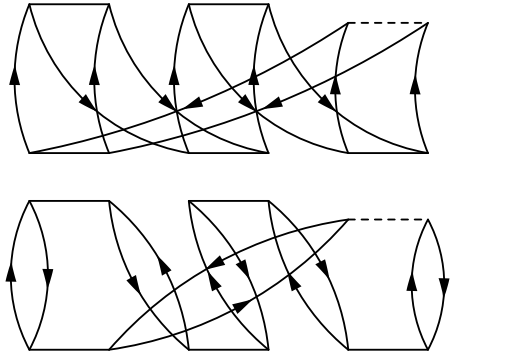
The canonical HF case has been assumed when constructing the diagrams. These are translated into algebraic expressions using the rules set forth in [10]. An extra rule must be added: if two sets of transformed excitation operator lines appear in one diagram, then it refers to the ${}_1\hat{T}$ operator. If only one set of lines appear, then the ${}_2\hat{T}$ operator must be used.

Following the same argument in Eq. 3.27, it can be shown that the QVCCD energy reduces to the CID expression for the case of two-electrons. However for the general N -electron case, all four cubic terms are generated:

$$\begin{aligned}
 \langle \hat{H} {}_2\hat{T} \rangle &= \frac{1}{8} \langle ij || ab \rangle {}_2t_{ij}^{ab} \\
 &= \frac{1}{8} \langle ij || ab \rangle \left\{ 2 \left[\frac{1}{2} (1 - \hat{\tau}_{ab}) ({}_A U^{-1})_a^c t_{cb}^{ij} \right] \right. \\
 &\quad + 2 \left[\frac{1}{2} (1 - \hat{\tau}_{ij}) ({}_B U^{-1})_k^i t_{ab}^{kj} \right] \\
 &\quad - 1 \left[\frac{1}{2} ({}_C U^{-1})_{kl}^{ij} t_{ab}^{kl} \right] \\
 &\quad \left. - 2 \left[\frac{1}{4} (1 - \hat{\tau}_{ij}) (1 - \hat{\tau}_{ab}) ({}_D U^{-1})_{ak}^{ic} t_{cb}^{kj} \right] \right\} \\
 &= \frac{1}{8} \langle ij || ab \rangle \left\{ t_{ij}^{ab} + \left[\frac{1}{2} (t_{cb}^{ij} t_{ca}^{ab} t_{ij}^{ca} - t_{ca}^{ij} t_{ij}^{ba} t_{cb}^{ca}) \right] \right. \\
 &\quad + \left[\frac{1}{2} (t_{ab}^{ij} t_{kj}^{ab} t_{ab}^{kj} - t_{ab}^{ji} t_{ki}^{ab} t_{ab}^{ki}) \right] \\
 &\quad - \left[\frac{1}{4} t_{ab}^{ij} t_{kl}^{ab} t_{ab}^{kl} \right] \\
 &\quad \left. - \left[\frac{1}{2} (t_{ab}^{ij} t_{kj}^{cb} t_{cb}^{kj} - t_{ab}^{ji} t_{ki}^{cb} t_{cb}^{ki} - t_{ba}^{ij} t_{kj}^{ca} t_{ca}^{kj} + t_{ba}^{ji} t_{ki}^{ca} t_{ca}^{ki}) \right] \right\} \\
 &= \frac{1}{8} \text{Diagram 1} \\
 &\quad + \frac{1}{16} \text{Diagram 2} - \frac{1}{16} \text{Diagram 3} \\
 &\quad + \frac{1}{32} \text{Diagram 4} + \frac{1}{16} \text{Diagram 5} \\
 &= O(t) + O(t^3). \tag{3.32}
 \end{aligned}$$

Much like LPFD(λ), a geometric series of these terms is captured by using the powers of the transformation matrix. Not only are all the $O(t^3)$ terms captured,

but also higher order terms. For example, the C- and D-type $O(t^5)$ terms are also included:



thereby introducing the effects of higher excitations into QVCCD. The new definition of the transformed excitation operator leads to a complete renormalisation of the CEPA(0) functional by all the $O(t^3)$ VCCD terms.

QVCCD is simply a modification of LPFD(λ) and so inherits all the properties of LPFD(λ); extensivity, exact for two electrons, scalar energy, scaling as $O(N^6)$. Moreover, it removes the parameters from LPFD(λ), thereby eliminating the inherent empiricism of the method.

QVCCD has been shown to have numerical improvements over both LPFD in strong non-dynamic regimes. [96] This is due to its success at capturing a complete and balanced set of VCCD cubic terms to infinite order and thereby correcting LPFD at the low $O(t^3)$ orders.

3.3 Existence of the \mathbf{U}^ρ tensors

Until now, it has been implicitly assumed that the \mathbf{U} tensors raised to a power exist. For a general matrix, \mathbf{U}^{-1} will only exist if \mathbf{U} is nonsingular, *i.e.* it possess a zero eigenvalue, thereby making $|\mathbf{U}| = 0$. [97]

Using the eigenvalue equation,

$$\mathbf{U}^{-\frac{1}{2}} = \mathbf{X}\epsilon^{-\frac{1}{2}}\mathbf{X}^\dagger, \quad (3.33)$$

for a real $\mathbf{U}^{-\frac{1}{2}}$ to exist, \mathbf{U} must not possess eigenvalues that are less than or equal to zero. Formally, \mathbf{U} must be a positive-definite matrix, *i.e.* for some vector in our Fock space, $\langle \mathbf{x} | \mathbf{U} | \mathbf{x} \rangle > 0$. [97]

It therefore needs to be shown that the \mathbf{U} tensors are positive-definite. This can be proved by realising that \mathbf{U} is simply a sum of the identity matrix and

a density matrix, therefore its eigenvalues will be one plus the eigenvalues of the density matrix. For \mathbf{U} to be positive-definite, the density matrix must be positive-semidefinite, meaning its eigenvalues can be greater or equal to zero.

It is easily recognised that the density matrices defined in Eq. 3.6 are Gramian, as they are formed from the inner product between a set of vectors, and therefore positive-semidefinite. [98] This satisfies the condition that $\mathbf{U}^{-\frac{q}{2}}$ ($q = \{1, 2\}$) exists. [13]

3.4 Single excitations

After doubles, the excitations that contribute the most to the energy and wavefunction are the singles. [7] Currently, within QVCCD theory, single excitations do not have an adequate mathematical form.

A naive approach would be to combine the singles and doubles amplitudes into the transformation matrix and so generate both single and double $O(t^3)$ terms. [13] For example,

$${}_{\mathcal{A}}U_b^a = \delta_b^a + t_b^i t_i^a + \frac{1}{2} t_{bc}^{ij} t_{ij}^{ac}. \quad (3.34)$$

In the two-electron case, this becomes,

$${}_{\mathcal{A}}U_{\bar{e}}^{\bar{e}} = \delta_{\bar{e}}^{\bar{e}} + t_{\bar{e}}^i t_i^{\bar{e}} + \frac{1}{2} t_{\bar{e}c}^{ij} t_{ij}^{\bar{e}c}. \quad (3.35)$$

However, the corresponding CISD denominator which needs to be captured is,

$$\langle \hat{T}_1^\dagger \hat{T}_1 \rangle = t_{\bar{e}}^i t_i^{\bar{e}} + t_{\bar{e}}^i t_i^{\bar{e}}. \quad (3.36)$$

Eq. 3.34 only produces one of these terms and so the energy expression would no longer be exact for the two-electron case.

Alternatively, including the effects of the singles can be achieved by using projective or variational Brueckner orbitals. [99] These two methods both omit the single excitations and instead incorporate the effects of these into a new set of orbitals. These two procedures will be briefly discussed here.

3.4.1 Projective Brueckner orbitals

Brueckner orbitals, Φ_B , can be defined *via* a series of projections, analogous to the CC equations, [100]

$$\langle \Phi_0 | \hat{H} \hat{X} | \Phi_0 \rangle = E \quad (3.37)$$

$$\langle \Phi_i^a | \hat{H} \hat{X} | \Phi_0 \rangle = 0 \quad (3.38)$$

$$\langle \Phi_{ij}^{ab} | \hat{H} \hat{X} | \Phi_0 \rangle = t_{ab}^{ij} E, \quad (3.39)$$

where \hat{X} is an excitation operator, either linear or exponential. Importantly, the equations for the singles coefficients are defined so that they vanish. The set of orbitals that satisfy these equations must be generated iteratively by mixing the virtual and occupied orbitals,

$$\chi'_i \rightarrow \chi_i + t_a^i \chi_a, \quad (3.40)$$

This procedure can be justified using Thouless theorem, which states that any SD can be transformed into any other SD by an exponential operator generating single excitations, *i.e.* mixing in virtual orbitals, [101]

$$|\Phi\rangle' = e^{\hat{T}_1} |\Phi\rangle, \quad (3.41)$$

The effects of the t_a^i coefficients can be combined into the orbitals every iteration, via Eq. 3.40, set to zero and the energy minimised with respect to the constraint in Eq. 3.38. [102] This often leads to slow convergence and so the effects of the singles can instead be included *via* a unitary rotation of the orbitals among themselves,

$$\chi'_i \rightarrow e^\Lambda \chi_i, \quad (3.42)$$

where Λ is an antisymmetric matrix constructed from the singles coefficients,

$$\Lambda_{ai} = t_a^i, \quad (3.43)$$

$$\Lambda_{ia} = -t_a^i, \quad (3.44)$$

$$\Lambda_{ij} = \Lambda_{ab} = 0, \quad (3.45)$$

$$-\mathbf{\Lambda} = \mathbf{\Lambda}^T. \quad (3.46)$$

This method defines the B(rueckner)CCD, BCID and BQVCCD family of methods.

3.4.2 Variational Brueckner orbitals

Instead of defining the Brueckner condition of Eq. 3.38, the energy functional can be minimised with respect to the orbitals,

$$\frac{\partial E}{\partial \chi} = 0. \quad (3.47)$$

Conceptually, the orbital gradient is constructed and then used as an update to the singles coefficients for the next iteration. The update is used to construct the unitary rotation in Eq. 3.42 and transform the orbitals. This is repeated until the orbital gradient and the energy gradient with respect to the amplitudes are a minimum. This method defines the variational Brueckner or Orbital Optimised family of methods (OCCD, OCID and OQVCCD). [103]

Both the projective and variational methods account for the singles excitations exactly, and so are used with LPFD(λ) and QVCCD theory to include these contributions. It should be noted that even though both methods do not include single excitations explicitly, both sets of orbitals are usually not equivalent and will give different answers for the energy and other molecular properties. [103]

A drawback with these procedures are that the orbitals change every iteration, leading to recalculation of the one- and two-electron integrals. The projective Brueckner method can avoid the recalculation of the computationally expensive integrals involving three virtual orbitals. [102] However, this method has been shown to produce failures when calculating potential energy surfaces, [104] while orbital optimisation is in general more reliable due to the variational minimisation of the orbitals.

The orbital optimisation method was subsequently used within both the old and new implementations of QVCCD.

3.5 Triple excitations

3.5.1 The (T) correction

The effect of triple excitations are often needed to produce chemically accurate answers, however if the exponential operator is truncated at \hat{T}_3 , CCSDT scales as $O(N^8)$ and so is too computationally expensive for many chemical systems of interest.

It has been shown that CCD is the same as MBPT up to third order [10], so instead of including the full triples terms, the CCSD energy can be corrected up to fourth-order in MBPT. Triply excited SDs are included and therefore some of the effects of triple excitations can be incorporated. This correction forms an extra non-iterative step which is added onto the CCSD energy after it has converged, denoted as CCSD[T],

$$E_{\text{CCSD[T]}} = E_{\text{CCSD}} + E_{\text{T}}^{(4)}. \quad (3.48)$$

This correction scales as $O(N^7)$ and so is significantly faster than including a complete description of the triples. [66] However this scheme tends to overestimate the effects of the triples and can produce incorrect potential energy surfaces. [105]

It was noted that if the singles and doubles terms were to balance properly in the [T] correction, extra fifth-order terms involving the singles should be included. These fifth-order terms usually have the opposite sign compared to the fourth-order terms and so offset the overcorrection by [T]. [66] This correction was denoted CCSD(T) and has been widely used ever since,³

$$E_{\text{CCSD(T)}} = E_{\text{CCSD}} + E_{\text{T}}^{(4)} + E_{\text{ST}}^{(5)}. \quad (3.49)$$

As noted in Chapter 2, CCSD(T) is widely used to investigate many different chemical problems and is often called the *Gold Standard* of computational chemistry. [67] The inclusion of the triples *via* (T) has been shown to be necessary to generate chemically accurate results with relatively little computational expense. This has led CCSD(T) being used in lieu of experimental results as a benchmark for comparing other computational methods. [106]

3.5.2 Triples correction for OQVCCD

CCD, VCCD and QVCCD are all equivalent up to fourth-order in MP theory, [13] if the singles coefficients are set to zero, so the standard (T) correction can be

³Stanton has provided an interesting rationale for the inclusion of $E_{\text{T}}^{(4)}$ and $E_{\text{ST}}^{(5)}$. [66] If the zeroth-order wavefunction replaces the HF reference in an MBPT treatment, then the leading order corrections are the $E_{\text{T}}^{(4)}$ and $E_{\text{ST}}^{(5)}$ terms.

applied to OQVCCD,⁴

$$E_{\text{OQVCCD(T)}} = E_{\text{OQVCCD}} + E_{\text{(T)}}, \quad (3.50)$$

$$E_{\text{(T)}} = \frac{1}{16} \frac{\langle \Phi_0 | \hat{T}_2^\dagger \hat{V} | \Phi_{ijk}^{abc} \rangle \langle \Phi_{ijk}^{abc} | \hat{V} \hat{T}_2^\dagger | \Phi_0 \rangle}{\epsilon_i + \epsilon_j + \epsilon_k - \epsilon_a - \epsilon_b - \epsilon_c}, \quad (3.51)$$

which defines OQVCCD(T).

This method has previously been investigated [107] and been shown to produce promising results for some diatomic dissociations, however, in some cases (*e.g.* the OH⁻ anion), OQVCCD(T) produces a maxima at long bond lengths before the energy starts to fall, thereby reproducing the behaviour of CCSD(T).

This sort of behaviour was blamed on the breakdown of the (T) correction which contains eigenvalues, ϵ_p , of the Fock operator in the denominator. If the energy difference between the occupied and virtual orbitals becomes small, for example, when the energies of the orbitals become closer in energy, then $E_{\text{(T)}}$ becomes large and over corrects for the effects of the triples and so leads to qualitative failures in the description of bond dissociations. [15] Often in systems with non-dynamic correlation, the MOs can be close in energy, meaning that the standard (T) will not work with such systems.

3.5.3 Renormalised triples

Several different authors have attempted to construct triples corrections which do not suffer from the degenerate orbital breakdown. These *renormalised triples* introduce a denominator into Eq. 3.51, which rescales the correction properly when the energy difference between the occupied and virtual orbitals becomes small. Piecuch *et al.* made use of this methodology in the Completely-Renormalised CC method (CR-CC). [108] This method has been through several reformulations, all of which suffer from problems. For example, the earliest attempt at renormalised triples was no longer extensive, [109] whereas the later CR-CC(2,3) method requires the calculation of the CCSD left eigenstates, thereby nearly doubling the computational expense compared to standard CCSD. [110]

A renormalised triples scheme can be developed by using an analysis by Nooijen and LeRoy; Eq. 3.51 can be derived in a different way which allows

⁴This is the same as the [T] correction as the singles terms vanish and so is less computationally expensive than the standard (T) correction for CCSD

the recognition of a renormalising denominator. [111] In preparation, new notation must be introduced: the complete excitation operator will be denoted as $\tilde{\mathbb{T}} = \tilde{\mathbb{T}}_1 + \tilde{\mathbb{T}}_2 + \tilde{\mathbb{T}}_3 + \dots$,⁵ while $\hat{\mathbb{T}} = \hat{\mathbb{T}}_1 + \hat{\mathbb{T}}_2$. The FCI Schrödinger equation can be written thus,

$$\langle \Phi_0 | e^{\tilde{\mathbb{T}}^\dagger} \hat{\mathbb{H}} = E_{\text{FCI}} \langle \Phi_0 | e^{\tilde{\mathbb{T}}^\dagger} . \quad (3.52)$$

Pre-multiplying by $e^{\hat{\mathbb{T}}} |\Phi_0\rangle$ gives the energy functional,

$$\langle \Phi_0 | e^{\tilde{\mathbb{T}}^\dagger} \hat{\mathbb{H}} e^{\hat{\mathbb{T}}} |\Phi_0\rangle = E_{\text{FCI}} \langle \Phi_0 | e^{\tilde{\mathbb{T}}^\dagger} e^{\hat{\mathbb{T}}} |\Phi_0\rangle , \quad (3.53)$$

$$E_{\text{FCI}} = \frac{\langle \Phi_0 | e^{\tilde{\mathbb{T}}^\dagger} \hat{\mathbb{H}} e^{\hat{\mathbb{T}}} |\Phi_0\rangle}{\langle \Phi_0 | e^{\tilde{\mathbb{T}}^\dagger} e^{\hat{\mathbb{T}}} |\Phi_0\rangle} . \quad (3.54)$$

The identity operator, $e^{\hat{\mathbb{T}}} e^{-\hat{\mathbb{T}}} = 1$, can be inserted into Eq. 3.54 and the Resolution Of the Identity (ROI) operator, $\mathbf{1} = \sum_k |k\rangle \langle k|$, introduced to produce a sum over the basis of reference and excited manifolds,

$$E_{\text{FCI}} = \sum_k \frac{\langle \Phi_0 | e^{\tilde{\mathbb{T}}^\dagger} e^{\hat{\mathbb{T}}} |k\rangle \langle k| e^{-\hat{\mathbb{T}}} \hat{\mathbb{H}} e^{\hat{\mathbb{T}}} |\Phi_0\rangle}{\langle \Phi_0 | e^{\tilde{\mathbb{T}}^\dagger} e^{\hat{\mathbb{T}}} |\Phi_0\rangle} , \quad (3.55)$$

$$E_{\text{FCI}} = E_{\text{CCSD}} + \sum_{k \in T, Q, \dots} \frac{\langle \Phi_0 | e^{\tilde{\mathbb{T}}^\dagger} e^{\hat{\mathbb{T}}} |k\rangle \langle k| e^{-\hat{\mathbb{T}}} \hat{\mathbb{H}} e^{\hat{\mathbb{T}}} |\Phi_0\rangle}{\langle \Phi_0 | e^{\tilde{\mathbb{T}}^\dagger} e^{\hat{\mathbb{T}}} |\Phi_0\rangle} . \quad (3.56)$$

Nooijen and LeRoy further identified the cancellation of unlinked terms between the denominator and numerator, thereby producing an explicitly linked term,

$$E_{\text{FCI}} = E_{\text{CCSD}} + \sum_{k \in T, Q, \dots} \langle \Phi_0 | e^{\tilde{\mathbb{T}}^\dagger} e^{\hat{\mathbb{T}}} |k\rangle_L \langle k| e^{-\hat{\mathbb{T}}} \hat{\mathbb{H}} e^{\hat{\mathbb{T}}} |\Phi_0\rangle . \quad (3.57)$$

If only the triply excited determinants are considered, the excitation operators can be explicitly written:

$$\delta E = \frac{1}{16} \langle \Phi_0 | e^{\tilde{\mathbb{T}}_2^\dagger + \tilde{\mathbb{T}}_3^\dagger} e^{\hat{\mathbb{T}}_2} |\Phi_{ijk}^{abc}\rangle_L \langle \Phi_{ijk}^{abc} | e^{-\hat{\mathbb{T}}} \hat{\mathbb{H}} e^{\hat{\mathbb{T}}} |\Phi_0\rangle , \quad (3.58)$$

$$\delta E \approx \frac{1}{16} \langle \Phi_0 | e^{\hat{\mathbb{T}}_2^\dagger} \hat{\mathbb{T}}_3^{(2)\dagger} e^{\hat{\mathbb{T}}_2} |\Phi_{ijk}^{abc}\rangle_L \langle \Phi_{ijk}^{abc} | e^{-\hat{\mathbb{T}}} \hat{\mathbb{H}} e^{\hat{\mathbb{T}}} |\Phi_0\rangle , \quad (3.59)$$

where the $\tilde{\mathbb{T}}_2$ operator has been approximated with the converged $\hat{\mathbb{T}}_2$ operator and $\tilde{\mathbb{T}}_3$ has been replaced by the second-order correction to the triples operator,

$$\hat{\mathbb{T}}_3^{(2)} |\Phi_0\rangle = \left(\frac{1}{3!}\right)^2 t_{abc}^{ijk(2)} |\Phi_{ijk}^{abc}\rangle , \quad (3.60)$$

$$t_{abc}^{ijk(2)} = \frac{\langle \Phi_{ijk}^{abc} | \hat{\mathbb{V}} \hat{\mathbb{T}}_2 |\Phi_0\rangle}{\epsilon_i + \epsilon_j + \epsilon_k - \epsilon_a - \epsilon_b - \epsilon_c} . \quad (3.61)$$

⁵This should not be confused with an excitation operator acting only on the $m_s = +\frac{1}{2}$ electrons.

Eq. 3.59 represents the standard (T) correction discussed above, but scaled by the CCSD norm. [15]

Robinson and Knowles recognised a connection between Eq. 3.59 and the QVCCD ansatz. The diagrams that appear here are the same family of diagrams that the \mathbf{U} transformation matrices produce, except contracted with a triples operator. A simple renormalised correction can therefore be produced by using the transformed excitation operator in the (T) correction and thereby approximate this term,

$$E_{\text{CR(T)}} = \frac{1}{16} \frac{\langle \Phi_0 | {}_2\hat{T}_2^\dagger \hat{V} | \Phi_{ijk}^{abc} \rangle \langle \Phi_{ijk}^{abc} | (\hat{V}\hat{T}_2 + \frac{1}{2!}\hat{V}\hat{T}_2^2) | \Phi_0 \rangle}{\epsilon_i + \epsilon_j + \epsilon_k - \epsilon_a - \epsilon_b - \epsilon_c}. \quad (3.62)$$

This will be denoted as the Completely-Renormalised Triples (CR(T)) correction.

The effect of using the transformed excitation operator can be examined by considering a three-electron system. Eq. 3.59 simplifies to,

$$\begin{aligned} \delta E &\approx \frac{1}{16} \frac{\langle \Phi_0 | \hat{T}_3^{(2)\dagger} | \Phi_{ijk}^{abc} \rangle_L \langle \Phi_{ijk}^{abc} | (\hat{V}\hat{T}_2 + \frac{1}{2!}\hat{V}\hat{T}_2^2) | \Phi_0 \rangle}{1 + \langle \hat{T}_2^\dagger \hat{T}_2 \rangle} \\ &= \frac{1}{16} \frac{\langle \Phi_0 | \hat{T}_2^\dagger \hat{V} | \Phi_{ijk}^{abc} \rangle \langle \Phi_{ijk}^{abc} | (\hat{V}\hat{T}_2 + \frac{1}{2!}\hat{V}\hat{T}_2^2) | \Phi_0 \rangle}{\left(1 + \langle \hat{T}_2^\dagger \hat{T}_2 \rangle\right) (\epsilon_i + \epsilon_j + \epsilon_k - \epsilon_a - \epsilon_b - \epsilon_c)}. \end{aligned} \quad (3.63)$$

In the limit, (T) is divided by the CI norm, which has been shown before to be the action of the transformed excitation operators, thereby justifying the choice in Eq. 3.62.

If the quadratic term in Eq. 3.62 is ignored, then a simpler correction is obtained,

$$\begin{aligned} E_{\text{AR(T)}} &= \frac{1}{16} \frac{\langle \Phi_0 | {}_2\hat{T}_2^\dagger \hat{V} | \Phi_{ijk}^{abc} \rangle \langle \Phi_{ijk}^{abc} | \hat{V}\hat{T}_2 | \Phi_0 \rangle}{\epsilon_i + \epsilon_j + \epsilon_k - \epsilon_a - \epsilon_b - \epsilon_c} \\ &= \frac{1}{16} \frac{V_{ijk}^{abc} W_{ijk}^{abc}}{\epsilon_i + \epsilon_j + \epsilon_k - \epsilon_a - \epsilon_b - \epsilon_c} \end{aligned} \quad (3.64)$$

This will be denoted as the Asymmetric-Renormalised Triples (AR(T)) correction.

The AR(T) correction requires the construction of two different intermediates, V_{ijk}^{abc} and W_{ijk}^{abc} , instead of just one in the standard (T) correction, thereby nearly doubling the computational time required to evaluate it. Another approximation can be formed if both excitation operators are replaced with transformed excitation operators,

$$E_{\text{R(T)}} = \frac{1}{16} \frac{\langle \Phi_0 | {}_1\hat{T}_2^\dagger \hat{V} | \Phi_{ijk}^{abc} \rangle \langle \Phi_{ijk}^{abc} | \hat{V} {}_1\hat{T}_2 | \Phi_0 \rangle}{\epsilon_i + \epsilon_j + \epsilon_k - \epsilon_a - \epsilon_b - \epsilon_c}, \quad (3.65)$$

which has been denoted as the (symmetric) Renormalised Triples (R(T)) correction. This agrees up to sixth-order in MP theory with Eq. 3.62 and so it is predicted that there will only be a small numerical difference between the R(T), AR(T) and CR(T) corrections. R(T) only requires the evaluation of one intermediate, and so has the same computational cost as the standard (T) correction.

Chapter 4

Quasi-Variational Coupled-Cluster: Implementation

The previous implementation of the QVCCD code was written in Fortran within Molpro. As a result of the implementation, the code is slow and not able to take advantage of multiple processors. Part of this project has been to totally rewrite the code to make it fast, parallel and able to carry out calculations on larger molecules.

This section will explore the re-derivation of the QVCCD equations used in the computer code and the issues that were faced in the implementation that are not obvious from a cursory glance at the equations.

4.1 Programmable equations

The QVCCD equations presented in Chapter 3 can not be programmed into a computer. These equations must first be manipulated using second quantisation to produce expressions involving electron integrals and transformed cluster amplitudes. An explicit expression for the derivative of the energy with respect to the doubles amplitudes must also be derived, so an energy minimum can be found.

The general spin-orbital equations will be presented first, before the spin-adapted equations used to investigate closed-shell systems.

4.1.1 Indices

Before the equations are presented, a new index notation for the rank-4 tensors will be introduced to remove any ambiguities in the implementation. This notation will be used in both the spin- and spatial-orbital equations.

Any rank-4 tensor can be written in tensor and matrix notations:

$$A_{pq}^{ij} = A_{[pi],[qj]} . \quad (4.1)$$

The composite index is formed between $[pi]$ and $[qj]$, *i.e.* the columns of the tensor. This is the convention followed by the cluster amplitudes and will be maintained for the transformation matrices.

4.1.2 Spin-orbital equations

QVCCD energy

The QVCCD energy can be written in terms of contractions between electron integrals and transformed cluster amplitudes,

$$\begin{aligned} E_{\text{QVCCD}} &= E_{\text{corr}} - E_0 = 2 \langle \hat{\mathbf{H}}_2 \hat{\mathbf{T}}_2 \rangle + \langle {}_1\hat{\mathbf{T}}_2^\dagger (\hat{\mathbf{H}} - \langle \hat{\mathbf{H}} \rangle) {}_1\hat{\mathbf{T}}_2 \rangle \\ &= 2 {}_2V_{ij}^{ab} {}_2t_{ab}^{ij} + {}_1V_{ij}^{ab} {}_1t_{ab}^{ij} , \end{aligned} \quad (4.2)$$

where,

$${}_2V_{ij}^{ab} = \langle \Phi_0 | \hat{\mathbf{H}} | \Phi_{ij}^{ab} \rangle , \quad (4.3)$$

$${}_1V_{ij}^{ab} = \langle \Phi_0 | {}_1\hat{\mathbf{T}}^\dagger (\hat{\mathbf{H}} - \langle \hat{\mathbf{H}} \rangle) | \Phi_{ij}^{ab} \rangle , \quad (4.4)$$

define various one- and two-electron integrals and the transformed cluster amplitudes,

$$\begin{aligned} {}_q t_{ab}^{ij} &= 2 \left[\frac{1}{2} (1 - \tau_{ab}) (\mathcal{A} U^{-\frac{q}{2}})_{ac} t_{cb}^{ij} \right] \\ &\quad + 2 \left[\frac{1}{2} (1 - \tau_{ij}) (\mathcal{B} U^{-\frac{q}{2}})_{ki} t_{ab}^{kj} \right] \\ &\quad - 1 \left[\frac{1}{2} (c U^{-\frac{q}{2}})_{ki}^{lj} t_{ab}^{kl} \right] \\ &\quad - 2 \left[\frac{1}{4} (1 - \tau_{ij}) (1 - \tau_{ab}) (\mathcal{D} U^{-\frac{q}{2}})_{ac}^{ik} t_{cb}^{kj} \right] . \end{aligned} \quad (4.5)$$

Powers of derivatives of the U matrices

Before the energy derivative is examined it will be useful to examine certain quantities that appear in it. Suffice to say derivatives of the transformation

matrices that appear in the transformed amplitude equations will be necessary. Explicit expressions for these derivatives have already been derived, interested readers are directed to Ref. [13]. The final result will be presented here:

$$\begin{aligned}
d(U^x)_{I,J} &= x \sum_{K=1}^{N_p} X_{I,K} X_{J,K} \epsilon_K^{x-1} \sum_{\substack{M=1 \\ N=1}}^{N_p} X_{M,K} d(U)_{M,N} X_{N,K} \\
&+ \sum_{\substack{K=1, L=1 \\ \epsilon_K \neq \epsilon_L}}^{N_p} \frac{\epsilon_K^x - \epsilon_L^x}{\epsilon_K - \epsilon_L} X_{I,L} X_{J,K} \sum_{\substack{M=1 \\ N=1}}^{N_p} X_{M,L} d(U)_{M,N} X_{N,K}, \quad (4.6)
\end{aligned}$$

In other words, the derivative of \mathbf{U} matrix raised to a power x is related to its eigenvectors, \mathbf{X} , eigenvalues, ϵ and the derivative of the unpowered matrix, $d\mathbf{U}$. The indices labelled by the capital Latin letters can represent standard indices or the composite indices of the rank-4 tensor.

A simplification occurs when near-degenerate eigenvalues of the \mathbf{U} tensors are encountered. If $\epsilon_L = \epsilon_K + \mu$, where μ is a small variable parameter, then the ratio in the second line of Eq. 4.6 becomes,

$$\frac{\epsilon_K^x - \epsilon_L^x}{\epsilon_K - \epsilon_L} = \frac{\epsilon_K^x - (\epsilon_K + \mu)^x}{\epsilon_K - (\epsilon_K + \mu)}. \quad (4.7)$$

In the limit, as $\mu \rightarrow 0$, the eigenvalues approach degeneracy and the ratio becomes,

$$\lim_{\mu \rightarrow 0} \frac{\epsilon_K^x - (\epsilon_K + \mu)^x}{\epsilon_K - (\epsilon_K + \mu)} = x \epsilon_K^{x-1}. \quad (4.8)$$

This can be reinserted back into Eq. 4.6 and used when the eigenvalues are degenerate or the difference between them is below a certain threshold.¹

For efficient code, Eq. 4.6 can be written as a tensor contraction,

$$d(U^x)_{I,J} = Q[\mathbf{U}, x]_{M,N}^{I,J} d(U)_{M,N}, \quad (4.9)$$

$$Q[\mathbf{U}, x]_{M,N}^{I,J} = Q[\mathbf{U}, x]_{N,M}^{J,I}, \quad (4.10)$$

where the tensor \mathbf{Q} has been written as a functional that depends explicitly on a \mathbf{U} matrix and a power. This is convenient to do as \mathbf{Q} can now be contracted with another intermediate quantity other than the derivative of the unpowered matrix.

¹This has been chosen to be 1×10^{-8} in the present implementation

Residual equation

To find the minimum, ground state, energy for a given set of nuclear coordinates, the energy must be minimised with respect to the set of doubles amplitudes, *i.e.* the parameters that determine the QVCCD wavefunction,

$$\begin{aligned} \frac{\partial E_{\text{QVCCD}}}{\partial t_{ab}^{ij}} &= 0 \\ &\equiv G_{ij}^{ab}, \end{aligned} \quad (4.11)$$

$$2 G_{ij}^{ab} = {}_2V_{ij}^{ab} \frac{\partial({}_2t_{ab}^{ij})}{\partial t_{ab}^{ij}} + {}_1V_{ij}^{ab} \frac{\partial({}_1t_{ab}^{ij})}{\partial t_{ab}^{ij}}, \quad (4.12)$$

where G_{ij}^{ab} is called the residual. This forms part of the update used in the DIIS procedure to generate a new set of cluster amplitudes and thereby a new energy.

The complete residual expression can be written as,

$$\begin{aligned} {}_qG_{ab}^{ij} &= (1 + \tau_{ab}\tau_{ij}) \left\{ \left[{}_q^A R_{ea} t_{eb}^{ij} + {}_qV_{cb}^{ij} ({}_A U^{-\frac{q}{2}})_{ca} \right] \right. \\ &\quad + \left[{}_q^B R_{im} t_{ab}^{mj} + {}_qV_{ab}^{kj} ({}_B U^{-\frac{q}{2}})_{ki} \right] \\ &\quad - \left[\frac{1}{4} {}_q^C R_{mi}^{nj} t_{ab}^{mn} + {}_qV_{ab}^{kl} ({}_C U^{-\frac{q}{2}})_{ki}^{lj} \right] \\ &\quad \left. - \left[2 {}_q^D R_{ni}^{af} t_{fb}^{nj} + {}_qV_{cb}^{kj} ({}_D U^{-\frac{q}{2}})_{ac}^{ik} \right] \right\}, \end{aligned} \quad (4.13)$$

with the following intermediate quantities,

$$\begin{aligned} {}_q^A R_{ea} &= Q[\mathbf{U}, x]_{e,a}^{f,c} {}_q^A F_{fc}, & {}_q^B R_{im} &= Q[\mathbf{U}, x]_{i,m}^{k,o} {}_q^B F_{ok}, \\ {}_q^C R_{mi}^{nj} &= Q[\mathbf{U}, x]_{mn,ij}^{op,kl} {}_q^C F_{ok}^{pl}, & {}_q^D R_{ni}^{af} &= Q[\mathbf{U}, x]_{na,if}^{lc,kd} {}_q^D F_{cd}^{lk}, \end{aligned} \quad (4.14)$$

$$\begin{aligned} {}_q^A F_{fc} &= {}_qV_{fg}^{mn} t_{mn}^{cg}, & {}_q^B F_{ok} &= {}_qV_{ef}^{on} t_{kn}^{ef}, \\ {}_q^C F_{ok}^{pl} &= {}_qV_{cd}^{op} t_{kl}^{cd}, & {}_q^D F_{cd}^{lk} &= {}_qV_{de}^{lm} t_{ce}^{km}. \end{aligned} \quad (4.15)$$

4.1.3 Spatial-orbital equations

In a closed-shell calculation, two electrons with opposite spin are allowed to occupy the same spatial-orbital. The equations above can thus be simplified if written in terms of spatial-orbitals. To achieve this, the different spin cases of the excitation operator must be explicitly written,

$$\hat{T}_2 = \frac{1}{4} t_{ab}^{ij} \hat{a}_a^\dagger \hat{a}_b^\dagger \hat{a}_j \hat{a}_i, \quad (4.16)$$

$$\begin{aligned} &= \frac{1}{4} t_{\bar{a}\bar{b}}^{\bar{i}\bar{j}} \hat{a}_a^\dagger \hat{a}_b^\dagger \hat{a}_j \hat{a}_i + \frac{1}{4} t_{\bar{a}\bar{b}}^{\bar{i}\bar{j}} \hat{a}_a^\dagger \hat{a}_b^\dagger \hat{a}_j \hat{a}_i \\ &\quad + t_{\bar{a}\bar{b}}^{\bar{i}\bar{j}} \hat{a}_a^\dagger \hat{a}_b^\dagger \hat{a}_j \hat{a}_i, \end{aligned} \quad (4.17)$$

where tilde and bar indicate an electron of $m_s = +\frac{1}{2}$ and $m_s = -\frac{1}{2}$ respectively.

These terms can be identified with the spin-coupled excitation operator, [43]

$$\hat{T}_2 = \frac{1}{2} T_{ab}^{ij} \hat{E}_{ai} \hat{E}_{bj}, \quad (4.18)$$

$$\hat{E}_{rs} = \hat{a}_r^\dagger \hat{a}_s + \hat{a}_r^\dagger \hat{a}_s, \quad (4.19)$$

$$\begin{aligned} \hat{T}_2 = & \frac{1}{2} T_{ab}^{ij} (\hat{a}_a^\dagger \hat{a}_i \hat{a}_b^\dagger \hat{a}_j + \hat{a}_a^\dagger \hat{a}_i \hat{a}_b^\dagger \hat{a}_j \\ & + \hat{a}_a^\dagger \hat{a}_i \hat{a}_b^\dagger \hat{a}_j + \hat{a}_a^\dagger \hat{a}_i \hat{a}_b^\dagger \hat{a}_j). \end{aligned} \quad (4.20)$$

The capital T now represents a cluster amplitude with respect to spatial-orbitals.

In a closed-shell system, $T_{\bar{a}\bar{b}}^{\bar{i}\bar{j}} = T_{\bar{a}\bar{b}}^{\bar{i}\bar{j}}$, implying,

$$t_{\bar{a}\bar{b}}^{\bar{i}\bar{j}} = 2 T_{ab}^{ij}. \quad (4.21)$$

It is convenient to work with anti-symmetrised cluster amplitudes, similar to antisymmetric two-electron integrals, so Eq. 4.21 becomes,

$$t_{\bar{a}\bar{b}}^{\bar{i}\bar{j}} = T_{ab}^{ij} - T_{ba}^{ij}. \quad (4.22)$$

Using the commutation relations between spin-creation and annihilation operators, the mixed spin cases of Eq. 4.20 can be rewritten,

$$\begin{aligned} \frac{1}{2} T_{ab}^{ij} (\hat{a}_a^\dagger \hat{a}_i \hat{a}_b^\dagger \hat{a}_j + \hat{a}_a^\dagger \hat{a}_i \hat{a}_b^\dagger \hat{a}_j) &= \frac{1}{2} T_{ab}^{ij} \hat{a}_a^\dagger \hat{a}_i \hat{a}_b^\dagger \hat{a}_j + \frac{1}{2} T_{ba}^{ji} \hat{a}_b^\dagger \hat{a}_j \hat{a}_a^\dagger \hat{a}_i \\ &= T_{ab}^{ij} \hat{a}_a^\dagger \hat{a}_i \hat{a}_b^\dagger \hat{a}_j, \end{aligned} \quad (4.23)$$

therefore,

$$t_{\bar{a}\bar{b}}^{\bar{i}\bar{j}} = T_{ab}^{ij}. \quad (4.24)$$

In summary, to turn the set of spin-orbital equations into spatial-orbital equations, the spin cases where $t_{\bar{a}\bar{b}}^{\bar{i}\bar{j}}$, should be written out explicitly. The spin-orbital cluster amplitudes can simply be replaced with the spatial-orbital cluster amplitudes using the following relationships from above, [112]

$$\begin{aligned} t_{\bar{a}\bar{b}}^{\bar{i}\bar{j}} = t_{\bar{a}\bar{b}}^{\bar{i}\bar{j}} &= T_{ab}^{ij} - T_{ba}^{ij}, \\ t_{\bar{a}\bar{b}}^{\bar{i}\bar{j}} &= T_{ab}^{ij}, \end{aligned} \quad (4.25)$$

Only the $G_{\bar{a}\bar{b}}^{\bar{i}\bar{j}}$ case needs to be considered, and not $G_{\bar{a}\bar{b}}^{\bar{i}\bar{j}}$ *etc.*, as this will form the update to the $t_{\bar{a}\bar{b}}^{\bar{i}\bar{j}}$ amplitudes which can be used to construct the same spin amplitudes.

Spin-adapted transformation matrices

Before proceeding to the transformed amplitude and residual equations, the specific spin cases of the \mathbf{U} matrices needs to be examined.

There are only two non-zero spin cases for ${}_{\mathcal{A}}\mathbf{U}$ and ${}_{\mathcal{B}}\mathbf{U}$: $\alpha\alpha$ or $\beta\beta$. In spatial-orbitals, these two cases are the same,

$${}_{\mathcal{A}}U_{ba} = \delta_{ba} + 2T_{bc}^{ij}T_{ac}^{ij} - T_{bc}^{ij}T_{ca}^{ij}, \quad (4.26)$$

$${}_{\mathcal{B}}U_{ji} = \delta_{ji} + 2T_{ab}^{ik}T_{ab}^{jk} - T_{ab}^{ik}T_{ba}^{jk}. \quad (4.27)$$

${}_{\mathcal{C}}\mathbf{U}$ consists of three different spin cases that arise through the density matrix,

$${}_{\mathcal{C}}\eta_{ki}^{lj} = \begin{pmatrix} & \tilde{k}\tilde{l} & \tilde{k}\bar{l} & \bar{k}\tilde{l} & \bar{k}\bar{l} \\ \tilde{j}\tilde{i} & \mathcal{C}_1 & \mathbf{0} & \mathbf{0} & \mathbf{0} \\ \tilde{j}\bar{i} & \mathbf{0} & \mathcal{C}_2 & \mathcal{C}_2 & \mathbf{0} \\ \bar{j}\tilde{i} & \mathbf{0} & \mathcal{C}_2 & \mathcal{C}_2 & \mathbf{0} \\ \bar{j}\bar{i} & \mathbf{0} & \mathbf{0} & \mathbf{0} & \mathcal{C}_3 \end{pmatrix},$$

From Eq. 4.5, only the \mathcal{C}_2 case is needed,

$${}_{\mathcal{C}}U_{ki}^{lj} = \delta_{ki}\delta_{lj} + T_{ab}^{ij}T_{kl}^{ab}. \quad (4.28)$$

An issue arises with ${}_{\mathcal{D}}\mathbf{U}$, as the different spin cases are not independent of one another,

$${}_{\mathcal{D}}\eta_{ab}^{ij} = \begin{pmatrix} & \tilde{j}\tilde{b} & \tilde{j}\bar{b} & \bar{j}\tilde{b} & \bar{j}\bar{b} \\ \tilde{a}\tilde{i} & \mathcal{D}_1 & \mathbf{0} & \mathbf{0} & \mathcal{D}_2 \\ \tilde{a}\bar{i} & \mathbf{0} & \mathcal{D}_3 & \mathbf{0} & \mathbf{0} \\ \bar{a}\tilde{i} & \mathbf{0} & \mathbf{0} & \mathcal{D}_3 & \mathbf{0} \\ \bar{a}\bar{i} & \mathcal{D}_2 & \mathbf{0} & \mathbf{0} & \mathcal{D}_1 \end{pmatrix},$$

$${}_{\mathcal{D}_1}\eta_{ab}^{ij} = 2T_{ac}^{ik}T_{bc}^{jk} - T_{ca}^{ik}T_{bc}^{jk} - T_{ac}^{ik}T_{cb}^{jk} + T_{ca}^{ik}T_{cb}^{jk}, \quad (4.29)$$

$${}_{\mathcal{D}_2}\eta_{ab}^{ij} = 2T_{ac}^{ik}T_{bc}^{jk} - T_{ca}^{ik}T_{bc}^{jk} - T_{ac}^{ik}T_{cb}^{jk}, \quad (4.30)$$

$${}_{\mathcal{D}_3}\eta_{ab}^{ij} = T_{ca}^{ik}T_{cb}^{jk}. \quad (4.31)$$

\mathcal{D}_1 and \mathcal{D}_2 are coupled. This becomes a problem when powers of the ${}_{\mathcal{D}}\mathbf{U}$ matrix are formed, because the separate blocks cannot be raised to a power independently of each other.

A simple rotation can be applied to uncouple and derive explicit expressions for the \mathcal{D}_1 and \mathcal{D}_2 blocks:

$$\mathbf{Q} = \frac{1}{\sqrt{2}} \begin{pmatrix} \mathbf{1} & \mathbf{1} \\ \mathbf{1} & -\mathbf{1} \end{pmatrix},$$

$$\mathbf{\Delta} = \begin{pmatrix} \mathcal{D}_1 & \mathcal{D}_2 \\ \mathcal{D}_2 & \mathcal{D}_1 \end{pmatrix},$$

$$\mathbf{Q}^\dagger \mathbf{\Delta} \mathbf{Q} = \begin{pmatrix} (\mathcal{D}_1 + \mathcal{D}_2) & \mathbf{0} \\ \mathbf{0} & (\mathcal{D}_1 - \mathcal{D}_2) \end{pmatrix} = \mathbf{D}, \quad (4.32)$$

which produces a diagonal matrix. The power of the matrix can be formed and rotated back to produce explicit expressions for the powered \mathcal{D}_1 and \mathcal{D}_2 blocks,

$$\begin{aligned} \mathbf{\Delta} &= \mathbf{Q} \mathbf{D} \mathbf{Q}^\dagger, \\ \mathbf{\Delta}^{-\frac{a}{2}} &= \mathbf{Q} \mathbf{D}^{-\frac{a}{2}} \mathbf{Q}^\dagger \\ &= \frac{1}{2} \begin{pmatrix} \mathbf{1} & \mathbf{1} \\ \mathbf{1} & -\mathbf{1} \end{pmatrix} \begin{pmatrix} (\mathcal{D}_1 + \mathcal{D}_2)^{-\frac{a}{2}} & \mathbf{0} \\ \mathbf{0} & (\mathcal{D}_1 - \mathcal{D}_2)^{-\frac{a}{2}} \end{pmatrix} \begin{pmatrix} \mathbf{1} & \mathbf{1} \\ \mathbf{1} & -\mathbf{1} \end{pmatrix} \\ &= \frac{1}{2} \begin{pmatrix} (\mathcal{D}_1 + \mathcal{D}_2)^{-\frac{a}{2}} + (\mathcal{D}_1 - \mathcal{D}_2)^{-\frac{a}{2}} & (\mathcal{D}_1 + \mathcal{D}_2)^{-\frac{a}{2}} - (\mathcal{D}_1 - \mathcal{D}_2)^{-\frac{a}{2}} \\ (\mathcal{D}_1 + \mathcal{D}_2)^{-\frac{a}{2}} - (\mathcal{D}_1 - \mathcal{D}_2)^{-\frac{a}{2}} & (\mathcal{D}_1 + \mathcal{D}_2)^{-\frac{a}{2}} + (\mathcal{D}_1 - \mathcal{D}_2)^{-\frac{a}{2}} \end{pmatrix}, \end{aligned} \quad (4.33)$$

$$\mathcal{D}_1 = \frac{1}{2} \left\{ (\mathcal{D}_1 + \mathcal{D}_2)^{-\frac{a}{2}} + (\mathcal{D}_1 - \mathcal{D}_2)^{-\frac{a}{2}} \right\}, \quad (4.34)$$

$$\mathcal{D}_2 = \frac{1}{2} \left\{ (\mathcal{D}_1 + \mathcal{D}_2)^{-\frac{a}{2}} - (\mathcal{D}_1 - \mathcal{D}_2)^{-\frac{a}{2}} \right\}. \quad (4.35)$$

Two quantities can be defined,

$$\mathbf{Y} = \mathcal{D}_1 + \mathcal{D}_2, \quad (4.36)$$

$$\begin{aligned} \mathbf{W} &= \mathcal{D}_1 - \mathcal{D}_2 \\ &= \mathcal{D}_3, \end{aligned} \quad (4.37)$$

$$\mathcal{D}_1^{-\frac{a}{2}} = \frac{1}{2} \left(\mathbf{Y}^{-\frac{a}{2}} + \mathbf{W}^{-\frac{a}{2}} \right), \quad (4.38)$$

$$\mathcal{D}_2^{-\frac{a}{2}} = \frac{1}{2} \left(\mathbf{Y}^{-\frac{a}{2}} - \mathbf{W}^{-\frac{a}{2}} \right), \quad (4.39)$$

$$\mathcal{D}_3^{-\frac{a}{2}} = \mathbf{W}^{-\frac{a}{2}}. \quad (4.40)$$

As a result, \mathcal{D}_1 , \mathcal{D}_2 , and \mathcal{D}_3 need to be constructed, so as to construct \mathbf{Y} and \mathbf{W} . This can be simplified by recognising $\mathcal{D}_3 = \mathcal{D}_1 - \mathcal{D}_2$, which gives:

$$W_{ab}^{ij} = \delta_{ab} \delta_{ij} + T_{ca}^{ik} T_{jk}^{cb} \quad (4.41)$$

$$Y_{ab}^{ij} = W_{ab}^{ij} + 4T_{ac}^{ik} T_{jk}^{bc} - 2T_{ca}^{ik} T_{jk}^{bc} - 2T_{ac}^{ik} T_{jk}^{cb} \quad (4.42)$$

Spin-adapted amplitudes

The spin-adapted transformed amplitude equations can be written as,

$$\begin{aligned} {}_q T_{ab}^{ij} &= \left[(\mathcal{A} U^{-\frac{a}{2}})_{ac} T_{cb}^{ij} + (\mathcal{A} U^{-\frac{a}{2}})_{bc} T_{ac}^{ij} \right] \\ &+ \left[(\mathcal{B} U^{-\frac{a}{2}})_{ki} T_{ab}^{kj} + (\mathcal{B} U^{-\frac{a}{2}})_{kj} T_{ab}^{ik} \right] \\ &- \left[(\mathcal{C} U^{-\frac{a}{2}})_{ki}^{lj} T_{ab}^{kl} \right] \\ &- \frac{1}{2} (1 + \tau_{ij} \tau_{ab}) \left[(Y^{-\frac{a}{2}})_{ac}^{ik} (T_{cb}^{kj} - \frac{1}{2} T_{bc}^{kj}) \right. \\ &\left. + \frac{1}{2} (W^{-\frac{a}{2}})_{ac}^{ik} T_{bc}^{kj} + (W^{-\frac{a}{2}})_{ac}^{jk} T_{cb}^{ik} \right], \end{aligned} \quad (4.43)$$

where the tensors defined in Eq. 4.36 have been used.

Spin-adapted residual

Finally, the residual in terms of spatial-orbitals becomes,

$$\begin{aligned}
{}_q G_{ab}^{ij} = & (1 + \tau_{ab}\tau_{ij}) \left\{ \left[({}^A R_{af} + {}^A R_{fa})(2T_{eb}^{ij} - T_{be}^{ij}) + {}_q V_{cb}^{ij} ({}^A U^{-\frac{q}{2}})_{ca} \right] \right. \\
& + \left[({}^B R_{oi} + {}^B R_{io})(2T_{ab}^{oj} - T_{ba}^{oj}) + {}_q V_{ab}^{kj} ({}^B U^{-\frac{q}{2}})_{ik} \right] \\
& - \left[({}^C R_{oi}^{pj} + {}^C R_{io}^{jp})T_{ab}^{op} + {}_q V_{ab}^{kl} ({}^C U^{-\frac{q}{2}})_{ik}^{jl} \right] \\
& - \frac{1}{2} \left[{}^{\mathcal{D}} R_{ag}^{io} (8T_{gb}^{oj} - 4T_{bg}^{oj}) \right. \\
& - {}^{\mathcal{D}} R_{bg}^{io} (4T_{ga}^{oj} - 2T_{ag}^{oj}) + 2 {}^{\mathcal{D}} R_{bg}^{io} T_{ag}^{oj} \\
& + {}_q V_{cb}^{kj} (Y^{-\frac{q}{2}})_{ca}^{ki} - \frac{1}{2} {}_q V_{ca}^{kj} (Y^{-\frac{q}{2}})_{cb}^{ki} \\
& \left. + \frac{1}{2} {}_q V_{ca}^{kj} (W^{-\frac{q}{2}})_{cb}^{ki} + {}_q V_{cb}^{ik} (W^{-\frac{q}{2}})_{ca}^{kj} \right] \left. \right\}, \tag{4.44}
\end{aligned}$$

where the intermediate quantities are defined:

$$\begin{aligned}
{}^A R_{ea} &= Q[\mathbf{U}, x]_{e,f}^{a,c} {}^A F_{ac}, & {}^B R_{im} &= Q[\mathbf{U}, x]_{o,m}^{k,i} {}^B F_{ki}, \\
{}^C R_{om}^{pn} &= Q[\mathbf{U}, x]_{op,mn}^{kl,ij} {}^C F_{ki}^{lj}, & {}^{\mathcal{D}}_1 R_{eg}^{mo} &= Q[\mathbf{Y}, x]_{em,go}^{ai,ck} {}^{\mathcal{D}}_1 F_{ac}^{ik}, \\
{}^{\mathcal{D}}_2 R_{eg}^{mo} &= Q[\mathbf{W}, x]_{em,go}^{ai,ck} ({}^{\mathcal{D}}_2 F + {}^{\mathcal{D}}_3 F)_{ac}^{ik},
\end{aligned} \tag{4.45}$$

$$\begin{aligned}
{}^A F_{ac} &= {}_q V_{ab}^{ij} T_{cb}^{ij}, & {}^B F_{ki} &= {}_q V_{ab}^{ij} T_{ab}^{kj}, \\
{}^C F_{ki}^{lj} &= {}_q V_{ab}^{ij} T_{ab}^{kl}, & {}^{\mathcal{D}}_1 F_{ac}^{ik} &= (T_{cb}^{kj} - \frac{1}{2} T_{bc}^{kj}) {}_q V_{ab}^{ij}, \\
{}^{\mathcal{D}}_2 F_{ac}^{ik} &= \frac{1}{2} T_{bc}^{kj} {}_q V_{ab}^{ij}, & {}^{\mathcal{D}}_3 F_{ac}^{ik} &= T_{cb}^{kj} {}_q V_{ab}^{ij},
\end{aligned} \tag{4.46}$$

4.1.4 Contravariant configurations

The doubly excited SDs that are generated by the transformed excitation operators are not orthogonal, [43]

$$\langle \Phi_{ij}^{ab} | \Phi_{kl}^{cd} \rangle = 4\delta_{ac}\delta_{bd}\delta_{jl}\delta_{ik} + 4\delta_{bc}\delta_{ad}\delta_{jk}\delta_{il} - 2\delta_{ac}\delta_{bd}\delta_{il}\delta_{jk} - 2\delta_{bc}\delta_{ad}\delta_{jl}\delta_{ik}, \tag{4.47}$$

making terms like Eq. 4.4 difficult to evaluate.

Instead, it is useful to project onto the space spanned by the orthogonal complement to $|\Phi_{ij}^{ab}\rangle$, [102, 113]

$$\langle \check{\Phi}_{ij}^{ab} | = \frac{1}{3} \langle \Phi_{ij}^{ab} | + \frac{1}{6} \langle \Phi_{ji}^{ab} |. \tag{4.48}$$

This yields the desired orthogonal relationship,

$$\langle \check{\Phi}_{ij}^{ab} | \Phi_{kl}^{cd} \rangle = \delta_{ik}\delta_{jl}\delta_{ac}\delta_{bd} + \delta_{il}\delta_{jk}\delta_{ad}\delta_{bc}, \tag{4.49}$$

where the normalisation is chosen to obey,

$$\langle \check{\Phi}_{ij}^{ab} | \Phi_{ij}^{ab} \rangle = 1 + \delta_{ij} \delta_{ab}. \quad (4.50)$$

Using the orthogonal complement also makes optimisation of the cluster amplitudes easier. For the iterative update, the second derivatives of the amplitudes are required. This can be approximated by a diagonal matrix that assumes the off-diagonal blocks of the Hessian to be small (a Quasi-Newton method). In the non-orthogonal basis, this is not necessarily true. The new basis minimises these blocks and allows this approximation to be made; the inverse of the Hessian matrix would need to be constructed otherwise.

As a result, two new tensors must be defined,

$${}_q \mathbb{V}_{ij}^{ab} = 2 {}_q V_{ij}^{ab} - {}_q V_{ji}^{ab}, \quad (4.51)$$

and inserted into the energy and residual expression instead of ${}_q V_{ij}^{ab}$. This allows the contravariant sum of the residual expression to be taken,

$$\mathbb{G}_{ab}^{ij} = \frac{1}{3} \frac{\partial E}{\partial T_{ab}^{ij}} + \frac{1}{6} \frac{\partial E}{\partial T_{ba}^{ij}}, \quad (4.52)$$

which defines the final residual used within the program.

4.2 Implementation

4.2.1 Integrated Tensor Framework

The spin-adapted equations presented in this chapter have been programmed into Molpro using the Integrated Tensor Framework (ITF). [14]. The philosophy behind the ITF is that of division of labour: the quantum chemist should work on theory and equations while the computer scientist should work on the implementation. This allows developers to easily program equations and generate fast and efficient code.

The ITF effectively forms a layer between the quantum chemical equations and the concrete implementation of these on a computer. It allows the input of a generic set of instructions, the tensor equations, which the computer decides how best to implement, *e.g.* memory allocation and addressing of tensors, spatial symmetry, parallelism and input-output operations. [74] It achieves this by

allowing the user to write in a domain specific language which is centred around binary tensor contractions, but hiding how the tensors are actually contracted and stored. Several python scripts are used to convert this high-level language into assembler code (postfixed by `.itfa`) which is read and executed by a virtual machine which contains fast matrix multiplication routines.

To date there has been little documentation about the ITF and its language, therefore the basics will be outlined here.

Code is written into a `.itfaa` algorithm file. Each of these files start with a declaration of the index space and a set of tensors that will be used in the code:

```

---- decl
index-space: ijklmn, Closed, c
index-space: abcd, External, e
index-space: CD, Core, C

tensor: aU[aa], !Create{type:disk}, aU
tensor: bU[ii], !Create{type:disk}, bU
tensor: cU[iiii], !Create{type:disk; sym:01/23}, cU
tensor: W[aa ii], !Create{type:disk; sym:01/23}, W
tensor: Y[aa ii], !Create{type:disk; sym:01/23}, Y

```

This block is headed by the `---- decl` header and continues until the start of a new header.

In the example above, a set of occupied and virtual indices are declared using the `Closed` and `External` keywords respectively. Core indices, *i.e.* orbitals in which no excitations occur, can also be declared with `Core`. The three index-spaces are labelled `c`, `e` and `C` for ease of reference.

A tensor can be declared using `tensor:`, followed by the name and index space. For example, the $\mathcal{A}\mathbf{U}$ tensor is only indexed within the external space, while \mathbf{W} and \mathbf{Y} rank-4 tensors have indices in both the closed and external spaces. For these tensors, the first and third form the first composite index, while the second and fourth form the second.

If the tensor does not already exist by default in the ITF, then it must be explicitly created by using the `!Create{type:disk}` option. The permutational symmetry of the indices can be optionally specified using the `sym:01/23` option; in this example, this

defines,

$$cU_{ki}^{lj} = cU_{ik}^{jl}. \quad (4.53)$$

The equations are then written into blocks of code that are called by the driver program. For example, the t_{ab}^{ij} equation of Eq. 4.43 can be directly written into the .itfaa file:

```

---- code ("QVCCD_qT")
alloc T1[abij]
load aUm05[*c]
.T1[abij] += aUm05[ac] C[cbij]
.T1[abij] += aUm05[bc] C[acij]
drop aUm05[*c]
load bUm05[k*]
.T1[abij] += bUm05[ki] C[abkj]
.T1[abij] += bUm05[kj] C[abik]
drop bUm05[k*]
load cUm05[kilj]
.T1[abij] -= cUm05[kilj] C[abkl]
drop cUm05[kilj]
load d3Um05[ac*k], Ym05[acik], L1[cbkj]
.T1[abij] -= Ym05[acik] L1[cbkj]
.T1[abij] -= 0.5 * d3Um05[acik] C[bckj]
.T1[abij] -= d3Um05[acjk] C[cbik]
drop L1[cbkj], Ym05[acik], d3Um05[ac*k]
store T1[abij]

```

Each block of equations starts with the ---- code header followed by a name which can be referred to in the driver program. This block continues until another code block is started or the ---- end footer is used.

Memory for tensors can be allocated on the stack using the `alloc` keyword; this also serves the purpose of initialising all elements to zero within the tensor. The `load` command can be used to reload previously initialised tensors back onto the stack. The tensor contractions then appear as they do in Eq. 4.43, without the need for any explicit loops; the ITF will generate code that automatically loops over the dummy indices. The indices can either be explicitly written or the wild card `*` can be used if there is no ambiguity as to which tensor object is being referred to. Finally a tensor can be

removed from the stack with `drop`, or placed into the heap with `store`.

The tensor names in the above code have been chosen so it is obvious as to what they refer to. The only difference with the naming convention of Eq. 4.43 is the `L1` intermediate which is just,

$$(L1)_{cb}^{kj} = T_{cb}^{kj} - \frac{1}{2}T_{bc}^{kj}. \quad (4.54)$$

Loops over specific indices can be used to load in certain blocks of the tensor at one time, thereby reducing the memory consumption. For example,

```
for [i,j]:

    alloc V1[**ij]
    load K4E[**ij]
    .V1[**ij] += K4E[**ij]
    drop K4E[**ij]

    load Ki[**ij]
    .V1[**ij] += T1[**kl] Ki[klij]
    drop Ki[**ij]
```

This loads in and loops over the blocks indexed by the closed indices. The syntax follows that of Python, where a loop is indicated by the level of indentation.

Finally, if-statements can also be simulated. In essence, these create another `.itfca` file which Molpro will then use. To do this, the different `.itfca` files must be defined at the start of the code:

```
#algo QVCCD
#algo OQVCCD: orb_opt
```

This will create two files, `QVCCD.itfca` and `OQVCCD.itfca`. The ‘if-statements’ can then be placed in the code, for example:

```
#if orb_opt
// Update singles residual
...
#endif
```

The singles residual should be updated when running a `OQVCCD` calculation, but not for a `QVCCD` calculation. With the `#if` and `#endif` statements, the `QVCCD.itfca` file

will not include this code and therefore will not execute it, while the OQVCCD code will.

All the code generated by the ITF is fully parallelised, allowing for a significant speed up to occur when using several processors.

4.2.2 Auxiliary code

At the present time, the ITF has several limitations that require auxiliary C++ code to be written. For example, the ITF can not diagonalise tensors, so forming powers of the \mathbf{U} tensors and forming the \mathbf{Q} intermediate must occur outside of the ITF.

This means that the ITF code must be structured around these calls to the C++ code. For example, the transformation matrices must be formed in the ITF, before being extracted and raised to a power in the C++. All of the tensors in the ITF map onto class objects and can be easily manipulated.

qTransform

The \mathbf{Q} intermediate of Eq. 4.6 must be formed outside of the ITF. This can be split into several intermediates,

$$Q_{ij} = (C_{ik} + A_{ik})X_{kj}^T, \quad (4.55)$$

$$C_{mk} = \begin{cases} \sum_{\substack{k,l,m \\ k \neq l}} \frac{\epsilon_k^x - \epsilon_l^x}{\epsilon_k - \epsilon_l} B_{kl} X_{ml}, & \epsilon_k - \epsilon_l > 1 \times 10^{-8} \\ x \sum_{\substack{k,l,m \\ k \neq l}} \frac{\epsilon_k^x}{\epsilon_k} B_{kl} X_{ml}, & \epsilon_k - \epsilon_l \leq 1 \times 10^{-8} \end{cases} \quad (4.56)$$

$$A_{mk} = x \sum_{k,m} B_{kk} \frac{e_k^x}{e_k} X_{mk}, \quad (4.57)$$

$$B_{ij} = D_{ik} X_{kj}, \quad (4.58)$$

$$D_{ij} = F_{ik} X_{kj}, \quad (4.59)$$

where \mathbf{X} and ϵ are the eigenvectors and eigenvalues of \mathbf{U} ,² x is the power and \mathbf{F} are the intermediates defined in Eq. 4.46.

The BLAST library has been used where possible, however, this can not be used when forming the \mathbf{C} intermediate. The computational expense of forming this step can be mitigated by using the MPI library to make the loop run on parallel processors.

²By modifying the existing C++ object, the eigenvectors and eigenvalues can be calculated once per iteration, stored, then used to form the powers of \mathbf{U} and \mathbf{Q} intermediate.

Orbital Optimisation

The previous chapter discussed the inclusion of single excitations implicitly into the QVCCD energy.

For the orbital optimisation procedure, the energy derivative with respect to the orbitals needs to be constructed. The spin-adapted expression can be written as, [96, 103]³

$$\begin{aligned}
\frac{\partial E}{\partial \phi} = f_a = & F_a^i - T_j^i F_a^j - T_a^b F_b^i \\
& - T_l^k (2 \langle il|ak \rangle - \langle li|ak \rangle) \\
& + T_d^c (2 \langle id|ac \rangle - \langle di|ac \rangle) \\
& + {}_1T_{cd}^{ik} {}_1\tilde{T}_{jl}^{cd} \langle jl|ak \rangle - {}_1\tilde{T}_{ac}^{kl} {}_1T_{kl}^{bd} \langle ic|bd \rangle \\
& - \frac{1}{2} ({}_1\tilde{T}_{bd}^{ik} {}_1\tilde{T}_{jk}^{cd} + 3 {}_1T_{bd}^{ki} {}_1T_{kj}^{cd}) \langle jb|ac \rangle \\
& + \frac{1}{2} ({}_1\tilde{T}_{ac}^{jl} {}_1\tilde{T}_{kl}^{bc} + 3 {}_1T_{ac}^{lj} {}_1T_{lk}^{ac}) \langle ik|bj \rangle \\
& + {}_1\tilde{T}_{bd}^{ik} {}_1\tilde{T}_{jk}^{cd} \langle bj|ac \rangle - {}_1\tilde{T}_{ac}^{jl} {}_1\tilde{T}_{kl}^{bc} \langle ik|jb \rangle \\
& + 2\tilde{T}_{bc}^{ij} \langle bc|aj \rangle - 2\tilde{T}_{ab}^{jk} \langle ib|jk \rangle, \tag{4.60}
\end{aligned}$$

where the intermediate quantities are defined as,

$$\begin{aligned}
q\tilde{T}_{ab}^{ij} &= 2 {}_qT_{ab}^{ij} - qT_{ba}^{ij}, \\
T_j^i &= {}_1\tilde{T}_{ab}^{ik} {}_1T_{jk}^{ab}, \\
T_a^b &= {}_1\tilde{T}_{ac}^{ij} {}_1T_{ij}^{bc}, \\
F_q^p &= h_q^p + (2 \langle pi|qi \rangle - \langle pi|iq \rangle). \tag{4.61}
\end{aligned}$$

This can be simplified for a more efficient implementation by collecting together terms

³There is a typo in the original paper by Robinson. Lines two and six of Eq.4.60 were written:

$$\begin{aligned}
& - \frac{1}{2} ({}_1\tilde{T}_{bd}^{ik} {}_1\tilde{T}_{cd}^{jk} + 3 {}_1\tilde{T}_{bd}^{ki} {}_1\tilde{T}_{cd}^{kj}) \langle ja|bc \rangle \\
& + \frac{1}{2} ({}_1\tilde{T}_{ac}^{jl} {}_1\tilde{T}_{bc}^{kl} + 3 {}_1\tilde{T}_{ac}^{lj} {}_1\tilde{T}_{bc}^{lk}) \langle ib|kj \rangle
\end{aligned}$$

that involve the same Coulomb or exchange integrals,

$$\begin{aligned}
f_a^i &= F_a^i - T_j^i F_a^j - T_a^b F_b^i \\
&+ {}_1N_{ik}^{jl}(ja|lk) - {}_2N_{ac}^{bd}(ib|cd) \\
&+ {}_3N_{bc}^{ij}(ja|bc) \\
&+ {}_4N_{ab}^{jk}(ib|kj) \\
&+ {}_5N_{bc}^{ij}(ba|jc) + {}_6N_{ab}^{jk}(ij|kb), \tag{4.62}
\end{aligned}$$

where the following intermediates are defined as,

$$\begin{aligned}
{}_1N_{ik}^{jl} &= {}_1T_{cd}^{ik} {}_1\tilde{T}_{cd}^{jl}, \\
{}_2N_{ac}^{bd} &= {}_1\tilde{T}_{ac}^{kl} {}_1T_{bd}^{kl}, \\
{}_3N_{bc}^{ij} &= 2\delta_{ij}T_b^c - \frac{1}{2}({}_1\tilde{T}_{bd}^{ik} {}_1\tilde{T}_{cd}^{jk} + 3{}_1\tilde{T}_{bd}^{ki} {}_1\tilde{T}_{cd}^{kj}), \\
{}_4N_{ab}^{jk} &= \frac{1}{2}({}_1\tilde{T}_{ac}^{jl} {}_1\tilde{T}_{bc}^{kl} + 3{}_1\tilde{T}_{ac}^{lj} {}_1\tilde{T}_{bc}^{lk}) - 2\delta_{ab}T_j^k, \\
{}_5N_{bc}^{ij} &= {}_1\tilde{T}_{bd}^{ik} {}_1\tilde{T}_{cd}^{jk} + 2\tilde{T}_{bc}^{ij} - \delta_{ij}T_b^c, \\
{}_6N_{ab}^{jk} &= \delta_{ab}T_k^j - {}_1\tilde{T}_{ac}^{jl} {}_1\tilde{T}_{bc}^{kl} - 2\tilde{T}_{ab}^{jk}. \tag{4.63}
\end{aligned}$$

Within the program, ${}_3N_{bc}^{ij}$ and ${}_5N_{bc}^{ij}$ are constructed then contracted with the three external integrals using an external call to the Fortran code within Molpro. The rest of the integral contractions take place within the ITF.

For an OQVCCD calculation, Eq. 4.62 is constructed and passed from the C++ code into Fortran. It is used to call a previously existing function called *absorb*, which creates the exponential operator from the residual. This rotates the orbitals and a new set of integrals are calculated, which are used in the next iteration.

Triples corrections

The triples correction from Chapter 3 can be rewritten as a series of tensor contractions, [114, 115]

$$\begin{aligned}
E_{(T)} &= -\frac{1}{3}W_{ijk}^{abc}R_{abc}^{ijk}, \\
R_{abc}^{ijk} &= \left(4W_{ijk}^{abc} + W_{kij}^{abc} + W_{jki}^{abc} - 2W_{kji}^{abc} - 2W_{ikj}^{abc} - 2W_{jik}^{abc}\right)/D_{ijk}^{abc}, \\
W_{ijk}^{abc} &= P_{ijk}^{abc}\left(T_{ij}^{ad}\langle cb|kd\rangle - T_{ij}^{ad}\langle cl|kj\rangle\right), \\
D_{ijk}^{abc} &= \epsilon_i + \epsilon_j + \epsilon_k - \epsilon_a - \epsilon_b - \epsilon_c. \tag{4.64}
\end{aligned}$$

P_{ijk}^{abc} is a permutation operator that permutes the occupied and virtual indices simultaneously.

This correction can only be applied to a canonical set of orbitals due to the eigenvalues of these being in the denominator. However, with orbital optimisation, the orbitals are rotated every iteration and so are no longer canonical.

Two schemes can be devised that can result in a canonical set of orbitals. The off-diagonal blocks in the Fock matrix (F_{ai}) can be set to zero and the resulting matrix diagonalised every iteration and a new set of integrals calculated. Alternatively, the Fock matrix can be diagonalised after the energy has converged, a new set of integrals calculated and the cluster amplitudes rotated using the eigenvectors of the Fock matrix.

The second approach requires passing the eigenvectors of the Fock matrix into the ITF, or passing the cluster amplitudes from the ITF into the Fortran code. The first scheme, doesn't require this and so was attempted first due to apparent ease of implementation. Numerical tests however proved to be disappointing as changing the Fock matrix affected the convergence of the method. The second scheme was implemented and was successful in matching the number of iterations from the old implementation.

Renormalised triples

The renormalised triples can be easily implemented into the ITF after the standard triples code has been made to work. This only requires rotating the ${}_1T$ transformed cluster amplitudes instead of the standard cluster amplitudes, then sending these to the triples code. This means replacing the cluster amplitudes in Eq. 4.64 with ${}_1T_{ij}^{ad}$

The asymmetric triples requires an extra tensor intermediate; one formed from the ${}_2T$,

$$E_{(T)} = -\frac{1}{3}V_{ijk}^{abc}R_{abc}^{ijk}, \quad (4.65)$$

$$V_{ijk}^{abc} = P_{ijk}^{abc} \left({}_2T_{ij}^{ad} \langle cb|kd \rangle - {}_2T_{ij}^{ad} \langle cl|kj \rangle \right). \quad (4.66)$$

All intermediate quantities are the same as in Eq. 4.64. This can be achieved without an increase in memory, as both intermediates do not appear on the stack at the same time.

Chapter 5

Benchmarking and applications

To date there have been several performance studies of the Quasi-Variational Coupled-Cluster Doubles family of methods, hereafter collectively denoted as the QV methods. [107, 116, 117]. This work will be continued by applying the QV methods to larger and more interesting examples.

In Section 5.1, the Potential Energy Curves (PECs) for third-row diatomic molecules will be examined and compared to those obtained with multireference methods. Section 5.2 will examine the differences in using the QV methods, as opposed to other single-reference methods, to calculate activation and reaction energies. Numerical tests will be carried out in Section 5.3 with the asymmetric-renormalised triples correction and compared to OQVCCDR(T). Finally the computational timings and scaling of the QV methods will be presented in Section 5.4.

5.1 PECs and diatomic constants

It is well documented that traditional Coupled-Cluster methods, like CCSD, produce errors in the wavefunction and energy when used to describe chemical systems with strong non-dynamic correlation [64].

For molecules, this occurs typically when covalent bonds are extended, and is most pronounced for the breaking of double and triple bonds. Normally, such situations have to be investigated with multireference (MR) methods, which means choosing a suitable active space into which the approximate wavefunction can be expanded. The use of MCSCF, with subsequent treatment of dynamical correlation effects through MRCI or related approaches, has been very successful in generating global ground and excited state potential energy surfaces for small molecules.

However, for larger molecules, the difficulty of choosing a suitable active space,

the computational scaling with system size, and the lack of a practical general size-extensive formulation, all provide an impetus for seeking alternative approaches. The QV methods can bridge this gap between a single-reference formalism and capturing non-dynamic correlation.

The previous computational implementation of the QVCCD method suffered from long computational times, meaning that previous studies were limited in the size of system that could be addressed. In the current work, the QVCCD code has been completely rewritten within the Integrated Tensor Framework (ITF) (as described in Chapter 4), to allow calculation of larger systems.

PECs and vibrational constants of third-row diatomic molecules will be investigated and compared with CCSD(T), MRCI and the Distinguishable Cluster (DCSD) approximation. Size consistency errors will also be determined by comparing the asymptotic values of the QV methods and the dissociation energy calculated with the separated atoms.

5.1.1 Computational details

All calculations have been carried out using Molpro and the ITF implementation of the QV methods. For each system, a potential energy curve has been calculated, from which diatomic constants can be determined by polynomial fitting. The number of points in the curve and the degree of the polynomial were increased until the constants converged to an answer. All energies and spectroscopic quantities have been calculated using CCSD(T), the three QV methods (OQVCCD(T), OQVCCDR(T), OQVCCDAR(T)), DCSD and MRCI, with and without cluster corrections. The valence space was chosen for each active space, apart from Cl₂ which has been extended to produce smooth curves for the calculation of the spectroscopic constants. For comparison with empirical values, [118] CCSD(T) calculations have been carried out by correlating the core orbitals and including relativistic scalar effects *via* the second-order Douglas-Kroll-Hess Hamiltonian. [119]

All energy calculations have been extrapolated from the cc-pVQZ and cc-pV5Z basis sets, while the relativistic calculations have been extrapolated from cc-pwCVQZ-dk and cc-pwCV5Z-dk.¹

The size consistency error was estimated for these methods by taking the difference of the dissociation energy calculated from the asymptotic limit and the dissociation energy calculated from the separate atoms. Open-shell QV methods are currently not

¹Please see Ref. [120] for relevant data and Molpro inputs.

available, so the atomic energies were calculated using RCCSD(T). These are predicted to differ little from the hypothetical open-shell QV methods.

The OQVCCDAR(T) PECs have not been included on the graphs for clarity. Discussion of the performance of this method compared to OQVCCDR(T) will be deferred until Section 5.3.

5.1.2 Singly bonded molecules

A majority of chemical reactions involve breaking and forming single bonds. Therefore it is important for a quantum chemical method to describe this phenomenon correctly. To start, we investigate the breaking of three singly bonded molecules; HCl, BCl and Cl₂.

HCl

For the dissociation of HCl, Fig. 5.1, we observe the typical behaviour of CCSD(T) at long bond lengths: the energy forms a maximum, in this case around 3.0 Å, before falling rapidly. OQVCCD(T) also matches this behaviour, illustrating the breakdown of the (T) correction. Eigenvalues of the Fock matrix appear in the denominator of this correction and so can lead to an over-estimation of the effects of the triples when these eigenvalues are close in energy. This problem can be corrected by using a renormalised triples scheme.

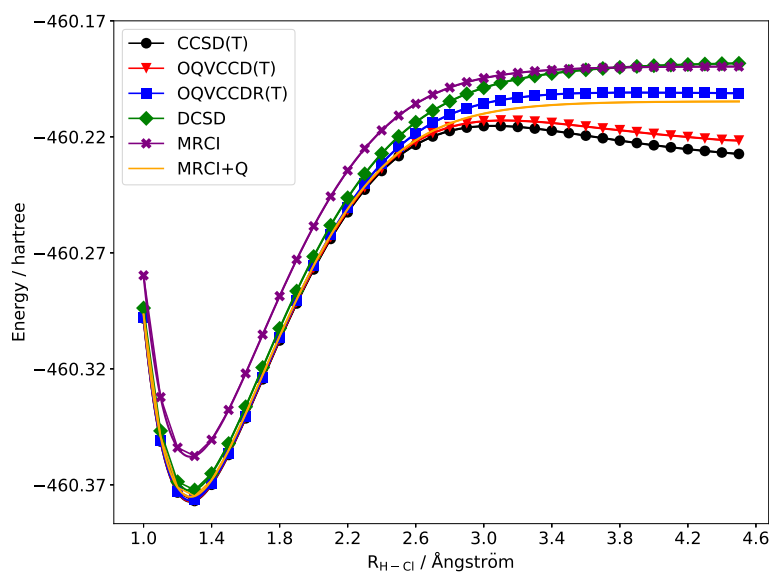


Figure 5.1: Calculated potential energy curves for HCl with extrapolated cc-pVQZ:cc-pV5Z basis set.

OQVCCDR(T) performs well, leading to a flat dissociation limit of around -460.201 hartree, which is bounded by both the MRCI and MRCI+Q energies. DCSD also performs well, leading to a dissociation energy slightly above the MRCI energy. The size consistency error for the renormalised QV methods, shown in Table 5.2, is an order of magnitude larger than the MRCI error, however it is an order of magnitude less than the OQVCCD(T) error.

All the QV methods predict a first vibrational constant in agreement with the CCSD(T) value (Table 5.1); there is a slight over prediction of around 5 cm^{-1} from the renormalised QV methods.

BCl

For BCl (Fig. 5.2) the error in the CCSD(T) energy comes mainly from the inability to model multi-reference systems, as OQVCCD(T) produces an energy that is qualitatively similar to the MR methods. At around 4.0 \AA , the CCSD(T) energy sharply drops. The Renormalised QV methods do not form this maximum and flatten out to asymptotic limits. The symmetric- and asymmetric-renormalised triples predict a slightly higher energy than the standard triples at long bond lengths; the difference being 0.014 hartree. Surprisingly, the standard triples correction produces a lower size consistency error than the renormalised QV methods by two orders of magnitude.

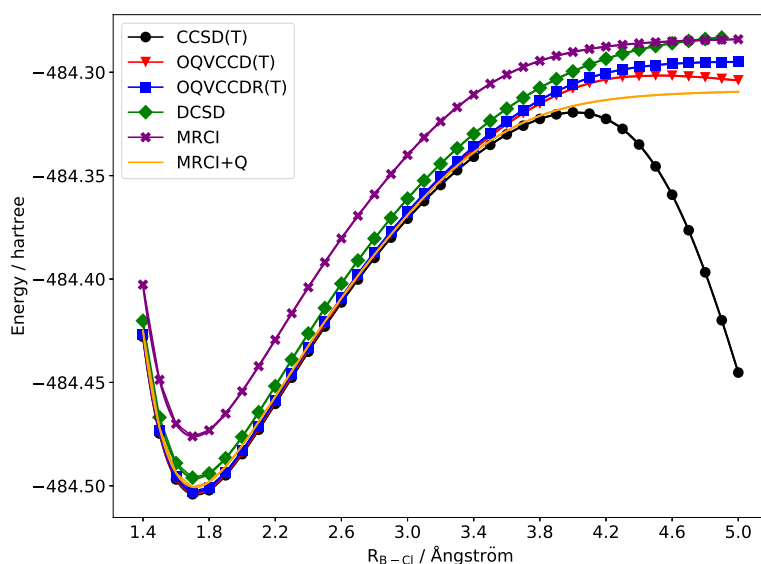


Figure 5.2: Calculated potential energy curves for BCl with extrapolated cc-pVQZ:cc-pV5Z basis set.

The QV methods and DCSD predict vibrational constants which are close to the

CCSD(T) and empirical values.

Cl₂

Coupled-cluster theory again produces a maximum at long bond lengths for Cl₂, in part due to the breakdown of the triples correction (Fig. 5.3). Both renormalised QV methods follow the MCRI+Q energy, with an over prediction in energy from 3.0 Å. The energy for both these methods does start to fall slowly at 4.3 Å, the difference between here and 6.5 Å being 1.8×10^{-3} hartree. This can be explained by the non-variational nature of the QV methods; the energy is not bounded from below by the exact Schrödinger energy.

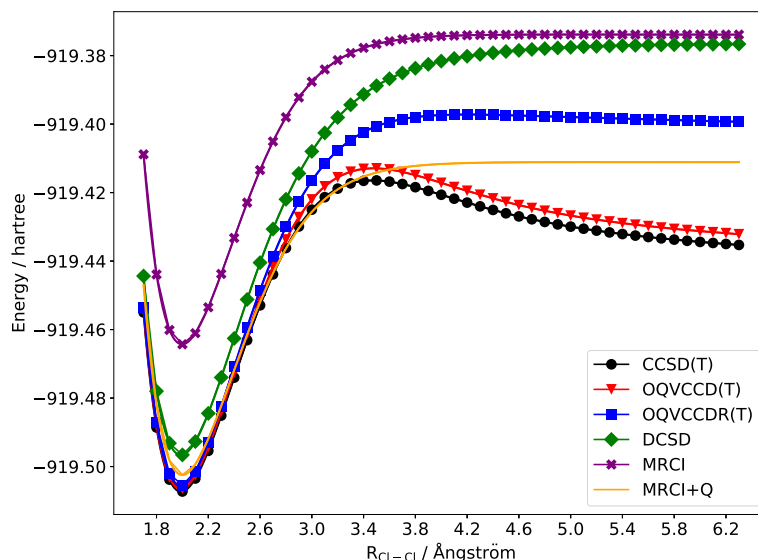


Figure 5.3: Calculated potential energy curves for Cl₂ with extrapolated cc-pVQZ:cc-pV5Z basis set.

The renormalised QV methods and MRCI converge to a larger asymptotic limit compared to OQVCCD(T) and MRCI+Q. The size consistency error for all the QV methods is an order of magnitude greater than the MR methods.

Again, all the QV methods predict vibrational constants that are close to the CCSD(T) values.

AlO⁻

Fig. 5.4 shows the potential energy curve for AlO⁻, formally a singly bonded anion. CCSD(T) fails when the MR nature of the the system becomes too large at around 3.4 Å. The QV methods are able to dissociate the molecule and lead to an asymptotic

	HCl	BCl	Cl ₂	AlO ⁻	S ₂	P ₂	SiO
CCSD(T)	2996.1	841.3	561.4	971.1	699.0	786.7	1241.8
CCSD(T)+	2997.1	841.3	561.4	972.8	702.1	792.9	1249.0
OQVCCD(T)	2999.0	842.6	565.2	978.6	707.8	797.2	1251.0
OQVCCDR(T)	3002.0	843.2	567.5	979.9	713.8	801.6	1253.1
OQVCCDAR(T)	3002.0	843.1	567.3	983.4	713.9	801.9	1252.8
DCSD	3001.8	844.2	564.1	987.4	700.2	787.9	1263.4
MRCI	2992.8	869.7	559.2	958.9	693.6	778.8	1227.8
MRCI+Q	2989.8	856.0	556.0	951.4	697.4	776.6	1222.0
Empirical	2991.0	839.1	559.7	-	699.7	1241.6	780.8

Table 5.1: ω_e/cm^{-1} with extrapolated cc-pVQZ:cc-pV5Z basis set. Empirical values taken from the NIST Chemistry WebBook. [118]

limit. The renormalised triples methods are bounded by the MRCI and MRCI+Q energies, but lead to an asymptotic limit at around -316.985 hartree, which is lower than the MRCI+Q energy by 0.02 hartree. All the QV and MR methods predict a lower asymptotic limit, producing a size consistency errors that are comparable in magnitude, however the cluster correction on MRCI appears to increase this error by an order of magnitude.

DCSD follows the MRCI+Q curve well, however flattens off earlier. After 3.1 Å it becomes difficult to converge the cc-PVQZ and cc-PV5Z answer to the same state and therefore interferes with the extrapolation.

All QV methods predict spectroscopic constants in agreement with CCSD(T).

	HCl	BCl	Cl ₂	AlO ⁻	S ₂
OQVCCD(T)	-0.019280	-0.000896	-0.020608	-0.022369	0.013717
OQVCCDR(T)	0.004131	0.012843	0.012595	0.002785	0.055709
OQVCCDAR(T)	0.004121	0.012866	0.012609	0.002837	0.057487
MRCI	-0.000213	0.030943	0.004076	-0.007330	0.018244
MRCI+Q	0.000009	0.034257	-0.001939	-0.021658	0.004454

Table 5.2: Size consistency error / hartree with extrapolated cc-pVQZ:cc-pV5Z basis set.

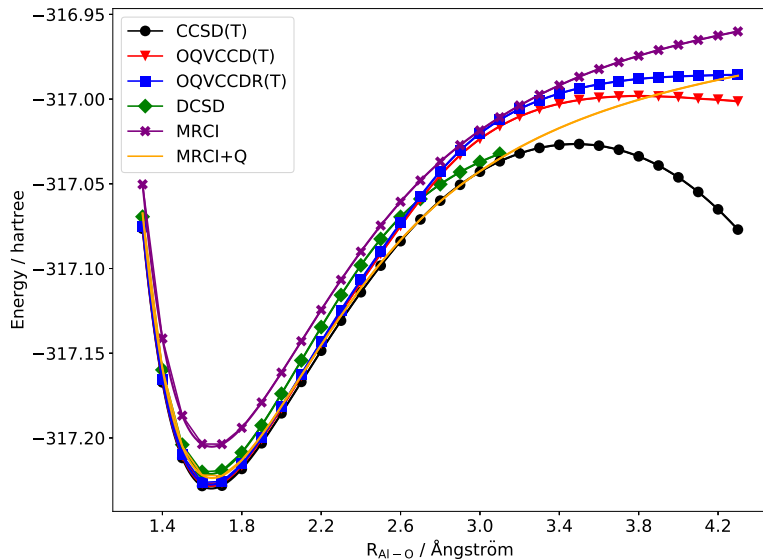


Figure 5.4: Calculated potential energy curves for AlO^- with extrapolated cc-pVQZ:cc-pV5Z basis set.

5.1.3 Multiply bonded molecules

Dissociation of doubly bonded molecules present another challenge. The S_2 molecule, an analogue of O_2 , is investigated.

S_2

For the Σ_g^+ excited state of S_2 , the QV methods are able to dissociate the molecule and produce a qualitatively correct PEC. Renormalised QV methods predict a slightly higher asymptotic value than MRCI, while the standard triples flattens out to a limit above the MRCI+Q energy. The multireference energies are quicker to reach an asymptotic limit compared to the renormalised QV methods, which is characteristic of ionic character in the wavefunction at long bond lengths. This behaviour is also mimicked with the DCSD method leading to very similar PECs beyond the equilibrium bond length. Interestingly the standard triples QV method does not exhibit this ionic character and follows the MRCI+Q energy well, nevertheless its energy gradually begins to fall at longer bond lengths.

The QV and MR methods over predict the dissociation energy with the largest size consistency error being produced by OQVCCDAR(T) of 0.057 hartree. The cluster correction to MRCI reduces this error by an order of magnitude compared to MRCI without the correction.

All QV methods predict larger vibrational constants than is expected from the

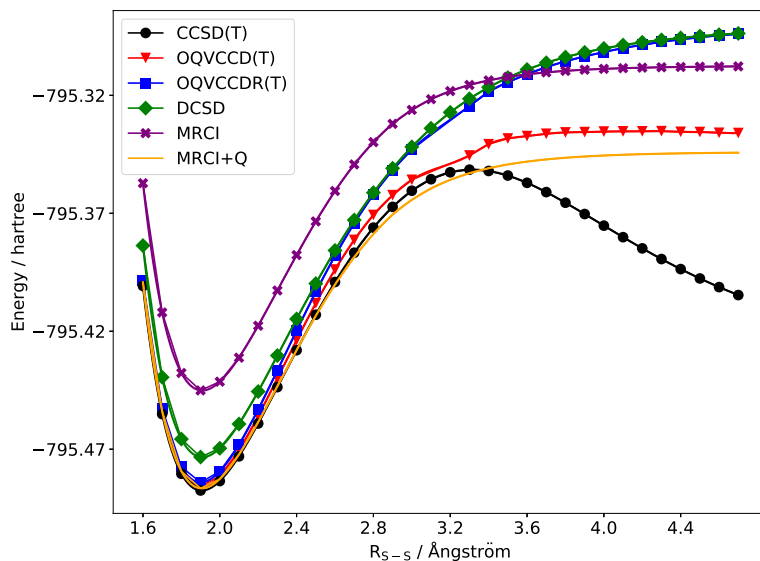


Figure 5.5: Calculated potential energy curves for S_2 with extrapolated cc-pVQZ:cc-pV5Z basis set.

CCSD(T); the renormalised methods both deviate from this value by around 15 cm^{-1} .

P_2

To break a triple bond, excitations up to hexuples should be included in the wavefunction expansion. CCSD(T) does not disprove this as the energy shows the unphysical maximum in Fig. 5.6. The QV results show a marked improvement even for these challenging systems. This is most likely due to the implicit inclusion of higher excitations *via* the $\mathbf{U}^{-\frac{q}{2}}$ tensors.

The QV energy for P_2 , an analogue of N_2 , shows it is able to predict a qualitatively correct PEC, even in large non-dynamic correlation regimes. The standard triples correction appears to perform better in this case, as the energy closely follows the MRCI energy, whereas the renormalised methods, including DCSD, exhibit strong ionic character, leading to larger asymptotic limits.

The QV methods all over predict the first vibrational constant; in this respect CCSD(T) provides a better estimate of this constant.

SiO

Again, all the QV methods can dissociate SiO without the energy dropping towards negative infinity, however all the triples schemes predict a higher energy at long bond lengths compared to MRCI (Fig. 5.7). The energy is no longer bounded by the MRCI

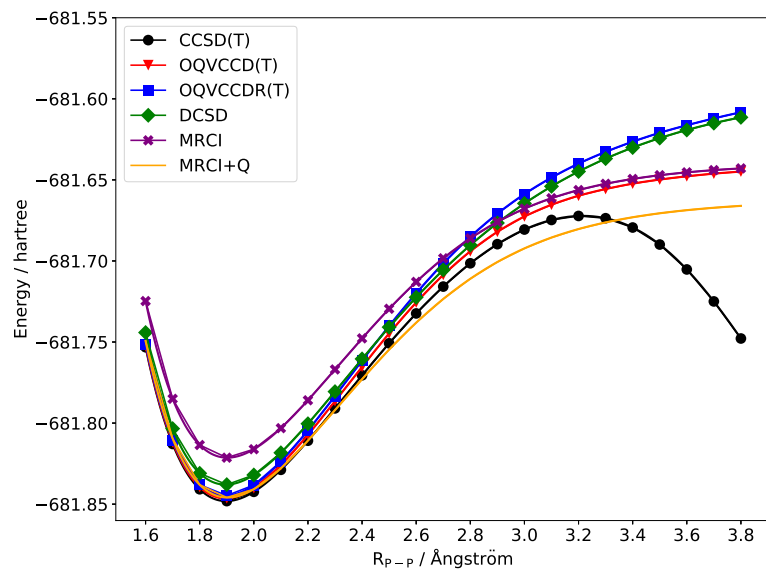


Figure 5.6: Calculated potential energy curves for P₂ with extrapolated cc-pVQZ:cc-pV5Z basis set.

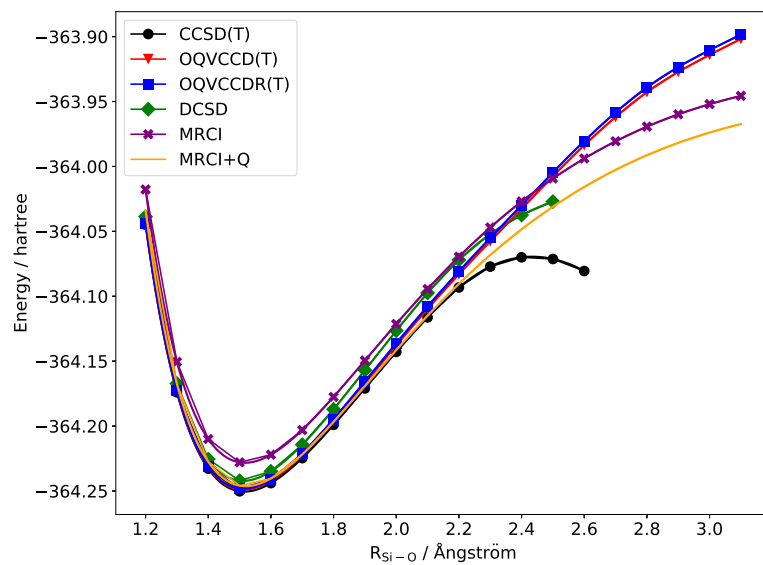


Figure 5.7: Calculated potential energy curves for SiO with extrapolated cc-pVQZ:cc-pV5Z basis set.

and MRCI+Q result. The standard (T) correction produces a very similar answer to the renormalised methods.

DCSD appears to flatten off to an asymptotic limit earlier than the MR methods. No further points could be calculated as the energy jumps to an excited state at beyond 2.5 Å.

The QV methods over predict the first vibrational constant by around $10\text{-}12\text{ cm}^{-1}$ compared with the CCSD(T) result.

Breaking two single bonds

Breaking more than one chemical bond at a time presents another challenge to single reference methods. As an accompaniment to the diatomic molecules, the PECs for the BeCl_2 were calculated and compared. This was achieved by symmetrically moving the Cl atoms away from the central Be atom (Fig. 5.8).

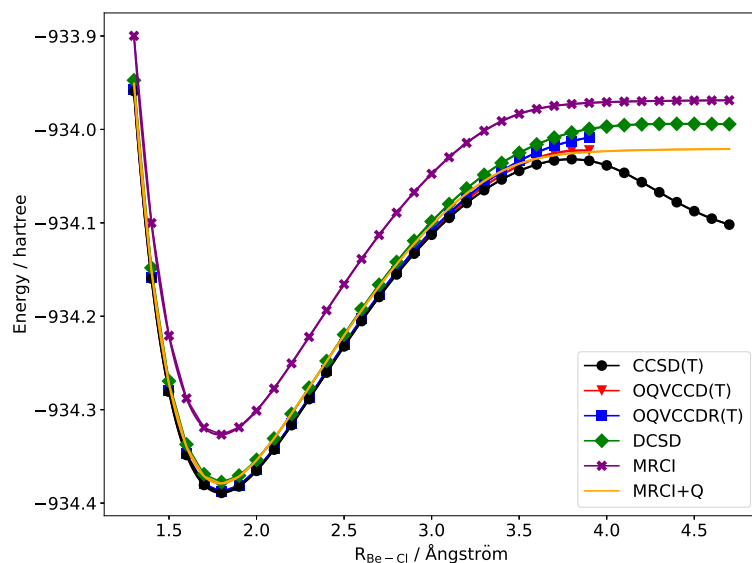


Figure 5.8: Calculated potential energy curves for BeCl_2 with extrapolated cc-pVQZ:cc-pV5Z basis set.

CCSD(T) again forms the familiar maximum at around 3.5 Å, whereas MRCI and DCSD dissociate to a flat limit above the MRCI+Q energy. The QV methods appear to also flatten out to asymptotic limits, however it became difficult to converge to the QV solution past 3.9 Å.

5.1.4 Conclusions

This investigation has provided more cases where the QV methods behave well when dissociating and breaking apart singly and multiply bonded molecules. The sharp maximum that is encountered when calculating PECs with CCSD(T) is avoided in all cases with the QV methods, apart from OQVCCD(T), which is susceptible to the breakdown of the non-iterative (T) correction. DCSD has also been shown to dissociate these diatomics while avoiding the unphysical maximum of CCSD(T).

The QV methods can provide reasonable estimates to the vibrational wavenumber and first anharmonicity constants, though, as has previously been recognised, they do not perform as well as CCSD(T). CCSD(T) generally behaves well in the immediate region of PEC minima and is therefore well suited to calculating these diatomic constants.

Estimates of the QV size consistency error have shown that there are large energy differences between the apparent asymptotic limit and the energy of the separated atoms. From the molecules examined, the largest difference is around 0.057 hartree for OQVCCDAR(T) and S₂. Several errors can account for these results. Firstly, it becomes difficult to converge the QV energy at bond lengths longer than the ones presented in the PECs, therefore the energy may not have completely converged to a limit. Another error must occur by using RCCSD(T) on the separated atoms instead of a QV method. Both of these problems are unfortunately unavoidable.

Finally, unpromising behaviour has been detected in the PECs of the multiply bonded molecules. The renormalised QV methods tend to over predict the energy at longer bond lengths for molecules like S₂, P₂ and SiO. The same results are seen with DCSD for S₂ and P₂. This is characteristic of residual ionic character in the wavefunction; a remnant from the single-reference wavefunction.

5.2 Determination of activation and reaction energies

The determination of activation and reaction energy changes is of great importance to theoretical chemistry. With an accurate description of the reactive potential energy surface, the kinetics and dynamics of the reaction can be investigated. With the energy changes of reaction, mechanistic pathways can be developed and intermediate species identified.

The determination of the activation energy can potentially pose a problem for

Traditional Coupled-Cluster methods such as CCSD(T). This is due to the fact that the transition state may possess multireference character owing to the often strained nature of the system. Therefore, a simple single-reference approach may not fully capture the non-dynamic correlation effects.

Instead of examining individual chemical reactions, large databases of pre-defined molecules and reactions can be employed. This allows the determination of statistical measurements for the quantities being calculated and thereby provide a more reliable picture of how different methods perform against each other.

In this current work, six different chemical databases are employed to determine the effects that the QV and TCC methods have when calculating activation and reaction energies.

5.2.1 Computational details

Two closed-shell databases were selected for the calculation of activation energies (E_a):

- **CRBH20** contains 20 cycloreversion transition states, the reverse processes of cycloaddition reactions. These include the fragmentation of 5-membered heterocyclic rings (10 dioxazoles and 10 oxathiazoles) into cyanate and carbonyl products [121]. These reactions also involve the migration of a hydrocarbon or hydrofluorocarbon substituent across a C=N bond.
- **BHPERI** consists of 26 transition states for pericyclic reactions compiled by Goerigk and Grimme. [122] These include 10 pericyclic reactions with unsaturated hydrocarbons such as an electrocyclic reaction of cyclobutene, Diels-Alder reactions with cyclopentadiene and cycloreversions of large molecules such as cis-triscyclopropacyclohexane. [123] Also included are three classes of 1,3-dipolar cycloadditions, involving diazonium, nitrilium and azomethine betaines to form 5-membered heterocyclic rings. [124] Finally, 7 Diels-Alder reactions are incorporated, involving the addition of ethylene to different 5-membered heterocycles. [125]

Two databases were chosen to investigate solely reaction energies (ΔE):

- **ISOMER20**. A closed-shell subset of this database was constructed from the 20 original organic isomerisation reactions; [126] this now consists of reaction energies for 16 endothermic reactions. These include isomerisations of small molecules like hydrogen cyanide and isocyanic acid, and larger molecules like ketene and acetaldehyde.

- **DARC** consists of 14 exothermic Diels-Alder reactions. [122, 127] These include reactions of dienes like butadiene and cyclopentadiene with ethene, ethyne, maleine and maleinimide.

Finally two databases were chosen that consist of both activation and reaction energies:

- **O3ADD6** contains 2 reactions with the addition of ozone to ethene and ethyne. [122, 128] The database is comprised of 2 barrier heights, 2 reaction energies and 2 van der Waals (vdW) energies for the associated ozonide complex.
- **CRIEGEE** is a newly constructed database which comprises of a reaction pathway, as shown in Fig. 5.9, involving a Criegee intermediate. This pathway consists of 3 sequential transition states and so in total provides a set of 3 activation energies and 1 exothermic and 2 endothermic reaction energies.

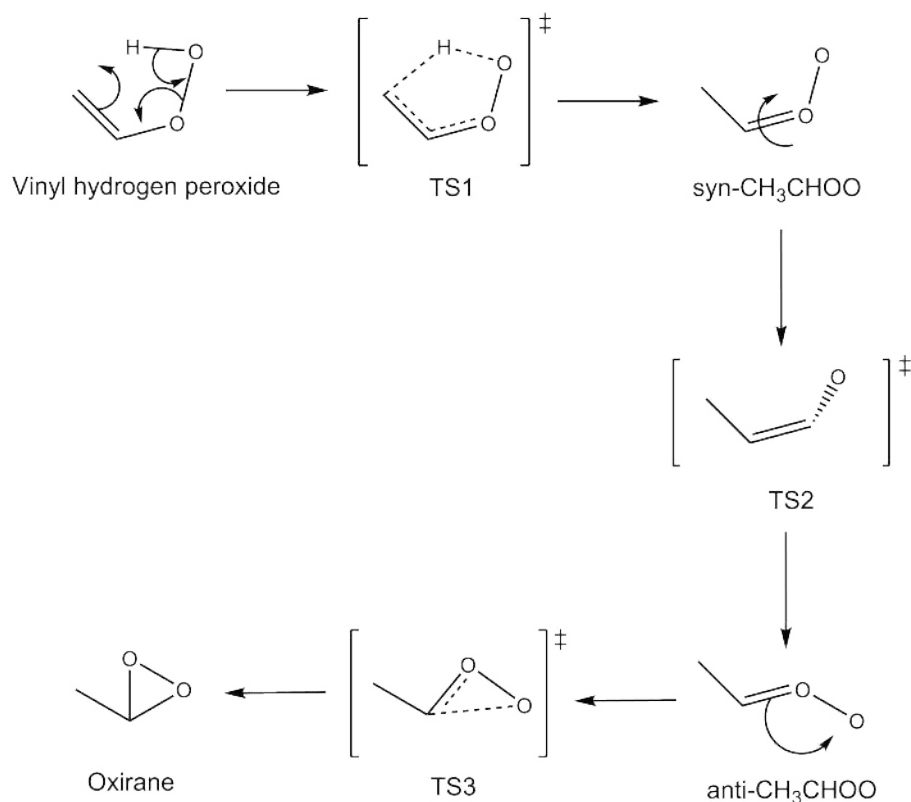


Figure 5.9: Mechanism for the CRIEGEE database

In total, these databases contain 153 distinct chemical species that are used to calculate 51 activation energies and 37 reaction energies.

A framework exists within Molpro [14] for carrying out calculations with databases. This employs the XML language to mark-up the molecular geometries and define reactions. This facilitates the batch calculation of the single point energies for all the

molecules in the database. The energy differences and related statistics can also be calculated for each of the defined reactions using Python scripts that are supplied with Molpro.

This framework was applied to the six databases using MP2, CCSD, CCSD(T), DCSD, OQVCCD, OQVCCD(T), OQVCCDR(T) and OQVCCDAR(T). The mean, standard deviation (σ), mean absolute deviation (MAD) and absolute maximum difference were calculated for each method relative to OQVCCDAR(T). Several different basis sets were used, however only the largest basis set results are presented here.² For the O3ADD6 database, the systems were small enough to use CCSDT as the benchmark and investigate the effects of the full inclusion of triple excitations. These calculations were carried out using Molpro's interface to the MRCC program of M. Kallay. [130]

5.2.2 Results and discussion

O3ADD6

The energy differences for the defined reactions in the O3ADD6 database are displayed in Table 5.3. The values reported, apart from the CCSDT results, are differences from the CCSDT energies.

The first point to note is the large differences of MP2, CCSD and OQVCCD with the thermochemistry predicted by CCSDT. MP2 greatly over predicts the reaction energies of the adduct formation by 40.6 and 134.0 kJ mol⁻¹. CCSD and OQVCCD both produce more negative reaction energies by around 30 kJ mol⁻¹. DCSD, on the other hand, produces very impressive results for both reaction energies which are within chemical accuracy compared to CCSDT.

The non-iterative (T) correction decreases these differences substantially. For CCSD(T), the differences for the adduct reaction energies are below 1 kJ mol⁻¹. OQVCCD(T) still predicts a more negative energy by around 5 kJ mol⁻¹ for both reactions. The effect of the renormalisation is to decrease this quantity even more by 3.5 kJ mol⁻¹; the AR(T) decreases this further by 0.03 kJ mol⁻¹.

For the van der Waals (vdW) energies, all methods, apart from MP2 predict values close to CCSDT. DCSD excels here by producing the smallest differences. CCSD and OQVCCD both produce larger energies, with a maximum difference of 1.5 and 1.7 kJ mol⁻¹ respectively for reaction 4.

The effect of the standard triples correction is to reduce these quantities further. OQVCCD(T) produces more negative vdW energies than CCSD(T). These are closer to

²Please see Ref. [129] for all single point energies, statistics and Molpro inputs.

Method	C ₂ H ₂ + O ₃			C ₂ H ₄ + O ₃		
	1. vdW	2. TS	3. Adduct	4. vdW	5. TS	6. Adduct
CCSDT	-9.656	33.812	-259.425	-11.202	16.119	-226.177
CCSD(T)	-0.392	-3.264	-0.714	-0.546	-2.929	-0.904
OQVCCD(T)	-0.235	-2.184	-4.926	-0.242	-1.703	-5.173
OQVCCDR(T)	-0.219	-1.483	-7.759	-0.133	-0.949	-8.668
OQVCCDAR(T)	-0.217	-1.468	-7.789	-0.130	-0.934	-8.699
MP2	-4.234	-13.624	40.638	98.392	83.326	134.089
CCSD	0.679	5.494	-26.672	1.502	5.735	-31.378
DCSD	0.038	2.639	-0.010	-0.024	1.910	-2.981
OQVCCD	0.791	6.906	-30.165	1.740	7.038	-34.866

Table 5.3: Energy differences with CCSDT / kJ mol⁻¹ for the O3ADD6 database with cc-pVDZ basis set. In the case of CCSDT, the actual energies are reported.

the CCSDT reference by around 0.3 kJ mol⁻¹ for reaction 4. The renormalisation serves to decrease these quantities again; for the second reaction OQVCCDAR(T) lowers this by around 0.1 kJ mol⁻¹

The calculation of the activation energies shows larger differences than the vdW energies. MP2 produces inconsistent results; it over estimates the first E_a by 13.6 kJ mol⁻¹ and under estimates the second by 83 kJ mol⁻¹. CCSD and OQVCCD improve upon these results; CCSD predicts higher barrier heights of 5.5 and 5.7 kJ mol⁻¹ for each reaction, while OQVCCD increases this difference to around 7 kJ mol⁻¹. DCSD shows good agreement to CCSDT.

The effect of the triples correction is to lower these barrier heights below the full triples result. OQVCCD(T) predicts larger barrier heights than CCSD(T) by around 0.6 kJ mol⁻¹ for the second reaction. Renormalisation corrects this lowering by the (T) correction and increases the barrier heights again.

The QV methods with triples corrections produce the smallest differences compared to CCSDT, with OQVCCDAR(T) differing by around 1 kJ mol⁻¹ for both reactions. The activation energies that are calculated are in between the CCSD(T) and CCSDT results. The QV methods appear to correct for the lowering of the barrier height by the (T) correction.

CRBH20

The statistics for the CRBH20 database with an OQVCCDAR(T) reference are shown in Table 5.4. The largest deviation occurs for MP2 with a mean difference and MAD of 23 kJ mol⁻¹. OQVCCD shows the next largest deviation with a mean and MAD of 10.4 kJ mol⁻¹. The triples correction for the QV methods and CCSD clearly make a large contribution to the overall activation energies. DCSD however, shows one of the smallest deviations from OQVCCDAR(T), apart from OQVCCD(T) and OQVCCDR(T), with a mean difference of 1.98 kJ mol⁻¹.

Method	Mean	σ	MAD	Max
MP2	23.005	3.513	23.005	30.514
CCSD	6.587	2.182	6.587	10.511
DCSD	1.980	0.968	1.986	3.315
OQVCCD	10.369	2.643	10.369	15.170
CCSD(T)	-3.250	0.876	3.250	5.345
OQVCCD(T)	-0.748	0.246	0.748	1.209
OQVCCDR(T)	-0.013	0.003	0.013	0.021

Table 5.4: E_a statistics / kJ mol⁻¹ for the CRBH20 database with cc-pVTZ basis set.

Overall, the triples has the effect of lowering the activation energy. The QV methods predict higher activation energies than CCSD(T), with a mean difference approaching 3.4 kJ mol⁻¹. The effect of the renormalised triples corrections is to increase the energy barrier. The asymmetric-renormalised triples leads to further increases, though only by around 0.01 kJ mol⁻¹ when compared to OQVCCDR(T).

The largest individual reaction difference of 5.4 kJ mol⁻¹ occurs for reaction 11, which involves the simplest oxathiazole ring. However, there are no energy differences that approach 5 kJ mol⁻¹ for the remaining nine oxathiazole rings.

The largest difference for OQVCCD of 15 kJ mol⁻¹ occurs for reaction 3, which is an ethyl substituted dioxazole ring. The second largest energy difference occurs for reaction 14; a fluoromethyl substituted dioxazole ring. There appears no correlation between these large energy differences and the two types of hetrocyclic ring.

BHPERI

Table 5.5 shows the results for the BHPERI database.

Large mean differences are observed for MP2, CCSD, DCSD, OQVCCD. For this database, MP2 completely under predicts the barrier heights by a mean of 33.9 kJ mol⁻¹; the largest difference occurs for reaction 9 with an error of 55 kJ mol⁻¹. OQVCCD and CCSD both show similar differences, each over predicting the barrier height, with the largest difference also occurring for reaction 9 (a Diels-Alder reaction involving two cyclopentadienes).

Method	Mean	σ	MAD	Max
MP2	-33.937	10.780	33.937	55.070
CCSD	17.517	4.337	17.517	25.257
DCSD	9.044	2.846	9.044	14.641
OQVCCD	18.241	4.648	18.241	26.170
CCSD(T)	-2.881	1.028	2.881	5.003
OQVCCD(T)	-1.454	0.470	1.454	2.259
OQVCCDR(T)	0.017	0.175	0.050	0.873

Table 5.5: Statistics for the BHPERI database with cc-pVTZ basis set

The triples corrections again lead to a lowering of the barrier heights. CCSD(T) produces answers that are close to OQVCCDAR(T), with a mean difference of -2.9 kJ mol⁻¹. In general, the QV methods lead to a increase of the activation energies. Differences greater than 4 kJ mol⁻¹ occur for reactions 11 and 14 (1,3-dipolar cycloadditions).

The effects of the renormalised triples are to increase the barrier heights slightly by a mean of 1.4 kJ mol⁻¹. The asymmetric-renormalised triples leads to a further increase compared to the symmetric-renormalisation. The difference between these two methods is small; the largest difference being 0.9 kJ mol⁻¹.

DARC

Table 5.6 presents the statistics for the reaction energies of the DARC database. Overall, these results do not show strong derivations from the OQVCCDAR(T) energies unlike the activation energies in Tables 5.4-5.5. Again, the largest difference occurs with MP2, which tends to under predict the energy change with a mean difference of -13.9 kJ mol⁻¹. The maximum absolute difference is around 23.7 kJ mol⁻¹, far beyond the 4 kJ mol⁻¹ of ‘chemical accuracy’.

DCSD shows the next largest difference after MP2, with a mean difference of 6.3 kJ

mol^{-1} . OQVCCD shows the closest match to the OQVCCDAR(T) energies, compared to the other methods without triples corrections.

Method	Mean	σ	MAD	Max
MP2	-13.868	7.892	13.868	23.718
CCSD	2.931	1.799	2.931	5.869
DCSD	6.251	1.203	6.251	8.509
OQVCCD	2.451	1.859	2.618	5.124
CCSD(T)	1.623	0.383	1.623	2.017
OQVCCD(T)	0.737	0.285	0.737	0.941
OQVCCDR(T)	0.005	0.002	0.005	0.009

Table 5.6: ΔE statistics / kJ mol^{-1} for the DARC database with cc-pVTZ basis set.

OQVCCDAR(T) predicts more exothermic reaction energies than all the methods, though OQVCCDR(T) produces results that are very similar; the mean difference being $0.005 \text{ kJ mol}^{-1}$. CCSD(T) also shows little deviation with a mean difference of 1.6 kJ mol^{-1} . The renormalised triples correction serves to decrease the reaction energies by about 1 kJ mol^{-1} compared to the standard (T) correction.

ISOMER20

Table 5.7 shows the statistics for a close-shell subset of the ISOMER20 database. All the methods give a mean difference within 1 kJ mol^{-1} of the reference values, apart from MP2. However, CCSD and OQVCCD have large σ values, indicating a large distribution of values that happen to cancel out each other when the mean is taken. Large absolute maximum differences for both methods occur for the isocyanic acid isomerisation to fulminic acid (reaction 8).

There is also a small mean difference for DCSD, however this is also due to a wide spread of relative results.

Overall, the QV methods with the triples predict more endothermic reaction energies than CCSD(T) and DCSD. There is little difference between the symmetric- and asymmetric-renormalisation corrections. The renormalisation does serve to slightly increase the reaction energies.

Method	Mean	σ	MAD	Max
MP2	8.599	14.196	12.550	33.652
CCSD	0.618	5.554	3.905	12.665
DCSD	-0.270	2.956	2.272	6.262
OQVCCD	0.586	6.294	4.353	14.355
CCSD(T)	-0.324	1.441	0.991	2.910
OQVCCD(T)	-0.214	0.519	0.381	1.110
OQVCCDR(T)	-0.001	0.007	0.005	0.015

Table 5.7: ΔE statistics / kJ mol^{-1} for a subset of the ISOMER20 database with cc-pV5Z basis set.

CRIEGEE

Tables 5.8-5.9 show the statistics for the CRIEGEE database. For the activation energies, all methods have small mean differences apart from MP2, CCSD and OQVCCD. For OQVCCD, the barrier height for TS1 differs by 16.7 kJ mol^{-1} . It is this reaction that also produces the largest errors for CCSD. Again, DCSD produces surprisingly close results for a method without any triples correction.

Reaction	Mean	σ	MAD	Max
MP2	6.648	9.824	9.702	13.656
CCSD	4.474	8.132	5.157	13.815
DCSD	-0.442	2.588	2.138	2.544
OQVCCD	6.577	8.809	6.577	16.696
CCSD(T)	-1.617	1.455	1.617	3.293
OQVCCD(T)	-0.157	0.579	0.391	0.822
OQVCCDR(T)	-0.005	0.007	0.005	0.013

Table 5.8: E_a statistics / kJ mol^{-1} for the CRIEGEE database with cc-pV5Z basis set.

CCSD(T), OQVCCD(T) and OQVCCDR(T) all produce similar answers to OQVCCDAR(T). In general, the QV methods produce higher barrier heights than CCSD(T). The effect of the renormalised triples is to increase this quantity. The largest difference with CCSD(T) occurs for reaction 1.

Table 5.9 presents the statistical results for the reaction energies. Again, from the mean differences, all the methods appear to be in good agreement. However MP2 and

Reaction	Mean	σ	MAD	Max
MP2	-3.505	18.351	12.431	23.905
CCSD	0.435	6.224	4.540	7.462
DCSD	-1.787	3.156	1.971	5.421
OQVCCD	0.663	9.407	6.728	11.087
CCSD(T)	-0.301	4.614	3.113	5.121
OQVCCD(T)	-0.034	0.689	0.493	0.790
OQVCCDR(T)	-0.001	0.010	0.007	0.013

Table 5.9: ΔE statistics / kJ mol^{-1} for the CRIEGEE database with cc-pV5Z basis set.

OQVCCD show large deviations for the first and third reactions. On average, compared to CCSD(T), the QV methods produce more endothermic reaction energies for the first and second reactions, while producing a more exothermic energy for the third reaction. The largest difference for CCSD(T) again occurs for reaction 1 with a lower energy of 5.1 kJ mol^{-1} .

5.2.3 Conclusions

There are several conclusions that can be drawn from the statistical information provided. Firstly, unsurprisingly, MP2 performs poorly for the calculation of accurate activation and reaction energies. Differences from the OQVCCDAR(T) answer of $23\text{-}50 \text{ kJ mol}^{-1}$ have been observed for all databases, while a difference of 134 kJ mol^{-1} was calculated in the O3ADD6 database, when compared to CCSDT. These errors stem from the inability of MP2 to properly describe the dynamic and non-dynamic correlation effects in these systems.

OQVCCD has also been shown to perform poorly, especially for the calculation of activation energies. It is therefore vital to include a triples correction to OQVCCD to produce reliable results. DCSD has produced impressive answers for the O3ADD6 and CRBH20 databases, with differences below chemical accuracy. For the BHPERI database, the errors increased, but were still below those of OQVCCD. For the calculation of reaction energies, OQVCCD performed better for DARC, whereas DCSD performed better with the ISOMER20 subset.

In general, use of the QV methods leads to an increase in the activation energies and an increase in absolute reaction energies when compared to CCSD(T). From the

mean differences and standard deviations, these methods produce higher barrier heights by around 2–3 kJ mol⁻¹. However, there are individual barrier heights that CCSD(T) underestimates by 4–5 kJ mol⁻¹. These transition states exhibit some non-dynamical correlation effects, which are, however, generally small. For the calculation of reaction energies, CCSD(T) and the QV methods are in agreement, with differences approaching 3 kJ mol⁻¹. When compared to CCSDT, the effect of the QV methods are to correct for the limitations of the non-iterative triples and increase the barrier height. This error is again reduced with the renormalised triples corrections.

5.3 Asymmetric-renormalised triples correction

The symmetric and asymmetric renormalised triples corrections (which define the OQVCCDR(T) and OQVCCDAR(T) methods) have previously been discussed in Chapter 3. Numerical tests have been carried out to compare these two methods and determine whether the symmetric approximation is valid, *i.e.* if

$$\frac{\langle \Phi_0 | {}_2\hat{T}_2^\dagger \hat{V} | \Phi_{ijk}^{abc} \rangle \langle \Phi_{ijk}^{abc} | \hat{V} \hat{T}_2 | \Phi_0 \rangle}{\epsilon_i + \epsilon_j + \epsilon_k - \epsilon_a - \epsilon_b - \epsilon_c} \approx \frac{\langle \Phi_0 | {}_1\hat{T}_2^\dagger \hat{V} | \Phi_{ijk}^{abc} \rangle \langle \Phi_{ijk}^{abc} | \hat{V} {}_1\hat{T}_2 | \Phi_0 \rangle}{\epsilon_i + \epsilon_j + \epsilon_k - \epsilon_a - \epsilon_b - \epsilon_c}. \quad (5.1)$$

5.3.1 Potential energy curves

Plotted in Fig. 5.10-5.11 are the PECs for Cl₂ and P₂ respectively. For most of the diatomic molecules investigated in Section 5.1, there appears to be no discernible difference between the OQVCCDR(T) and OQVCCDAR(T) energies, thereby producing graphs like Fig. 5.10, where the OQVCCDAR(T) energy overlays the OQVCCDR(T) energy. However, a small difference in energy can be observed for triply bonded P₂ towards the end of the curve as both methods approach the asymptotic limit.

The differences in energy can be seen more clearly in Fig. 5.12-5.14 which show the differences between the OQVCCDAR(T) and OQVCCDR(T) energies. For Cl₂, the differences in energy are around 1×10⁻⁵ hartree and so are minimal throughout the PEC. The difference rises to a maximum at around 3.4 Å before falling to an apparent limiting difference at longer bond lengths.

This behaviour is not observed for P₂, where the energy difference is of the order of 1×10⁻³ hartree, *i.e.* in the range of chemical accuracy (the largest difference being 6.8 kJ/mol at 3.8 Å). After 3.8 Å it becomes difficult to converge the OQVCCD energy and so it is not possible to determine if the energy difference converges to a limiting value at longer bond lengths.

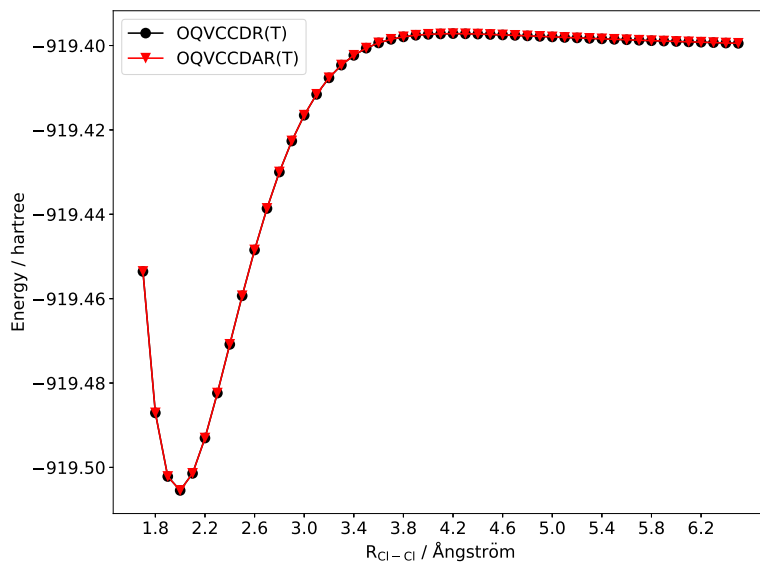


Figure 5.10: Calculated potential energy curves for Cl₂ with extrapolated cc-pVQZ:cc-pV5Z basis set.

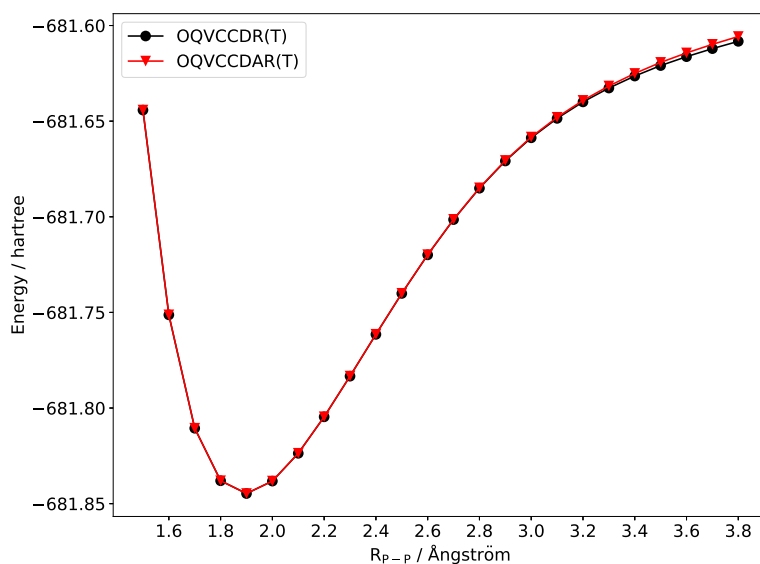


Figure 5.11: Calculated potential energy curves for P₂ with extrapolated cc-pVQZ:cc-pV5Z basis set.

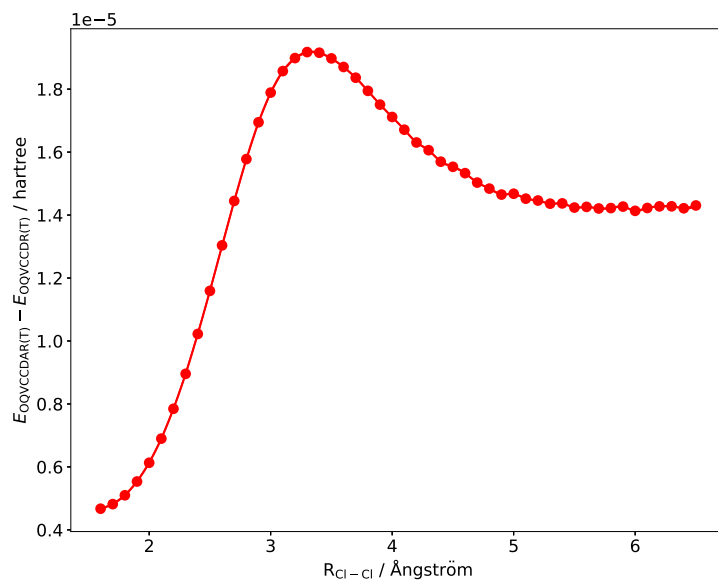


Figure 5.12: Energy difference between OQVCCDAR(T) and OQVCCDR(T) for the stretching of Cl₂ with extrapolated cc-pVQZ:cc-pV5Z basis set.

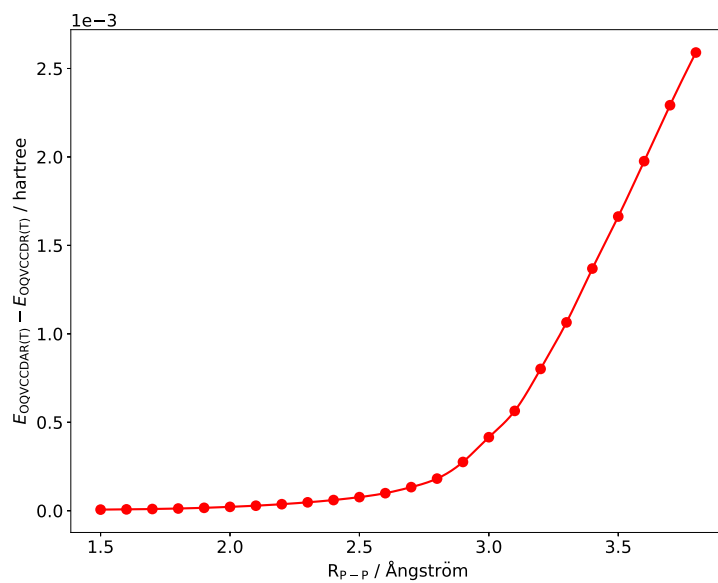


Figure 5.13: Energy difference between OQVCCDAR(T) and OQVCCDR(T) for the stretching of P₂ with extrapolated cc-pVQZ:cc-pV5Z basis set.

Energy differences have also been calculated for three more triply bonded molecules (N_2 , CO and SiO, Fig. 5.14-5.16), to investigate the effect of the asymmetric-renormalised triples.

The energy differences for the N_2 PEC mirrors the behaviour observed for P_2 ; as the bond is stretched, the energy difference becomes larger, of the order 1×10^{-3} hartree. CO and SiO replicate this behaviour, however the differences at the largest distances are an order of magnitude less than P_2 or N_2 . For SiO, the energy differences appear to be approaching a maximum.

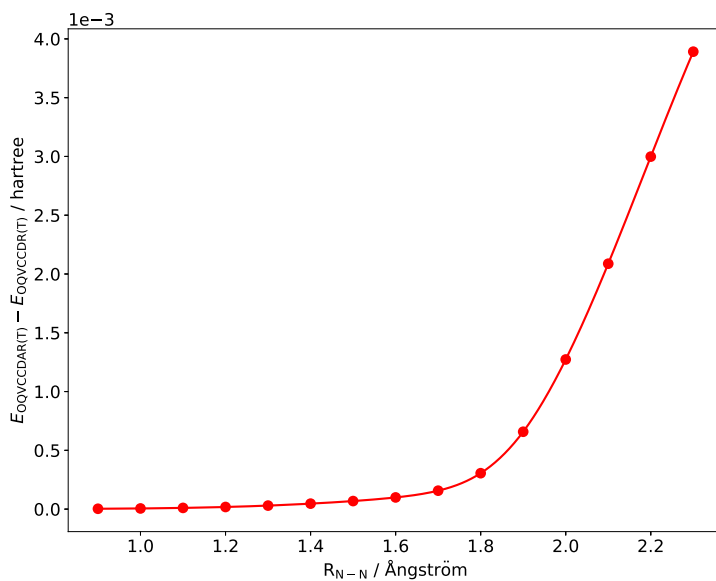


Figure 5.14: Energy difference between OQVCCDAR(T) and OQVCCDR(T) for the stretching of N_2 with extrapolated cc-pVQZ:cc-pV5Z basis set.

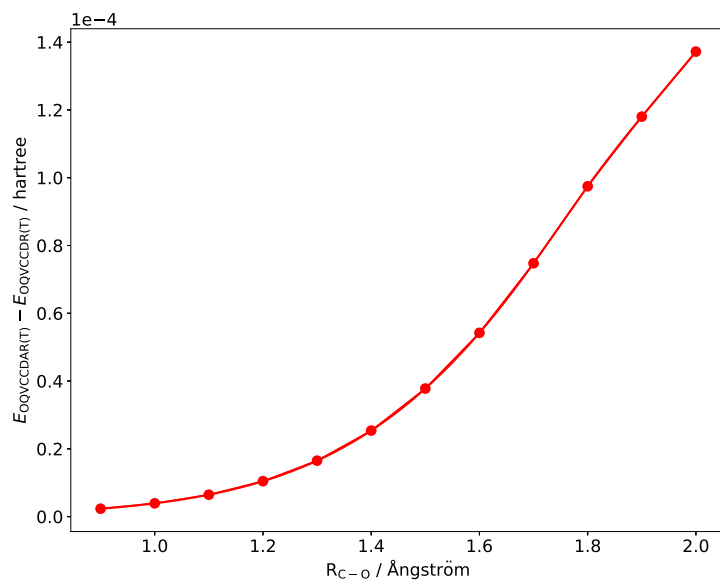


Figure 5.15: Energy difference between OQVCCDAR(T) and OQVCCDR(T) for the stretching of CO with extrapolated cc-pVQZ:cc-pV5Z basis set.

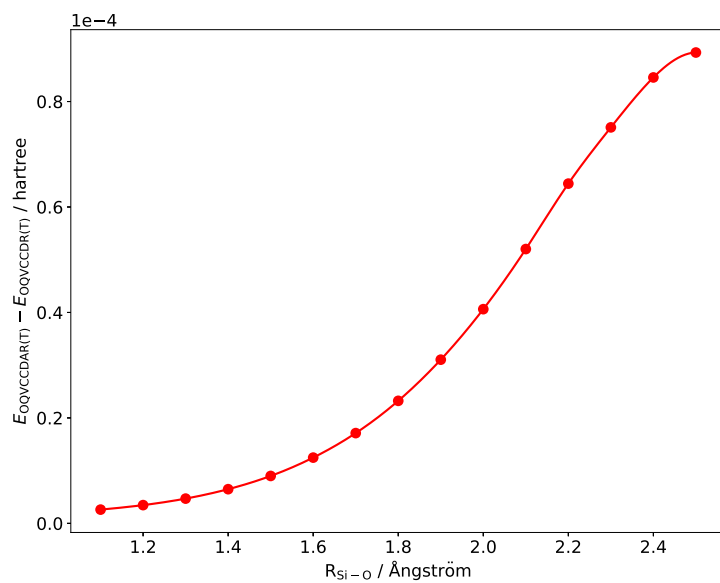


Figure 5.16: Energy difference between OQVCCDAR(T) and OQVCCDR(T) for the stretching of SiO with extrapolated cc-pVQZ:cc-pV5Z basis set.

5.3.2 Spectroscopic constants

The spectroscopic constants for third-row diatomic molecules were calculated with OQVCCDR(T) and OQVCCDAR(T) using the method outlined in Section 5.1. The results are presented in Table 5.10.

All the OQVCCDAR(T) results are similar OQVCCDR(T) with only small differences appearing for ω_e and $\omega_e x_e$. The largest differences in values occurs for AlO^- where the OQVCCDAR(T) ω_e is 3.51 cm^{-1} larger and $\omega_e x_e$ is 0.55 cm^{-1} larger. Equilibrium bond length and energy are both similar with small differences that are no larger than the other results.

System	Method	$R_e/\text{\AA}$	ω_e/cm^{-1}	$\omega_e x_e/\text{cm}^{-1}$	$E_n/\text{hartree}$
HCl	OQVCCDR(T)	1.276	3002.0	53.3	-460.376699
	OQVCCDAR(T)	1.276	3001.9	53.0	-460.376694
BCl	OQVCCDR(T)	1.721	843.2	5.4	-484.502851
	OQVCCDAR(T)	1.721	843.1	5.3	-484.502847
Cl_2	OQVCCDR(T)	1.987	567.5	2.6	-919.505526
	OQVCCDAR(T)	1.987	567.3	2.5	-919.505519
AlO^-	OQVCCDR(T)	1.643	979.9	4.8	-317.227567
	OQVCCDAR(T)	1.644	983.4	5.3	-317.227557
S_2	OQVCCDR(T)	1.900	713.8	2.8	-795.484077
	OQVCCDAR(T)	1.900	713.9	2.8	-795.484063
P_2	OQVCCDR(T)	1.893	801.6	2.7	-681.844750
	OQVCCDAR(T)	1.893	801.9	2.7	-681.844735
SiO	OQVCCDR(T)	1.513	1253.1	4.4	-364.248231
	OQVCCDAR(T)	1.513	1252.8	3.9	-364.248219

Table 5.10: Comparison between OQVCCDR(T) and OQVCCDAR(T) spectroscopic constants with extrapolated cc-pVQZ:cc-pV5Z basis set.

For P_2 where significant differences in energy were seen at long bond lengths, there appears to be no substantial difference in any of the diatomic properties. This is because these properties rely on a description of the minimum well, which both methods describe similarly as can be seen in Fig. 5.13.

5.3.3 Harmonic frequencies

A comparison of the calculated $1A_g$ normal modes for the halides was carried out with OQVCCDR(T) and OQVCCDAR(T). This procedure used central differences to construct the Hessian matrix. All calculations except At_2 were carried out at equilibrium bond lengths as defined in the NIST Chemistry WebBook [118]. No experimental data exists for At_2 , so the bond length of 3.11 Å was taken from a DFT/B3LYP3 calculation with a Douglas-Kroll Hamiltonian. These results are presented in Table 5.11.

Molecule	OQVCCDR(T)	OQVCCDAR(T)
F_2	946.97	946.97
Cl_2	581.87	581.88
Br_2	341.18	341.18
I_2^a	230.31	230.31
At_2^a	89.54	89.54

^a Calculated with cc-pVTZ-PP basis set.

Table 5.11: Harmonic vibrational wavenumbers corresponding to the $1A_g$ normal modes / cm^{-1} calculated with the cc-pVTZ basis set.

All the vibrational wavenumbers are exactly the same for both methods, except for Cl_2 where the difference is 0.01 cm^{-1} .

5.3.4 Computational time

The computational times for the calculation of the standard (T) correction and the asymmetric-renormalised (T) correction (AR(T)) were measured for a variety of alkanes and basis sets. The ratios of these timings are presented in Table 5.12. A number < 1 indicates a slower time to calculate the AR(T) correction.

For small systems and small basis sets, the time taken to calculate AR(T) is comparable to the standard (T); for methane at cc-pVDZ and cc-pVTZ, the ratio is close to 1.0. However as the basis set and system size are both increased, the ratio converges to around 0.5. This is as expected as the AR(T) code contains double the number of tensor contractions that scale as $O(N^7)$ than the standard (T) code. Nevertheless, in total, the number of tensor contractions in AR(T) is less than double compared to (T) and so will never take exactly twice as long to compute.

Basis	Methane	Ethane	Propane	Butane	Pentane	Hexane
cc-pVDZ	0.76	0.44	0.61	0.86	0.52	0.57
cc-pVTZ	0.87	0.66	0.62	0.63	0.55	0.57
cc-pVQZ	0.65	0.54	0.55	0.52	-	-
cc-pV5Z	0.64	0.56	0.52	-	-	-

Table 5.12: Ratios of the (T) and AR(T) code timings.

5.3.5 Discussion and conclusions

From the results presented in this and the previous sections, there appears to be little difference between the symmetric- and asymmetric-renormalised triples corrections. The energies that are produced differ slightly, however, they are not the same. For all the diatomic cases and database calculations, OQVCCDAR(T) predicts a higher energy than OQVCCDR(T), which suggests,

$$\langle \Phi_0 | {}_2\hat{T}_2^\dagger \hat{V} | \Phi_{ijk}^{abc} \rangle \langle \Phi_{ijk}^{abc} | \hat{V} \hat{T}_2 | \Phi_0 \rangle > 2 \langle \Phi_{ijk}^{abc} | \hat{V}_1 \hat{T}_2 | \Phi_0 \rangle . \quad (5.2)$$

For the triply bonded molecules like P₂ and N₂, the energy difference between the two corrections become larger at longer bond lengths. In fact the two corrections produce differences that are larger than the 4 kJ mol⁻¹ of chemical accuracy. However, around the equilibrium well, both methods produce similar energies, which is reflected in the diatomic constants results.

For other triply bonded diatomics like CO and SiO, the energy difference between the two methods is of the order of 1×10⁻⁴ hartree and therefore within the limits of chemical accuracy.

To conclude, the OQVCCDAR(T) method doesn't appear to have many benefits over OQVCCDR(T). The energies and vibrational wavenumbers that it produces are very similar to OQVCCDR(T); the problem is that it takes nearly double the time to compute the $E_{\text{AR(T)}}$ energy than $E_{\text{R(T)}}$. The only advantage of using OQVCCDAR(T) would be in the production of accurate dissociation curves for multiply bonded molecules, or for benchmarking energies where the added computational expense was acceptable.

5.4 Scaling and timings

Part of the current work has been to rewrite the QVCCD code, including the orbital optimisation and triples corrections, as stated in Chapter 4. This was undertaken in

the hope to make the code faster and therefore of more use to the scientific community.

This section will compare the new and old QVCCD implementations and see how quickly they can calculate the energy of a system. It is also of use to compare how fast QVCCD is compared to the TCC methods and determine their usability instead of the CC methods. Finally, QVCCD formally scales as $O(N^6)$, with a large time spent calculating terms involving $\mathcal{D}U$, which scales as $O(o^3v^3)$. It is this coupled with matrix diagonalisations that makes QVCCD slower than CCD. The scaling pre-factor for these terms will be estimated.

5.4.1 Comparisons with the old code

The timings for sections of the old and new QVCCD code were collected and compared. These sections represent the most time intensive parts of an OQVCCD(T) calculation. They include:

1. Construction of the \mathbf{U} tensors.
2. Construction of ${}_qT$ ($q = \{1, 2\}$).
3. Construction of the orbital optimisation derivative, $\frac{\partial E}{\partial \phi}$.
4. Construction of the QVCCD residual, \mathbf{G} .
5. Construction of the non-iterative (T) correction.
6. The total wall time of the calculation.

Single-point energy calculations were carried out on a selection of simple alkanes and various different basis sets on one Intel Xeon (Westmere / X5660) 2.80GHz processor. Only the cc-pVTZ and cc-PVQZ results will be presented here as the other basis sets add nothing new to these comparisons.³

Ratios calculated with cc-pVTZ are presented in Table 5.13. A ratio > 1 means that the new code is faster, while a ratio < 1 indicates the old code is faster.

Overall, the new code is significantly faster in all areas except the construction of the (T) correction. Significant time savings have been made in the construction of the \mathbf{U} tensors, ${}_qT$ and \mathbf{G} .

For the construction of the \mathbf{U} tensors, the new code is around 4 times faster for methane; this ratio increases to 4.8 for pentane. The residual equation is also constructed 2.8 times faster than the old code, however this ratio rises more quickly as the size of the alkane is increased. For pentane, the new code is 6.2 times faster than the old code. This represents a time difference of around 60 hours.

³Please see Ref. [131] for all timing data and input files.

Code	Methane	Ethane	Propane	Butane	Pentane
1. U	4.0	4.4	4.4	4.3	4.8
2. ${}_qT$	15.2	45.4	50.3	50.0	60.4
3. $\frac{\partial E}{\partial \phi}$	1.0	1.2	1.2	1.0	1.1
4. G	2.8	5.7	5.6	5.6	6.2
5. (T)	0.5	0.9	0.8	0.8	0.9
6. Total time	1.9	6.3	6.4	6.4	7.2

Table 5.13: Ratios of the old code and new code timings calculated with cc-pVTZ basis.

The largest speed up occurs for the construction of the transformed amplitude equations, which are 15.2 times faster than the old code for methane, but 60.4 times faster for pentane. Unfortunately, the new QVCCD code spends about 4% of the time in this section of the code, therefore these large ratios do not translate into large ratios of the total time.

For the orbital optimisation derivative, the timings are generally the same, however there is a slight increase of the ratios for ethane, propane and pentane. the new code is on average 0.1 times faster than the old code.

The only area where the new code is slower is the construction of the (T) correction. For methane, this takes twice as long to evaluate than in the old code, however this ratio rises as the size of the alkanes is increased. The slowness of the (T) correction can be contributed to summing over the virtual orbitals instead of the occupied. As there are generally more virtual orbitals in a calculation, a sum over them will take longer than a sum of the occupied orbitals. However this procedure takes up less memory and so becomes more relevant when a calculation uses multiple processors with a maximum amount of memory between them.

The overall total time taken shows that the new code is faster than the old one, especially for larger molecules. For methane the speed up is 1.9, whereas for pentane it is 7.2; this represents a time saving of 98 hours.

Similar speed ups are seen in the cc-pVQZ results in Table 5.14. Again, the new code is generally faster. Significant savings are seen in the construction of the **U** tensors, ${}_qT$ and **G**. All of these ratios increase as the size of the alkane increases. The largest ratios occur again for the construction of ${}_qT$, which is 70.4 times faster in the new code for propane.

The (T) correction remains slower in the new code, but the ratio rises to 1.0 for propane, meaning both codes take the same amount of time.

Code	Methane	Ethane	Propane
1. U	5.4	5.5	5.7
2. ${}_qT$	43.9	54.6	70.4
3. $\frac{\partial E}{\partial \phi}$	1.7	1.8	1.5
4. G	5.5	5.8	7.0
5. (T)	0.6	0.9	1.0
6. Total time	5.0	6.1	7.5

Table 5.14: Ratios of the old code and new code timings calculated with cc-pVQZ basis.

As the basis set is increased, all the ratios are increased. Compared to the old code, the new code becomes even faster as the basis set grows. This is shown clearly in the total times take for propane. The new code is 6.4 times faster at cc-pVTZ and 7.5 times faster at cc-pVQZ. This last ratio represents a saving of around 60 hours.

5.4.2 Comparisons with the CC program

The QV methods are designed to be a substitute for the TCC methods when investigating multireference systems. In general, the QV methods will always be slower than than CCD, CCSD and CCSD(T) due to the evaluation of the cubic VCCD terms. However, it will be useful to compare TCC and QV methods to gauge how feasible it is to replace a TCC calculation with a QV one.

QVCCD/CCD, OQVCCD/CCSD and OQVCCD(T)/CCSD(T) wall timing ratios were taken for the collection of alkanes and different basis sets.

The QVCCD/CCD timing ratios are presented in Table 5.15. Overall, QVCCD is slower than CCD, with larger timing ratios occurring for larger systems. QVCCD takes 72 minutes longer than CCD to calculate the energy of hexane with cc-pVDZ. As the basis set increases, the ratios appear to decrease; a calculation of methane with cc-pV5Z basis takes nearly twice as long with QVCCD than CCD. However, this only represents a difference of 7 minutes.

These trends are caused by the evaluation of ${}_D U$ terms and the diagonalisation of matrices which occur in QVCCD, but not in CCD. From Chapter 4, QVCCD requires the evaluation of at least thirteen $O(o^3v^3)$ terms plus four matrix diagonalisations per iteration. Four of the terms are carried out in the qTransform function, which makes use of highly optimised matrix multiplication routines, yet must rely on native C++ loops to evaluate the most expensive parts. There also exists $O(o^3v^3)$ terms

Basis	Methane	Ethane	Propane	Butane	Pentane	Hexane
cc-pVDZ	3.85	8.30	7.52	10.17	12.51	12.75
cc-pVTZ	5.05	6.22	7.34	9.41	10.61	11.15
cc-pVQZ	3.41	4.31	5.33	7.07	-	-
cc-pV5Z	2.38	3.31	4.11	-	-	-

Table 5.15: Ratios of the QVCCD and CCD wall timings.

like $\langle \Phi_{ab}^{ij} | \hat{H} \hat{T}_2^2 | \Phi_0 \rangle$ which are part of the CCD amplitude equations, but absent in QVCCD. However, there are around six of these terms and all of them make use of the fast matrix multiplication routines. [102]

The QVCCD code must also evaluate cU terms that scale as $O(o^4v^2)$. It is likely that these terms contribute the increasing ratios as the number of occupied orbitals are increased. Both set of terms serve to slow down the QVCCD code compared to CCD.

OQVCCD will always be slower than CCSD because of the integral transformation it has to carry out every iteration. This is illustrated in the large ratios in Table 5.16.

For a small system and basis set, these ratios can be ignored as the absolute timings are on the order of a 1-20 seconds. For larger basis sets and systems, these ratios become important because as the time differences become larger. For example, CCSD is around 5.7 times faster than OQVCCD in calculating the energy of propane/cc-pV5Z. In absolute time differences, OQVCCD takes 41 minutes more to complete than CCSD.

Basis	Methane	Ethane	Propane	Butane	Pentane	Hexane
cc-pVDZ	12.15	10.60	7.44	13.35	13.17	13.70
cc-pVTZ	9.19	9.01	11.15	13.79	14.55	13.97
cc-pVQZ	6.62	7.37	8.60	8.18	-	-
cc-pV5Z	4.35	6.45	5.74	-	-	-

Table 5.16: Ratios of the OQVCCD and CCSD wall timings.

The two trends observed for the QVCCD/CCD ratios are seen here as well, though the OQVCCD ratios are slightly larger: As the system size increases, the ratios become larger, however, as the basis set becomes larger (more virtual orbitals) the ratios decrease in size.

For the OQVCCD(T)/CCSD(T) ratios (Table 5.17), as the system size grows, the ratios do not necessarily grow, however as the basis set is increased, the ratios do

decrease. In general these ratios are lower than in Table 5.16, which is possible due to the longer time lengths being calculated.

Basis	Methane	Ethane	Propane	Butane	Pentane	Hexane
cc-pVDZ	5.97	7.12	7.73	6.75	5.13	5.13
cc-pVTZ	3.22	2.89	2.50	2.65	2.46	3.61
cc-pVQZ	3.69	3.24	3.05	2.70	-	-
cc-pV5Z	3.09	2.69	2.20	-	-	-

Table 5.17: Ratios of the OQVCCD(T) and CCSD(T) wall timings

For larger systems and basis sets, like propane/cc-pV5Z and pentane/cc-pVQZ, CCSD(T) is around 2-3 times faster than OQVCCD(T). In absolute terms, an OQVCCD(T) calculation of pentane/cc-pV5Z will take 38 minutes longer than CCSD(T).

To summarise, for single point energy calculations, the QV methods seem to perform well against TCC methods. For CCSD(T), these ratios appear to converge to around 2-3, meaning that the OQVCCD(T) calculation is 2-3 times slower than CCSD(T) (for these systems). Nonetheless, with the use of multiple processors, the time to carry out a QV calculation will fall and thereby make these methods more competitive with TCC methods.

5.4.3 Scaling factors

The previous section showed that the QV methods are slower than their TCC counterparts, even though both formally scale as $P \times O(N^6)$. The difference is due to the size of the pre-factor, P , and the terms that $O(N^6)$ includes.

Both CCD and QVCCD use the same code in Molpro to evaluate the set of external integrals; this scales as $O(o^2v^4)$. However, QVCCD has to evaluate terms that involve ${}_D U$ and diagonalise matrices, both of which scale as $O(o^3v^3)$.

With this in mind, if the number of occupied orbitals are kept the same, a polynomial function that describes the timing of the QVCCD method can be written:

$$a_0 + a_1v + a_2v^2 + a_3v^3 + a_4v^4.$$

The problem is then to find the size of the a_3 constant as this is the term that makes QVCCD slower than CCD. This polynomial can only be used as a estimate to derive a_3 . The QVCCD scaling function will also contain terms from the ${}_C U$ tensors that scale as $O(o^4v^2)$ which will ultimately effect the overall timing. Nevertheless, if a large basis set is used, then the $O(o^3v^3)$ terms will dominate.

QVCCD calculations were carried out on ethane with cc-pVQZ and cc-pV5Z basis sets to determine a_3 . From the resulting computational times, the timings for the evaluation of the external integrals (KEXTA) were subtracted. These points were plotted in seconds against the number of virtual orbitals and a cubic polynomial fitted using a least squares fit. [31] From this, it can be estimated that QVCCD will be $9.30 \times 10^{-5} v^3$ seconds slower in the limit of a large basis set.

The same procedure can be carried out by including the KEXTA times. This gives,

$$8.97 \times 10^{-5} v^3 + 5.33 \times 10^{-8} v^4. \quad (5.3)$$

This shows that the evaluation of the $O(o^2v^4)$ terms slightly decreases the scaling factor for the $O(o^3v^3)$ terms. But in this case, the v^3 terms still dominate the expression.

5.4.4 Parallel timings

As well as being more computationally expensive to run, the old QVCCD code does not take advantage of parallel processors. The ITF generates fully parallel code and sections of C++ code like *qTransform* have been written using MPI wrappers. These have been used to split the loops over multiple processors and sum all the components together, using a global sum, at the end of the function.

To examine the speed increase of using multiple processors, an energy calculation for propane was carried out with the new OQVCCD(T) code on 2^n Intel Xeon E5-2670 (Sandy Bridge) 2.60GHz processors, where $n = \{0, 1, 2, 3, 4, 5\}$. The CPU timings for these calculations alongside CCSD(T) are shown in Fig. 5.17.

As the number of processors increase, there is an exponential decrease in the CPU time for both methods. As the number of processors grow, both codes also show convergence to an absolute speed limit. If the number of processors were increased beyond 32, both codes would show little speed up.

Fig. 5.18 shows the absolute percentage change in CPU timings. By using two processors, the OQVCCD(T) code is sped up by 54.3%, while the CCSD(T) code becomes 65.4% faster. As the number of processors increases, this percentage decreases.

For 4 and 8 processors, both codes show similar percentage increases. For more processors, the OQVCCD(T) code shows smaller percentages of 7.6% and 11.8% for 16 and 32 processors respectively. CCSD(T) on the other hand continues to become 30-40% faster as the number of processors are doubled. This shows that the CCSD(T) code is parallelised more effectively than the OQVCCD(T) code. The main culprit for the decrease in percentage change is *qTransform*; the most expensive step in OQVCCD(T).

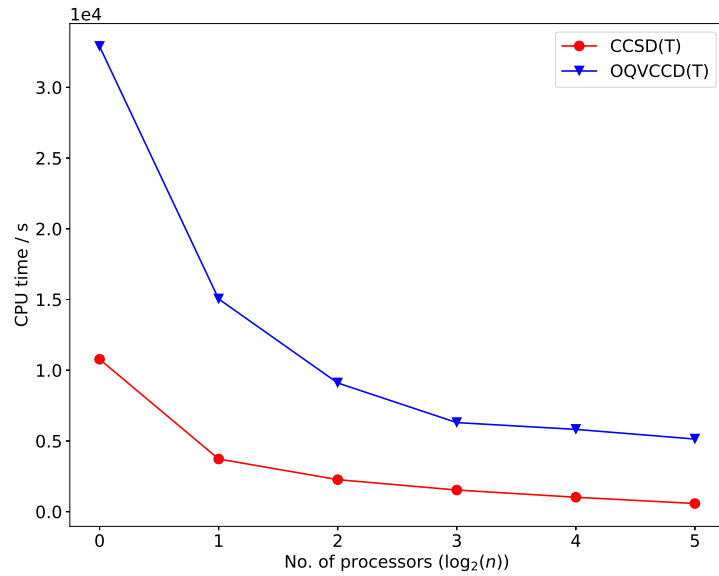


Figure 5.17: CPU timings for the energy calculation of propane with cc-pVQZ basis.

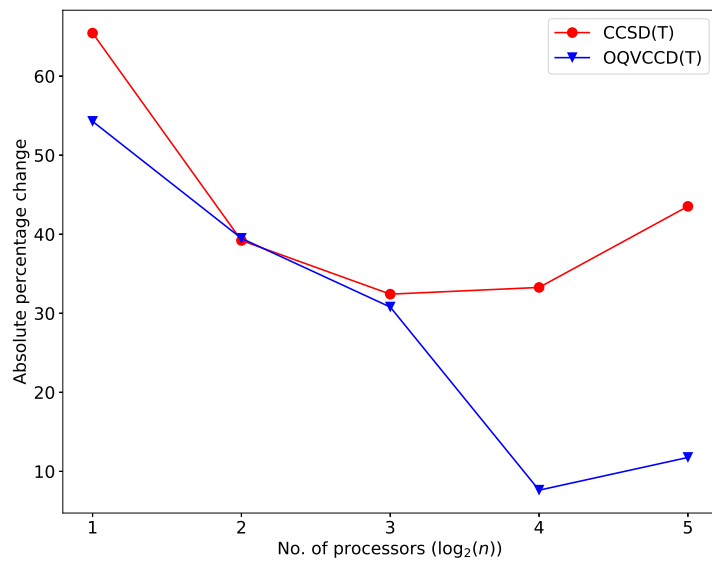


Figure 5.18: Absolute percentage change in CPU time for the energy calculation of propane with cc-pVQZ basis.

Though attempts have been made to make it run effectively in parallel, improvements can obviously be made that could help to increase the speed.

Chapter 6

Calculating reaction rates with Instanton theory

6.1 Reaction rates and rate constants

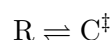
Calculating and understanding the rate of a chemical reaction is of fundamental importance to chemistry. How quickly a reaction proceeds, under certain conditions, allows for an understanding of macroscopic chemical change.

For a unimolecular reaction, the reaction rate and rate constant are related by, [132]

$$\frac{d[\text{P}]}{dt} = k[\text{R}], \quad (6.1)$$

where the concentration of a product, $[\text{P}]$, changes over time as a function of the reactant concentration, $[\text{R}]$, multiplied by a constant, k . If k is known, then $[\text{P}]$ is also known for any time.

Traditionally, Transition State Theory (TST) has been used to calculate k by constructing a model reaction. [23] Within this model, the reactants are assumed to be in a large pre-equilibrium (defined by an equilibrium constant K^\ddagger) with an activated complex, C^\ddagger :



This complex exists in a shallow potential well close to the transition state (TS) which vibrates classically. As a result, small vibrations along the reaction coordinate will push this complex through the TS and on towards the products.

Assuming that every activated complex goes forward to the TS and does not collapse back to the reactants, the overall rate constant will be proportional to the equilibrium constant and the rate constant describing $\text{C}^\ddagger \xrightarrow{k^\ddagger} \text{P}$.

These quantities can be derived by using a statistical mechanics approach involving the partition functions of the species involved. However, it is usually difficult to know the structure of the activated complex and so it is often simpler to use thermodynamic quantities and re-express K^\ddagger in terms of the Gibbs free energy of activation, $\Delta^\ddagger G$. [23]

The overall rate constant can be written as, [25]

$$k = \frac{k_B T}{h} e^{-\Delta^\ddagger G/RT}, \quad (6.2)$$

where k_B is the Boltzmann constant, R is gas constant, T is temperature. This is the general case of the Eyring equation. [133]

Semi-classical TST theory produces impressive results for specific reactions, however it fails to take account of the quantum behaviour of matter and therefore predicts qualitatively wrong results for reactions that involve quantum tunnelling.

Due to the wave-like nature of matter, when an atom experiences a potential energy barrier, there is a non-zero chance for it to ‘tunnel’ through it and appear on the other side. For a one dimensional, large ($\kappa L > 1$), rectangular potential barrier, the probability that a particle will pass through the barrier is given by, [1]

$$T = 16 \frac{E}{V} \left(1 - \frac{E}{V}\right) e^{-2\kappa L}, \quad (6.3)$$

$$\kappa = \frac{\left[2mV\left(1 - \frac{E}{V}\right)\right]^{\frac{1}{2}}}{\hbar}, \quad (6.4)$$

where E is the energy of the impending particle, V is the potential barrier height, L is the length of the barrier and m is the mass of the particle.

This simple model can give insights into the tunnelling phenomena. From Eq. 6.3, if the potential barrier increases or the energy decreases, the tunnelling probability will decrease. Importantly, the tunnelling factor is inversely proportional to both the mass and the size of the barrier. So particles of low mass will have a larger chance to tunnel through a narrow potential energy barrier.

In the context of chemical kinetics, this means that for hydrogen transfer reactions, the hydrogen atom can tunnel through the potential energy barrier separating the reactant and product. Less activation energy is needed to overcome the full TS barrier and so the reaction proceeds at a faster rate.

With the use of Ring Polymer Molecular Dynamics (RPMD) and Instanton theory, the reaction rate including the tunnelling factors can be calculated and compared to the semi-classical Eyring rate. [134, 135] In Section 6.2, the theory behind this procedure will be briefly set out.

6.1.1 Criegee intermediates

OH radicals are important in atmospheric chemistry. They react and breakdown many pollutants in the troposphere (lower atmosphere) such as NO_2 . During day time, under high light conditions, the majority of OH radicals are formed by the photolysis of ozone (O_3). At night time and in low light environments (such as cities), the most common pathway is alkene ozonolysis. [16,136] This occurs when ozone adds across the carbon-carbon double bond and splits the alkene into two molecules (Fig. 6.1).

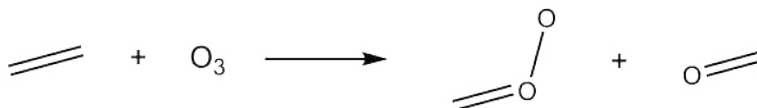


Figure 6.1: Ozonolysis reaction with ethene

The first molecule on the right in Fig. 6.1 is called a Criegee intermediate. [137] This molecule can extract a hydrogen from the terminal carbon *via* a transition state, and form a vinyl hydroperoxide product. The vinyl can then decompose into the OH radical and a vinoxy product.

The rate determining step in this mechanism is the hydrogen abstraction and migration. However, because a hydrogen transfer is involved, tunnelling factors are predicted to increase the rate of reaction.

The rates and tunnelling factors for the reaction involving the simplest Criegee intermediate CH_3CHOO , have been investigated using the Instanton method and the results presented in Section 6.4.

6.2 Theory

Calculating reaction rates using the *on-the-fly* instanton method requires calculation of the action (S). [17] From classical physics, an object will travel the path of least action. [138] For quantum mechanics, a particle has an equal probability of travelling down many paths and so all must be considered when describing the overall trajectory; each path is characterised by the action. In the classical limit, as $\hbar \rightarrow 0$, all the paths apart from the ones in the vicinity of the classical path cancel and so the classical result is obtained. [138] It is this trajectory, called the instanton, that passes from the reactants to the products *via* a first-order saddle point, that we wish to calculate.

6.2.1 Ring-polymer potential

To calculate the action for the instanton path, a new potential, called the ring-polymer potential is defined: [17]

$$U_N(\mathbf{x}) = \sum_{i=1}^N V(x_{i,1}, \dots, x_{i,f}) + \sum_{i=1}^N \sum_{j=1}^f \frac{m_j}{2\beta_N^2 \hbar^2} (x_{i,j} - x_{i-1,j})^2, \quad (6.5)$$

where $\beta_N = \beta/N$, $\beta = \frac{1}{k_B T}$ and $V(\mathbf{x}_i)$ is the energy at a point in the PES. This term is calculated whenever it is required (hence the name *on-the-fly*) by any electronic structure method of choice. The sum extends over N , which are a set of geometries close to the TS, known as ring-polymer beads.¹ This potential therefore describes a ring of ‘beads’ held together by Hookean springs (the second term in Eq.6.5). For a complete derivation of U_N from the quantum partition function, see Ref. [135].

The instanton path is found by optimising a set of beads with respect to the ring-polymer potential and the rate determined by converging the result to an increasing number of beads. This may require 128 bead geometries to be optimised, however because the system of beads is cyclic, half the beads lie on top of the other half, so only $N/2$ optimisation need to be carried out for a N bead calculation.

The number of optimisation steps can be reduced if the initial bead geometry is close to the final instanton geometry. This can be achieved by ‘laying’ a ring-polymer over the TS. Mathematically, this is realised by using, [17]

$$\mathbf{x}_i = \mathbf{x}^\ddagger + \Delta \cos\left(\frac{2\pi i}{N}\right) \mathbf{q}, \quad (6.6)$$

where the new bead geometry (labelled by i) is taken by adding a small contribution of the eigenvector which corresponds to the imaginary frequency (\mathbf{q}) of the TS geometry (\mathbf{x}^\ddagger). Δ is usually a small number that must be chosen by trial and error. For most cases $\Delta = 0.1$ has been found to be sufficient.

Eq.6.5 is a function of the chosen temperature, which should be chosen with knowledge of the shape of the potential barrier. The crossover temperature can be approximated by, [17]

$$T_c = \frac{\hbar\omega_b}{2\pi k_B}, \quad (6.7)$$

where ω_b is the imaginary vibrational wavenumber of the TS, multiplied by $i = \sqrt{-1}$.

This temperature represents the dividing point between two different tunnelling regimes. [139, 140] Above T_c all the beads of the ring-polymer sit in the saddle point

¹Not to be confused with chemical polymers. This ring-polymer is a purely mathematical construct.

and the instanton pathway collapses to the TS geometry. It is the fluctuations of the ring-polymer about the saddle point that describe the tunnelling effects. At large temperatures above T_c , these fluctuations disappear and the instanton rate reduces to the TST rate.

Below T_c , the ring-polymer corresponds to a set of delocalised geometries centred around the TS called the insanton. Fluctuations of the ring-polymer exist in this regime, which can by-pass the potential barrier and represent tunnelling effects.

For simple reactions, the instanton rate equations are only valid below T_c . Therefore it is recommended to pick a temperature 10–20 K below T_c , optimise the ring-polymer, then use that geometry as the starting point for a lower temperature.

6.2.2 Rate constants

Within Molpro, instanton (k_{inst}) and Eyring (k_{TST}) rates are both calculated and compared against each other. The Eyring rate is modified by using the partition functions from an N -bead ring-polymer.

$$k_{\text{TST}}Q_r = \frac{1}{2\pi\hbar\beta_N} Q_{\text{trans}}^{\ddagger} Q_{\text{rot}}^{\ddagger} Q_{\text{vib}}^{\ddagger} e^{-\beta V^{\ddagger}}, \quad (6.8)$$

where Q_r is the standard reactant partition function, and those labelled by \ddagger are the partition functions for the ring-polymer collapsed to the TS geometry; [17] these therefore represent the partition functions of the classical TS. As $N \rightarrow \infty$, k_{TST} reproduces the Eyring rate.

The instanton rate is an extension of Eq. 6.8,

$$k_{\text{inst}}Q_r = \frac{1}{\beta_N\hbar} \sqrt{\frac{B_N}{2\pi\beta_N\hbar^2}} Q_{\text{trans}} Q_{\text{rot}} Q_{\text{vib}} e^{-S/\hbar}, \quad (6.9)$$

$$B_N = \sum_{i=1}^N \sum_{j=1}^f m_j (\tilde{x}_{i+1,j} - \tilde{x}_{i,j})^2, \quad (6.10)$$

where the partition functions are now defined at the optimised ring-polymer geometry and $S = \beta_N U_N(\tilde{\mathbf{x}})$ is the action calculated using the potential at the optimised ring-polymer geometry.

The tunnelling factor is then defined as,

$$\kappa_{\text{tun}} \equiv \frac{k_{\text{inst}}}{k_{\text{TST}}}. \quad (6.11)$$

κ_{tun} gives information on how the rate has increased due to tunnelling effects. This is the final result that is calculated by the instanton algorithm in Molpro. Note also that the reactant partition function need not be calculated as it cancels out in Eq. 6.11.

6.3 Methodology and instanton scripts

Several python scripts and code modifications have been developed alongside Jeremy Richardson and will be available to use in Molpro. These scripts aim to semi-automate the generation of the initial bead geometries and Hessian matrices and thereby speed up instanton calculations.

To facilitate the optimisation and calculation of the instanton pathway, the geometry of several beads must be chosen *via* Eq. 6.6, which represent points close to the TS. The *initial_instanton.py* script will use the Hessian eigenvectors and TS geometry from a Molpro .xml file to generate an initial set of bead geometries and calculate T_c .

It is best to optimise a small set of beads, for example 16, before attempting 32, 64 and 128 bead calculations. To double the number of bead geometries in a file and thereby have a reasonable starting guess for the larger bead calculations, an interpolation scheme can be applied. This is carried out using the *interpolate_instanton.py* script that uses a set of bead geometries, interpolates between them and adds beads in-between the existing ones.

An instanton calculation requires the calculation of each bead Hessian before and after the optimisation routine. The interpolation script can also be used to generate an initial Hessian for larger bead geometries and thereby avoid having to calculate the Hessian before the optimisation. For example, a 16 bead Hessian can be saved to a file using the *savehess* option, interpolated using the *interpolate_instanton.py* script to a 32 bead Hessian and used in a 32 bead calculation. Only one set of bead Hessians should be calculated in each calculation.

The work flow for an instanton calculation could be as follows:

- Generate an initial set of bead geometries for a 16 bead instanton calculation using *initial_instanton.py* below T_c .
- Run the instanton calculation as specified in the Molpro manual. Use the *save* and *savehess* options to save the TS data and bead Hessian.
- Generate geometries and an initial Hessian for a 32 bead calculation using the *interpolate_instanton.py* script.
- Run the 32 bead instanton calculation remembering to reuse the previously calculated TS data and the *readhess* option to use the interpolated Hessian.
- Repeat this procedure for 64 and 128 bead calculations, or until the tunnelling factors converge.

6.4 Instanton calculations

The first transition state in the CRIEGEE database describes the Criegee intermediate (see Chapter 5). From the syn-CH₃CHOO reactant, a hydrogen is transferred from the terminal carbon to an oxygen, thus giving the VHP product that breaks down to form an hydroxyl radical. Because this step involves a hydrogen transfer process, it is possible that tunnelling will effect the rate of the reaction.

To investigate this effect, the instanton method was applied to TS1 using four different methods; Density Fitting Kohn-Sham Theory (DF-KS), Density Fitting MP2 (DF-MP2), CCSD and CCSD(T).² Both the TS and reactant geometry were optimised with each method and the cc-pVTZ basis set. The auxillary VTZ/JKFIT and VTZ/MP2FIT basis sets were also used for DF-KS and DF-MP2 respectively. The B3LYP3 hybrid functional was used for DF-KS;³ this is a standard functional that has been shown to perform well for organic molecules. [142, 143]

Crossover temperature

Before the instanton calculation, the imaginary wavenumber and crossover temperatures corresponding to each TS were calculated. These are shown in Table 6.1.

Method	$\omega_b / \text{cm}^{-1}$	T_c / K
DF-KS	1602.86	370.06
DF-MP2	1508.82	352.89
CCSD	1775.98	406.45
CCSD(T)	1695.28	388.14

Table 6.1: Imaginary wavenumbers and crossover temperatures for CRIEGEE TS1 with cc-pVTZ basis set.

Compared to the CCSD(T) result, DF-MP2 significantly under predicts the imaginary wavenumber by 186 cm⁻¹, while CCSD over predicts it by 81 cm⁻¹. This is reflected in the resulting crossover temperatures; DF-MP2 predicts a lower temperature, while CCSD predicts a higher one. DF-KS performs notably better than DF-MP2

²The density fitting method is used to approximate the two-electron integrals by using a auxiliary basis set to approximate two-electron densities. This results in considerable savings in computational time with little effect on the overall accuracy of the method. See Ref. [141] for details. Within Molpro, analytic gradients are available for both DF-KS and DF-MP2 methods.

³B3LYP3 is usually referred to as B3LYP in the literature.

in predicting the imaginary wavenumber and crossover temperature. The error compared to the CCSD(T) wavenumber is -92 cm^{-1} , which is comparable to the CCSD error. The resulting difference when compared to the CCSD(T) crossover temperature is -18 K .

Tunnelling factors

The Criegee reaction occurs in the middle of a sequential reaction mechanism. Molecules that cross over from the previous TS to form the Criegee intermediate will possess an amount of thermal energy. It is for this reason that the instanton calculations are carried out at different temperatures. The starting temperatures were chosen below the crossover temperature for each method and then lowered by 100 K intervals until 60 K. The resulting tunnelling factors are presented in Tables 6.2-6.3.

The first point to note is that as the number of beads (N) increases, the tunnelling factors for DF-KS and DF-MP2 appear to converge to an answer. It was not possible to obtain tunnelling factors with larger bead numbers for CCSD and CCSD(T) due to a non-reproducible bug in Molpro's CC program. The DF-KS and DF-MP2 results also show that it is necessary to use 128 beads in a calculation to guarantee convergence to an answer. This is less important for temperatures close to T_c (less than 100 K), as the tunnelling factors do not change orders of magnitude as N is increased. Instead, it becomes important for temperatures far from T_c as the factors can change many orders of magnitude as N increases.

It is expected that as the number of beads increases, κ_{tun} should increase. [17] However this is not observed for the DF-KS results at 260 K and 160 K or the DF-MP2 results at 160 K and 60 K. DF-KS also shows an anomaly at 360 K ($N=256$) to the converging behaviour. This is possibly due to the optimisation to a local minimum or a new saddle point.

For DF-MP2, the crossover temperature was significantly lower than the other methods and the instanton pathway only existed below 353 K. For CCSD, $T_c=406 \text{ K}$ and so a calculation could be carried out at 400 K. For comparison, only the 360 K result is presented for CCSD.

All the methods predict similar tunnelling factors at 360 K (340 K for DF-MP2). Therefore at this temperature, the reaction is predicted to proceed faster compared to the classical rate by a factor of 20.

For 260 K, the methods produce a larger range of results for the κ_{tun} . Compared to CCSD(T), both DF methods under predict this factor, with DF-MP2 predicting a slower reaction by a factor of 930.57. CCSD, on the other hand, predicts a larger factor

Method	N	360 K	260 K	160 K	60 K
DF-KS	16	19.90	333.95	2.35×10^9	4.54×10^{47}
	32	20.71	296.00	1.07×10^9	-
	64	20.47	287.51	8.96×10^8	-
	128	20.57	283.82	8.43×10^8	-
	256	13.62	284.55	8.12×10^8	-
CCSD	16	25.72	2874.38	2.18×10^{11}	-
CCSD(T)	16	21.35	948.40	1.52×10^{10}	6.48×10^{56}

Table 6.2: Tunnelling factors calculated with cc-pVTZ basis set.

Method	N	340 K	260 K	160 K	60 K
DF-MP2	16	6.46	6.73	4.33×10^6	1.26×10^{32}
	32	8.09	17.64	33964.40	1.27×10^{29}
	64	25.59	19.58	25408.12	4.01×10^{24}
	128	26.75	17.85	24576.59	9.89×10^{23}
	256	27.41	17.83	24942.40	7.12×10^{23}

Table 6.3: Tunnelling factors calculated with cc-pVTZ basis set.

than CCSD(T) by 1925.98. A warning must be made by comparing tunnelling factors to the CCSD(T) value as this was only carried out for 16 beads. However, it seems unlikely that the 360 K and 260 K values will change by an order of magnitude as N is increased.

The closest value to the CCSD(T) result is DF-KS, which predicts a slower reaction by a factor of 664. This is not surprising as DF-KS reproduced the barrier height well compared to CCSD(T) and is therefore capable of modelling the reactive PES.

Again, for 160 K and 60 K, DF-KS produces tunnelling factors that are closest to CCSD(T), with DF-MP2 severely under predicting the amount of tunnelling for both temperatures. It becomes difficult to converge the instanton calculations at low temperatures like this and so only a 16 bead calculation could be carried out with DF-KS.

Also presented in Table 6.4 are tunnelling for various temperatures calculated with CCSD(T)/cc-pVDZ. These can serve as a comparison to the limited CCSD(T)/cc-pVTZ results.

For the $N=16$ calculations, a smaller basis produces an enhanced tunnelling factor.

N	360 K	260 K	160 K	60 K
16	43.52	3451.58	1.7×10^{11}	1.5×10^{58}
32	55.33	3593.28	1.1×10^{11}	1.4×10^{64}
64	55.28	3573.25	8.4×10^{10}	2.2×10^{55}
128	53.98	3638.57	1.0×10^{11}	6.5×10^{60}

Table 6.4: Tunnelling factors for CCSD(T) calculated with cc-pVDZ

The most important differences are for κ_{tun} at 360 K and 260 K, each of which are increased by a factor of 0.5 and 0.3 respectively. For 160 K and 60 K the factors are enhanced by one order or magnitude and two orders of magnitude respectively.

It is also interesting to note that as N increases, the tunnelling factors increase. This is true, except at $N=64$ where the factors at all temperatures decrease, before increasing again at $N=128$. This could be a sign of possible oscillating behaviour in the convergence of the tunnelling factors.

Mass-weighted pathways

The differences in tunnelling factors can be investigated by plotting the potential energy along the mass-weighted instanton pathway. These pathways are defined by the action and show the effective barrier through which the tunnelling must occur.

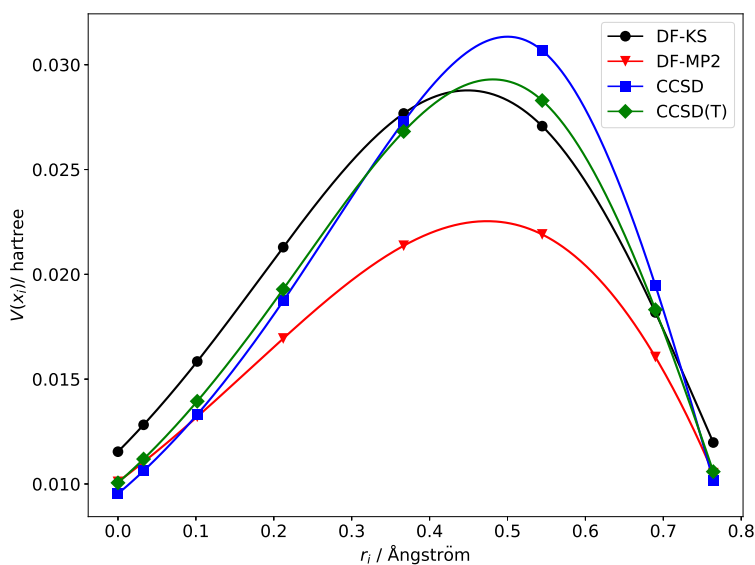


Figure 6.2: Potential energy along one half of a 16 bead instanton pathway at 260 K; calculated with cc-pVTZ basis.

Fig. 6.2 shows the mass-weighted pathways at 260 K and $N=16$. The DF-MP2 result produces a smaller and narrower pathway that passes closer to the saddle point and therefore results in a lower tunnelling factor. CCSD on the other hand produces a taller barrier which indicates a larger tunnelling factor. DF-KS and CCSD(T) show similar barrier heights and widths. CCSD(T) produces a slightly taller barrier, which corresponds to the larger tunnelling factors compared to DF-KS.

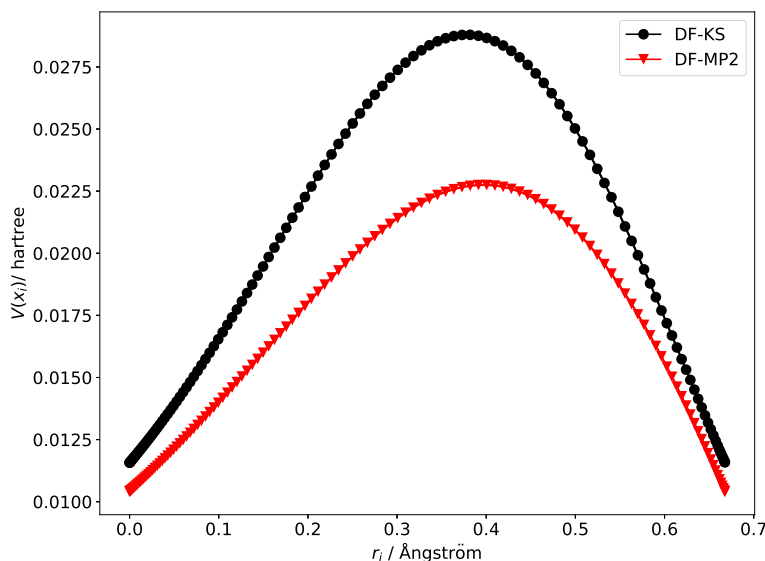


Figure 6.3: Potential energy along one half of a 256 bead instanton pathway at 260 K; calculated with cc-pVTZ basis.

Fig. 6.3 also shows the results of the DF-KS and DF-MP2 calculations at 260 K and $N=256$. These converged results mirror the behaviour for the $N=16$ bead calculations. DF-MP2 produces a smaller and narrower barrier which is closer to the TS saddle point, therefore producing a lower tunnelling factor. The DF-KS barrier is taller and wider which means it should produce larger tunnelling factors at 260 K.

Finally Fig. 6.4 compares the pathways for the 16 bead calculations of CCSD(T) with cc-pVDZ and cc-pVTZ basis sets. The two pathways are very similar, though the cc-pVDZ basis produces a slightly smaller and narrower barrier than cc-pVTZ. It is therefore expected that the tunnelling factor calculated with cc-pVDZ will be smaller, however this is not the case (compare Tables 6.2 and 6.3). This result should be used as a warning when comparing pathways characterised by similar action values; a 16 bead calculation may not provide enough structure to analyse the barrier in this qualitative manner.

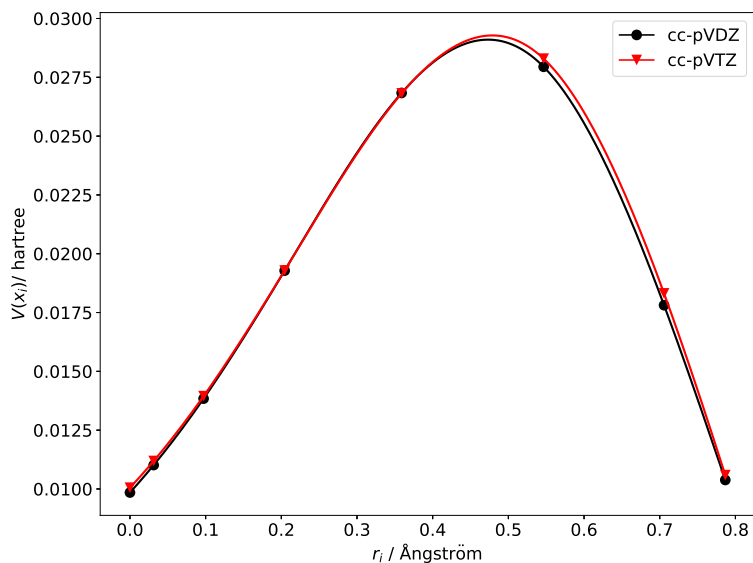


Figure 6.4: Potential energy along one half of a 16 bead instanton pathway at 260 K; calculated with CCSD(T).

Isoprene

Finally, as a comparison to the results presented above, the tunnelling factors for the Criegee intermediate based on isoprene [144] were calculated with DF-KS/B3LYP3 with cc-pVTZ and VTZ/JKFIT.

The imaginary wavenumber was calculated for the TS to be 1616.08 cm^{-1} , giving a crossover temperature of 370.06 K. Both these values are similar to the simple Criegee intermediate presented above. This is to be expected as both these imaginary wavenumbers correspond to similar vibrational modes.

The tunnelling factors for the isoprene derivative are shown in Table 6.5. The factors are similar to the DF-KS results in Table 6.2, though they are generally larger for isoprene. For example, at 260 K, the isoprene tunnelling factor is larger by a factor of 32, while at 160 K, it is larger by an order of magnitude. At 360 K the factors are similar, however the isoprene reaction is predicted to benefit less from tunnelling effects by a factor of 5.

In general, the tunnelling factors show convergence to an answer. The trend is to decrease the factors as the number of beads increases.

These results show that the isoprene system is likely to benefit more from tunnelling effects than the previously examined Criegee intermediate. This may simply be due to the barrier height being 1.86 kJ mol^{-1} higher for this reaction than the previous. The TST reaction rate will be slower, and so the instanton rate is relatively larger, thereby

N	360 K	310 K	260 K	210 K	160 K
16	18.62	35.81	374.12	66113.20	2.90×10^9
32	18.68	34.51	330.85	49706.60	1.40×10^9
64	18.76	34.25	320.00	45622.13	1.15×10^9
128	15.93	34.20	317.53	44800.66	1.08×10^9

Table 6.5: Tunnelling factors calculated at DF-KS/cc-pVTZ and cc-pVTZ/JKFIT

producing a larger tunnelling factor.

6.5 Conclusion

The reaction rates and tunnelling factors have been investigated for the simplest Criegee intermediate and an isoprene derivative using Molpro’s instanton program and four different electronic structure methods.

Overall, hydrogen tunnelling does lead to an increase in the rate of reaction compared to the TST for both reactions. For temperatures close to the crossover temperature (360 K), all methods predict an enhanced rate of by a factor of around 20. For lower temperatures, the tunnelling factors increase greatly and all methods give significant deviations from the classical rate.

For the simplest Criegee system, DF-MP2 leads to an under prediction of the imaginary wavenumber of the transition state and therefore a decrease in the crossover temperature. As a result, it predicts that lower tunnelling factors at the temperatures that were investigated compared to the (limited) CCSD(T) results.

CCSD, on the other hand, leads to an over prediction of the imaginary wavenumber and to an increase in the crossover temperature. This leads to larger tunnelling factors when compared to CCSD(T).

Surprisingly, DF-KS produces the closest results to CCSD(T) at all temperatures, apart from the anomalous results at 360 K ($N=256$). The instanton method is ultimately based upon a potential that is calculated by the electronic structure methods. DF-KS method manages to reproduce the barrier height of CCSD(T) and therefore describe the PES more accurately than the other methods. Due to its small computational cost and accurate results, it is recommended to use DF-KS in further instanton calculations involving organic molecules.

With this project, there is plenty of scope for further work. For example, it would be interesting to use OQVCCDR(T) in these calculations. In general, the QV methods

produce larger barrier heights (see Chapter 5) and therefore it is predicted that they will produce larger tunnelling factors than CCSD(T).

Other DFT functionals could and should be tested to see if they can produce closer answers that match the CCSD(T) result. B3LYP3 is a well known and reliable hybrid functional for organic molecules. However other modern functionals, such as the Minnesota M06-2X functional have been shown to reproduce barrier heights to high accuracy [91] and could therefore be of great use in instanton calculations.

Finally, only two Criegee intermediates have been investigated here. Other Criegee intermediates, such as derivatives of methylstyrene and α -pinene, occur naturally in the troposphere. Instanton calculations could be carried out on these to examine if the amount of hydrogen tunnelling increases or decrease with these systems. In these cases, it would become necessary to use DF-KS as CCSD would be too computationally expensive.

Chapter 7

Unrestricted Quasi-Variational Coupled Cluster theory

Many interesting molecular systems do not possess an even number of electrons; they are open-shell, not closed-shell. To date, only closed-shell QVCCD codes have been implemented within Molpro. An attempt towards an Unrestricted Quasi-Variational Coupled Cluster Doubles (UQVCCD) method has been made by deriving the open-shell equations. As a result of presenting these equations, it is hoped that the future development of a UQVCCD program will be made easier.

7.1 UQVCCD theory

It would be enough just to use the spin-orbital equations defined in Chapter 4 as the set of open-shell equations because the spin-orbitals are summed over the different spin cases. However, there would be many blocks in the transformed amplitude and residual tensors that would be zero due to conservation of the m_s quantum number; for example, $q\bar{t}_{\bar{a}\bar{b}}^{\bar{i}\bar{j}} = 0$. Significant computational savings can be made by explicitly deriving all the non-zero spin cases (*e.g.* \tilde{t} , \bar{t} and $t_{\bar{a}\bar{b}}^{\bar{i}\bar{j}}$).

7.1.1 Restricted and unrestricted formalisms

The choice of a reference wavefunction becomes important when proposing an open-shell QVCCD program. Both Unrestricted Hartree-Fock (UHF) and Restricted Open-Shell Hartree-Fock (ROHF) wavefunctions could be used as a reference as both are able to model open-shell systems.

UHF consists of two sets of simultaneous HF equations; one for the α electrons

and one for the β . [8] As a result, the wavefunction is comprised of two different sets of α and β orbitals. Usually, the UHF energy is lower than the RHF, however the wavefunction is no longer an eigenfunction of the total spin operator (\hat{S}^2) and so suffers from spin-contamination (*i.e.* the mixing of undesired higher spin-states). [145] This contamination becomes worse in high non-dynamic correlation regimes and so no longer becomes a valid reference for CC methods.¹

In the ROHF method, each pair of electrons are restricted to occupy the same spatial orbital. [146, 147] The unpaired electrons are then free to occupy single orbitals by themselves. The resulting equations look similar to the Roothaan-Hall equations of RHF (see Chapter 2). As a result, a single set of orbitals can be used for both α and β electrons, instead of the two sets used in UHF. This produces a single set of two-electron integrals, which allows for the different spin cases to be formulated explicitly. [148] Additionally, the ROHF wavefunction is an eigenfunction of \hat{S}^2 and so does not suffer from spin-contamination.

It is therefore simpler to use the ROHF wavefunction as the reference instead of the UHF wavefunction. However, \hat{S}^2 does not generally commute with \hat{T} and so an unrestricted CC wavefunction, like UCCSD, will still suffer from spin-contamination. [149, 150] Bartlett has shown that some of this spin-contamination is removed by left projection of the CC energy equation onto a proper spin-eigenfunction, like ROHF. [151] The remaining spin-contamination arises in the amplitude equations and higher powers of \hat{T} .

A different approach involves constructing the \hat{T}_1 and \hat{T}_2 operators so they commute with \hat{S}^2 . [149] The explicit spin excitation operators $\hat{e}_{\bar{a}\bar{i}}$ and $\hat{e}_{\bar{a}\bar{i}}$ can be replaced by a smaller set of spin summed operators like $\hat{E}_{\bar{a}\bar{i}} = \hat{e}_{\bar{a}\bar{i}} + \hat{e}_{\bar{a}\bar{i}}$ and their products. [148]. The resulting cluster operators will still produce a spin eigenfunction that spans the first order interaction space (*i.e.* the space that forms non-zero matrix elements with the reference wavefunction), but will be computationally cheaper. This describes the Restricted CCSD (RCCSD) method.

Spin contamination still remains a problem, but is predicted to be minimal. [148] An issue with RCCSD is that the working equations are more complicated than UCCSD.

It is proposed, for the reasons given above, that the ROHF wavefunction should be used as the reference for the future open-shell QVCCD program. The UQVCCD equations are presented here, however there is no reason that a RQVCCD program could be developed that would be computationally cheaper to execute.

¹“Once lost, good quantum numbers are hard to recover...” [146]

7.2 UQVCCD equations

7.2.1 Density matrices

$$\begin{aligned}
{}_{\mathcal{A}}U_{ba} &= \delta_{ba} + {}_{\mathcal{A}}\eta_{ba}, \\
{}_{\mathcal{A}}\tilde{U}_{ba} &= \tilde{\delta}_{ba} + \frac{1}{2}(t_{\tilde{b}\tilde{c}}^{\tilde{i}\tilde{j}}t_{\tilde{a}\tilde{c}}^{\tilde{i}\tilde{j}} + t_{\tilde{b}\tilde{c}}^{\tilde{i}\tilde{j}}t_{\tilde{a}\tilde{c}}^{\tilde{i}\tilde{j}}), \\
{}_{\mathcal{A}}\bar{U}_{ba} &= \bar{\delta}_{ba} + \frac{1}{2}(t_{\tilde{b}\tilde{c}}^{\tilde{i}\tilde{j}}t_{\tilde{a}\tilde{c}}^{\tilde{i}\tilde{j}} + t_{\tilde{b}\tilde{c}}^{\tilde{i}\tilde{j}}t_{\tilde{a}\tilde{c}}^{\tilde{i}\tilde{j}}).
\end{aligned} \tag{7.1}$$

$$\begin{aligned}
{}_{\mathcal{B}}U_{ji} &= \delta_{ji} + {}_{\mathcal{B}}\eta_{ji}, \\
{}_{\mathcal{B}}\tilde{U}_{ji} &= \tilde{\delta}_{ji} + \frac{1}{2}(t_{\tilde{a}\tilde{b}}^{\tilde{i}\tilde{k}}t_{\tilde{a}\tilde{b}}^{\tilde{j}\tilde{k}} + t_{\tilde{a}\tilde{b}}^{\tilde{i}\tilde{k}}t_{\tilde{a}\tilde{b}}^{\tilde{j}\tilde{k}}), \\
{}_{\mathcal{B}}\bar{U}_{ji} &= \bar{\delta}_{ji} + \frac{1}{2}(t_{\tilde{a}\tilde{b}}^{\tilde{i}\tilde{k}}t_{\tilde{a}\tilde{b}}^{\tilde{j}\tilde{k}} + t_{\tilde{a}\tilde{b}}^{\tilde{i}\tilde{k}}t_{\tilde{a}\tilde{b}}^{\tilde{j}\tilde{k}}).
\end{aligned} \tag{7.2}$$

$${}_{\mathcal{C}}U_{ki}^{lj} = \delta_{ki}\delta_{lj} + {}_{\mathcal{C}}\eta_{ki}^{lj},$$

$${}_{\mathcal{C}}\eta_{ki}^{lj} = \begin{pmatrix} & \tilde{k}\tilde{l} & \tilde{k}\tilde{l} & \tilde{k}\tilde{l} & \tilde{k}\tilde{l} \\ \tilde{j}\tilde{n} & \mathcal{C}_1 & \mathbf{0} & \mathbf{0} & \mathbf{0} \\ \tilde{j}\tilde{n} & \mathbf{0} & \mathcal{C}_2 & \mathcal{C}_2^\dagger & \mathbf{0} \\ \tilde{j}\tilde{n} & \mathbf{0} & \mathcal{C}_2 & \mathcal{C}_2 & \mathbf{0} \\ \bar{j}\bar{n} & \mathbf{0} & \mathbf{0} & \mathbf{0} & \mathcal{C}_3 \end{pmatrix},$$

$$\begin{aligned}
{}_{\mathcal{C}_1}\tilde{U}_{ki}^{lj} &= \tilde{\delta}_{ki}^{lj} + \frac{1}{2}t_{\tilde{a}\tilde{b}}^{\tilde{i}\tilde{j}}t_{\tilde{a}\tilde{b}}^{\tilde{k}\tilde{l}}, \\
{}_{\mathcal{C}_3}\bar{U}_{ki}^{lj} &= \bar{\delta}_{ki}^{lj} + \frac{1}{2}t_{\tilde{a}\tilde{b}}^{\tilde{i}\tilde{j}}t_{\tilde{a}\tilde{b}}^{\tilde{k}\tilde{l}}, \\
{}_{\mathcal{C}_2}U_{\tilde{k}\tilde{i}}^{\tilde{l}\tilde{j}} &= \delta_{\tilde{k}\tilde{i}}^{\tilde{l}\tilde{j}} + t_{\tilde{a}\tilde{b}}^{\tilde{i}\tilde{j}}t_{\tilde{a}\tilde{b}}^{\tilde{k}\tilde{l}}, \\
{}_{\mathcal{C}_2}U_{\tilde{k}\tilde{i}}^{\tilde{l}\tilde{j}} &= \delta_{\tilde{k}\tilde{i}}^{\tilde{l}\tilde{j}} + t_{\tilde{a}\tilde{b}}^{\tilde{i}\tilde{j}}t_{\tilde{a}\tilde{b}}^{\tilde{k}\tilde{l}}.
\end{aligned} \tag{7.3}$$

$${}_{\mathcal{D}}U_{ab}^{ij} = \delta_{ab}\delta_{ij} + {}_{\mathcal{D}}\eta_{ab}^{ij},$$

$${}_{\mathcal{D}}\eta_{ab}^{ij} = \begin{pmatrix} & \tilde{j}\tilde{b} & \tilde{j}\tilde{b} & \tilde{j}\tilde{b} & \tilde{j}\tilde{b} \\ \tilde{a}\tilde{i} & \mathcal{D}_1 & \mathbf{0} & \mathbf{0} & \mathcal{D}_5^\dagger \\ \tilde{a}\tilde{i} & \mathbf{0} & \mathcal{D}_2 & \mathbf{0} & \mathbf{0} \\ \tilde{a}\tilde{i} & \mathbf{0} & \mathbf{0} & \mathcal{D}_3 & \mathbf{0} \\ \bar{a}\bar{i} & \mathcal{D}_5 & \mathbf{0} & \mathbf{0} & \mathcal{D}_4 \end{pmatrix},$$

$$\begin{aligned}
{}_{\mathcal{D}_1}\tilde{U}_{ab}^{ij} &= \tilde{\delta}_{ab}\tilde{\delta}_{ij} + t_{\tilde{a}\tilde{c}}^{\tilde{i}\tilde{k}}t_{\tilde{b}\tilde{c}}^{\tilde{j}\tilde{k}} + t_{\tilde{a}\tilde{c}}^{\tilde{i}\tilde{k}}t_{\tilde{b}\tilde{c}}^{\tilde{j}\tilde{k}}, \\
{}_{\mathcal{D}_2}U_{\tilde{a}\tilde{b}}^{\tilde{i}\tilde{j}} &= \bar{\delta}_{ab}\tilde{\delta}_{ij} + t_{\tilde{a}\tilde{c}}^{\tilde{i}\tilde{k}}t_{\tilde{b}\tilde{c}}^{\tilde{j}\tilde{k}}, \\
{}_{\mathcal{D}_3}U_{\tilde{a}\tilde{b}}^{\tilde{i}\tilde{j}} &= \tilde{\delta}_{ab}\bar{\delta}_{ij} + t_{\tilde{a}\tilde{c}}^{\tilde{i}\tilde{k}}t_{\tilde{b}\tilde{c}}^{\tilde{j}\tilde{k}}, \\
{}_{\mathcal{D}_4}\bar{U}_{ab}^{ij} &= \bar{\delta}_{ab}\bar{\delta}_{ij} + t_{\tilde{a}\tilde{c}}^{\tilde{i}\tilde{k}}t_{\tilde{b}\tilde{c}}^{\tilde{j}\tilde{k}} + t_{\tilde{a}\tilde{c}}^{\tilde{i}\tilde{k}}t_{\tilde{b}\tilde{c}}^{\tilde{j}\tilde{k}}, \\
{}_{\mathcal{D}_5}U_{\tilde{a}\tilde{b}}^{\tilde{i}\tilde{j}} &= \delta_{\tilde{a}\tilde{b}}\delta_{\tilde{i}\tilde{j}} + t_{\tilde{a}\tilde{c}}^{\tilde{i}\tilde{k}}t_{\tilde{b}\tilde{c}}^{\tilde{j}\tilde{k}} + t_{\tilde{a}\tilde{c}}^{\tilde{i}\tilde{k}}t_{\tilde{b}\tilde{c}}^{\tilde{j}\tilde{k}}.
\end{aligned} \tag{7.4}$$

A simple rotation of the ${}_{\mathcal{D}}\eta_{ab}^{ij}$ matrix can no longer be used to uncouple the \mathcal{D}_1 , \mathcal{D}_4 and \mathcal{D}_5 blocks, like in the closed-shell equations; the complete matrix must be constructed and powered.

Overall, twelve different \mathbf{U} matrices need to be constructed to form the transformed amplitude and residual equations. Forming these matrices will therefore take about twice the time as QVCCD, which only requires six different \mathbf{U} matrices.

7.2.2 Transformed amplitudes

$$\begin{aligned}
q\bar{t}_{\bar{a}\bar{b}}^{\bar{i}\bar{j}} = & \left[(\mathcal{A}\tilde{\mathbf{U}}^{-\frac{q}{2}})_{ac} \bar{t}_{\bar{c}\bar{b}}^{\bar{i}\bar{j}} + (\mathcal{A}\bar{\mathbf{U}}^{-\frac{q}{2}})_{bc} \bar{t}_{\bar{a}\bar{c}}^{\bar{i}\bar{j}} \right] \\
& + \left[(\mathcal{B}\tilde{\mathbf{U}}^{-\frac{q}{2}})_{ki} \bar{t}_{\bar{a}\bar{b}}^{\bar{k}\bar{j}} + (\mathcal{B}\bar{\mathbf{U}}^{-\frac{q}{2}})_{kj} \bar{t}_{\bar{a}\bar{b}}^{\bar{i}\bar{k}} \right] \\
& - \frac{1}{2} \left[(\mathcal{C}\mathbf{U}^{-\frac{q}{2}})_{\bar{k}\bar{i}} \bar{t}_{\bar{a}\bar{b}}^{\bar{k}\bar{l}} + (\mathcal{C}\mathbf{U}^{-\frac{q}{2}})_{\bar{k}\bar{i}} \bar{t}_{\bar{a}\bar{b}}^{\bar{l}\bar{k}} \right] \\
& - \frac{1}{2} \left[(\mathcal{D}\mathbf{U}^{-\frac{q}{2}})_{\bar{a}\bar{c}} \bar{t}_{\bar{c}\bar{b}}^{\bar{k}\bar{j}} + (\mathcal{D}\mathbf{U}^{-\frac{q}{2}})_{\bar{a}\bar{c}} \bar{t}_{\bar{c}\bar{b}}^{\bar{j}\bar{k}} \right] \\
& - (\mathcal{D}\mathbf{U}^{-\frac{q}{2}})_{\bar{a}\bar{c}} \bar{t}_{\bar{c}\bar{b}}^{\bar{j}\bar{k}} \\
& - (\mathcal{D}\mathbf{U}^{-\frac{q}{2}})_{\bar{b}\bar{c}} \bar{t}_{\bar{c}\bar{a}}^{\bar{i}\bar{k}} \\
& + (\mathcal{D}\mathbf{U}^{-\frac{q}{2}})_{\bar{b}\bar{c}} \bar{t}_{\bar{c}\bar{a}}^{\bar{k}\bar{i}} + (\mathcal{D}\mathbf{U}^{-\frac{q}{2}})_{\bar{b}\bar{c}} \bar{t}_{\bar{c}\bar{a}}^{\bar{i}\bar{k}} \quad (7.5)
\end{aligned}$$

$$\begin{aligned}
q\bar{t}_{\bar{a}\bar{b}}^{\bar{i}\bar{j}} = & 2 \left[\frac{1}{2} (1 - \tilde{\tau}_{ab}) (\mathcal{A}\tilde{\mathbf{U}}^{-\frac{q}{2}})_{ac} \bar{t}_{\bar{c}\bar{b}}^{\bar{i}\bar{j}} \right] \\
& + 2 \left[\frac{1}{2} (1 - \tilde{\tau}_{ij}) (\mathcal{B}\tilde{\mathbf{U}}^{-\frac{q}{2}})_{ki} \bar{t}_{\bar{a}\bar{b}}^{\bar{k}\bar{j}} \right] \\
& - 1 \left[\frac{1}{2} (\mathcal{C}\tilde{\mathbf{U}}^{-\frac{q}{2}})_{\bar{k}\bar{i}}^{\bar{l}\bar{j}} \bar{t}_{\bar{a}\bar{b}}^{\bar{k}\bar{l}} \right] \\
& - 2 \left[\frac{1}{4} (1 - \tilde{\tau}_{ij}) (1 - \tilde{\tau}_{ab}) \left((\mathcal{D}\tilde{\mathbf{U}}^{-\frac{q}{2}})_{\bar{a}\bar{c}}^{\bar{i}\bar{k}} \bar{t}_{\bar{c}\bar{b}}^{\bar{k}\bar{j}} + (\mathcal{D}\mathbf{U}^{-\frac{q}{2}})_{\bar{a}\bar{c}} \bar{t}_{\bar{c}\bar{b}}^{\bar{i}\bar{k}} \right) \right] \quad (7.6)
\end{aligned}$$

$$\begin{aligned}
q\bar{t}_{\bar{a}\bar{b}}^{\bar{i}\bar{j}} = & 2 \left[\frac{1}{2} (1 - \bar{\tau}_{ab}) (\mathcal{A}\bar{\mathbf{U}}^{-\frac{q}{2}})_{ac} \bar{t}_{\bar{c}\bar{b}}^{\bar{i}\bar{j}} \right] \\
& + 2 \left[\frac{1}{2} (1 - \bar{\tau}_{ij}) (\mathcal{B}\bar{\mathbf{U}}^{-\frac{q}{2}})_{ki} \bar{t}_{\bar{a}\bar{b}}^{\bar{k}\bar{j}} \right] \\
& - 1 \left[\frac{1}{2} (\mathcal{C}\bar{\mathbf{U}}^{-\frac{q}{2}})_{\bar{k}\bar{i}}^{\bar{l}\bar{j}} \bar{t}_{\bar{a}\bar{b}}^{\bar{k}\bar{l}} \right] \\
& - 2 \left[\frac{1}{4} (1 - \bar{\tau}_{ij}) (1 - \bar{\tau}_{ab}) \left((\mathcal{D}\mathbf{U}^{-\frac{q}{2}})_{\bar{a}\bar{c}} \bar{t}_{\bar{c}\bar{b}}^{\bar{i}\bar{k}} + (\mathcal{D}\mathbf{U}^{-\frac{q}{2}})_{\bar{a}\bar{c}} \bar{t}_{\bar{c}\bar{b}}^{\bar{i}\bar{k}} \right) \right] \quad (7.7)
\end{aligned}$$

There are now six different transformed amplitude equations to construct in UQVCCD, compared to only two in QVCCD. It is expected that UQVCCD will take three times longer than QVCCD in calculating these quantities.

7.2.3 Residuals

$$\begin{aligned}
{}_q\tilde{g}_{ab}^{ij} &= (1 - \tilde{\tau}_{ab}) \left[\frac{1}{2} ({}^A\tilde{R}_{ae} + {}^A\tilde{R}_{ea}) \tilde{t}_{eb}^{ij} + ({}^A\tilde{U}^{-\frac{q}{2}})_{ca} {}_q\tilde{V}_{cb}^{ij} \right] \\
&+ (1 - \tilde{\tau}_{ij}) \left[\frac{1}{2} ({}^B\tilde{R}_{oi} + {}^B\tilde{R}_{io}) \tilde{t}_{ab}^{oj} + ({}^B\tilde{U}^{-\frac{q}{2}})_{ik} {}_q\tilde{V}_{ab}^{kj} \right] \\
&- \frac{1}{4} \left[({}^C\tilde{R}_{im}^{jn} + {}^C\tilde{R}_{mi}^{nj}) \tilde{t}_{ab}^{mn} + 2({}^C\tilde{U}^{-\frac{q}{2}})_{ik} {}_q\tilde{V}_{ab}^{kl} \right] \\
&- \frac{1}{2} (1 - \tilde{\tau}_{ij})(1 - \tilde{\tau}_{ab}) \left[({}^D\tilde{R}_{ag}^{io} + {}^D\tilde{R}_{ga}^{oi}) \tilde{t}_{gb}^{oj} + ({}^D\tilde{R}_{\bar{a}\bar{g}}^{\bar{i}\bar{o}} + {}^D\tilde{R}_{\bar{g}\bar{a}}^{\bar{o}\bar{i}}) \tilde{t}_{\bar{g}\bar{b}}^{\bar{o}\bar{j}} \right] \\
&+ ({}^D\tilde{U}^{-\frac{q}{2}})_{ca} {}_q\tilde{V}_{cb}^{kj} + ({}^D\tilde{U}^{-\frac{q}{2}})_{\bar{c}\bar{a}}^{\bar{k}\bar{i}} {}_q\tilde{V}_{\bar{c}\bar{b}}^{\bar{k}\bar{j}} \Big], \tag{7.8}
\end{aligned}$$

$$\begin{aligned}
{}^A\tilde{R}_{eg} &= \tilde{Q}_{e,g}^{a,c} {}^A\tilde{F}_{ac}, & {}^B\tilde{R}_{om} &= \tilde{Q}_{o,m}^{k,i} {}^B\tilde{F}_{ki}, \\
{}^C\tilde{R}_{om}^{pn} &= \tilde{Q}_{op,mn}^{kl,ij} {}^C\tilde{F}_{ki}^{lj}, & {}^D\tilde{R}_{eg}^{mo} &= \tilde{Q}_{em,go}^{ai,ck} {}^D\tilde{F}_{ac}^{ik}, \\
{}^D\tilde{R}_{\bar{e}\bar{g}}^{\bar{m}\bar{o}} &= Q_{\bar{e}\bar{m},\bar{g}\bar{o}}^{\bar{a}\bar{i},\bar{c}\bar{k}} {}^D\tilde{F}_{\bar{a}\bar{c}}^{\bar{i}\bar{k}}.
\end{aligned} \tag{7.9}$$

$$\begin{aligned}
{}^A\tilde{F}_{ac} &= {}_q\tilde{V}_{ab}^{ij} \tilde{t}_{cb}^{ij}, & {}^B\tilde{F}_{ki} &= {}_q\tilde{V}_{ab}^{ij} \tilde{t}_{ab}^{kj}, \\
{}^C\tilde{F}_{ki}^{lj} &= {}_q\tilde{V}_{ab}^{ij} \tilde{t}_{ab}^{kl}, & {}^D\tilde{F}_{ac}^{ik} &= {}_q\tilde{V}_{ab}^{ij} \tilde{t}_{cb}^{kj}, \\
{}^D\tilde{F}_{\bar{a}\bar{c}}^{\bar{i}\bar{k}} &= {}_q\tilde{V}_{\bar{a}\bar{b}}^{\bar{i}\bar{j}} \tilde{t}_{\bar{c}\bar{b}}^{\bar{k}\bar{j}}.
\end{aligned} \tag{7.10}$$

$$\begin{aligned}
{}_q\bar{g}_{ab}^{ij} &= (1 - \bar{\tau}_{ab}) \left[\frac{1}{2} ({}^A\bar{R}_{ae} + {}^A\bar{R}_{ea}) \bar{t}_{eb}^{ij} + ({}^A\bar{U}^{-\frac{q}{2}})_{ca} {}_q\bar{V}_{cb}^{ij} \right] \\
&+ (1 - \bar{\tau}_{ij}) \left[\frac{1}{2} ({}^B\bar{R}_{oi} + {}^B\bar{R}_{io}) \bar{t}_{ab}^{oj} + ({}^B\bar{U}^{-\frac{q}{2}})_{ik} {}_q\bar{V}_{ab}^{kj} \right] \\
&- \frac{1}{4} \left[({}^C\bar{R}_{im}^{jn} + {}^C\bar{R}_{mi}^{nj}) \bar{t}_{ab}^{mn} + 2({}^C\bar{U}^{-\frac{q}{2}})_{ik} {}_q\bar{V}_{ab}^{kl} \right] \\
&- \frac{1}{2} (1 - \bar{\tau}_{ij})(1 - \bar{\tau}_{ab}) \left[({}^D\bar{R}_{ag}^{io} + {}^D\bar{R}_{ga}^{oi}) \bar{t}_{gb}^{oj} + ({}^D\bar{R}_{\bar{a}\bar{g}}^{\bar{i}\bar{o}} + {}^D\bar{R}_{\bar{g}\bar{a}}^{\bar{o}\bar{i}}) \bar{t}_{\bar{g}\bar{b}}^{\bar{o}\bar{j}} \right] \\
&+ ({}^D\bar{U}^{-\frac{q}{2}})_{ca} {}_q\bar{V}_{cb}^{kj} + ({}^D\bar{U}^{-\frac{q}{2}})_{\bar{c}\bar{a}}^{\bar{k}\bar{i}} {}_q\bar{V}_{\bar{c}\bar{b}}^{\bar{k}\bar{j}} \Big], \tag{7.11}
\end{aligned}$$

$$\begin{aligned}
{}^A\bar{R}_{eg} &= \bar{Q}_{e,g}^{a,c} {}^A\bar{F}_{ac}, & {}^B\bar{R}_{om} &= \bar{Q}_{o,m}^{k,i} {}^B\bar{F}_{ki}, \\
{}^C\bar{R}_{om}^{pn} &= \bar{Q}_{op,mn}^{kl,ij} {}^C\bar{F}_{ki}^{lj}, & {}^D\bar{R}_{eg}^{mo} &= \bar{Q}_{em,go}^{ai,ck} {}^D\bar{F}_{ac}^{ik}, \\
{}^D\bar{R}_{\bar{e}\bar{g}}^{\bar{m}\bar{o}} &= Q_{\bar{e}\bar{m},\bar{g}\bar{o}}^{\bar{a}\bar{i},\bar{c}\bar{k}} {}^D\bar{F}_{\bar{a}\bar{c}}^{\bar{i}\bar{k}},
\end{aligned} \tag{7.12}$$

$$\begin{aligned}
{}^A\bar{F}_{ac} &= {}_q\bar{V}_{ab}^{ij} \bar{t}_{cb}^{ij}, & {}^B\bar{F}_{ki} &= {}_q\bar{V}_{ab}^{ij} \bar{t}_{ab}^{kj}, \\
{}^C\bar{F}_{ki}^{lj} &= {}_q\bar{V}_{ab}^{ij} \bar{t}_{ab}^{kl}, & {}^D\bar{F}_{ac}^{ik} &= {}_q\bar{V}_{ab}^{ij} \bar{t}_{cb}^{kj}, \\
{}^D\bar{F}_{\bar{a}\bar{c}}^{\bar{i}\bar{k}} &= {}_q\bar{V}_{\bar{a}\bar{b}}^{\bar{i}\bar{j}} \bar{t}_{\bar{c}\bar{b}}^{\bar{k}\bar{j}}.
\end{aligned} \tag{7.13}$$

$$\begin{aligned}
{}_q g_{\bar{a}\bar{b}}^{\bar{i}\bar{j}} = & \left[\frac{1}{2}({}^{\mathcal{A}}\tilde{\mathbf{R}}_{ae} + {}^{\mathcal{A}}\tilde{\mathbf{R}}_{ea})t_{\bar{c}\bar{b}}^{\bar{i}\bar{j}} + ({}^{\mathcal{A}}\tilde{\mathbf{U}}^{-\frac{q}{2}})_{ca} {}_q \mathbf{V}_{\bar{c}\bar{b}}^{\bar{i}\bar{j}} + \frac{1}{2}({}^{\mathcal{A}}\bar{\mathbf{R}}_{be} + {}^{\mathcal{A}}\bar{\mathbf{R}}_{eb})t_{\bar{a}\bar{e}}^{\bar{i}\bar{j}} + ({}^{\mathcal{A}}\bar{\mathbf{U}}^{-\frac{q}{2}})_{cb} {}_q \mathbf{V}_{\bar{a}\bar{c}}^{\bar{i}\bar{j}} \right] \\
& + \left[\frac{1}{2}({}^{\mathcal{B}}\tilde{\mathbf{R}}_{oi} + {}^{\mathcal{B}}\tilde{\mathbf{R}}_{io})t_{\bar{a}\bar{b}}^{\bar{o}\bar{j}} + ({}^{\mathcal{B}}\tilde{\mathbf{U}}^{-\frac{q}{2}})_{ik} {}_q \mathbf{V}_{\bar{a}\bar{b}}^{\bar{k}\bar{j}} + \frac{1}{2}({}^{\mathcal{B}}\bar{\mathbf{R}}_{oj} + {}^{\mathcal{B}}\bar{\mathbf{R}}_{jo})t_{\bar{a}\bar{b}}^{\bar{i}\bar{o}} + ({}^{\mathcal{B}}\bar{\mathbf{U}}^{-\frac{q}{2}})_{jk} {}_q \mathbf{V}_{\bar{a}\bar{b}}^{\bar{i}\bar{k}} \right] \\
& - \frac{1}{4} \left[({}^{\mathcal{C}}\mathbf{R}_{i\bar{m}}^{\bar{j}\bar{n}} + {}^{\mathcal{C}}\mathbf{R}_{\bar{m}\bar{i}}^{\bar{n}\bar{j}})t_{\bar{a}\bar{b}}^{\bar{m}\bar{n}} + 2({}^{\mathcal{C}}\tilde{\mathbf{U}}^{-\frac{q}{2}})_{\bar{i}\bar{k}}^{\bar{j}\bar{l}} {}_q \mathbf{V}_{\bar{a}\bar{b}}^{\bar{k}\bar{l}} + ({}^{\mathcal{C}}\mathbf{R}_{i\bar{m}}^{\bar{j}\bar{n}} + {}^{\mathcal{C}}\mathbf{R}_{\bar{m}\bar{i}}^{\bar{n}\bar{j}})t_{\bar{a}\bar{b}}^{\bar{m}\bar{n}} + 2({}^{\mathcal{C}}\mathbf{U}^{-\frac{q}{2}})_{\bar{i}\bar{k}}^{\bar{j}\bar{l}} {}_q \mathbf{V}_{\bar{a}\bar{b}}^{\bar{k}\bar{l}} \right] \\
& - \frac{1}{2} \left[({}^{\mathcal{D}}\mathbf{R}_{\bar{a}\bar{g}}^{\bar{i}\bar{o}} + {}^{\mathcal{D}}\mathbf{R}_{\bar{g}\bar{a}}^{\bar{o}\bar{i}})t_{\bar{g}\bar{b}}^{\bar{o}\bar{j}} + ({}^{\mathcal{D}}\mathbf{U}^{-\frac{q}{2}})_{\bar{c}\bar{a}}^{\bar{k}\bar{i}} {}_q \mathbf{V}_{\bar{c}\bar{b}}^{\bar{k}\bar{i}} + ({}^{\mathcal{D}}\tilde{\mathbf{R}}_{ag}^{\bar{i}o} + {}^{\mathcal{D}}\tilde{\mathbf{R}}_{ga}^{\bar{o}i})t_{\bar{g}\bar{b}}^{\bar{o}\bar{j}} + ({}^{\mathcal{D}}\tilde{\mathbf{U}}^{-\frac{q}{2}})_{ca}^{ki} {}_q \mathbf{V}_{\bar{c}\bar{b}}^{\bar{k}\bar{j}} \right. \\
& - ({}^{\mathcal{D}}\mathbf{R}_{\bar{a}\bar{g}}^{\bar{j}\bar{o}} + {}^{\mathcal{D}}\mathbf{R}_{\bar{g}\bar{a}}^{\bar{o}\bar{j}})t_{\bar{g}\bar{b}}^{\bar{o}\bar{i}} + ({}^{\mathcal{D}}\mathbf{U}^{-\frac{q}{2}})_{\bar{c}\bar{a}}^{\bar{k}\bar{j}} {}_q \mathbf{V}_{\bar{c}\bar{b}}^{\bar{k}\bar{i}} \\
& - ({}^{\mathcal{D}}\mathbf{R}_{\bar{b}\bar{g}}^{\bar{i}\bar{o}} + {}^{\mathcal{D}}\mathbf{R}_{\bar{g}\bar{b}}^{\bar{o}\bar{i}})t_{\bar{g}\bar{a}}^{\bar{o}\bar{j}} + ({}^{\mathcal{D}}\mathbf{U}^{-\frac{q}{2}})_{\bar{c}\bar{b}}^{\bar{k}\bar{i}} {}_q \mathbf{V}_{\bar{c}\bar{a}}^{\bar{k}\bar{j}} \\
& \left. + ({}^{\mathcal{D}}\mathbf{R}_{\bar{b}\bar{g}}^{\bar{j}\bar{o}} + {}^{\mathcal{D}}\mathbf{R}_{\bar{g}\bar{b}}^{\bar{o}\bar{j}})t_{\bar{g}\bar{a}}^{\bar{o}\bar{i}} + ({}^{\mathcal{D}}\mathbf{U}^{-\frac{q}{2}})_{\bar{c}\bar{b}}^{\bar{k}\bar{j}} {}_q \tilde{\mathbf{V}}_{ca}^{ki} + ({}^{\mathcal{D}}\bar{\mathbf{R}}_{bg}^{\bar{j}o} + {}^{\mathcal{D}}\bar{\mathbf{R}}_{gb}^{\bar{o}j})t_{\bar{g}\bar{a}}^{\bar{o}\bar{i}} + ({}^{\mathcal{D}}\bar{\mathbf{U}}^{-\frac{q}{2}})_{cb}^{kj} {}_q \mathbf{V}_{\bar{c}\bar{a}}^{\bar{k}\bar{i}} \right], \tag{7.14}
\end{aligned}$$

$$\begin{aligned}
{}^{\mathcal{A}}\tilde{\mathbf{F}}_{gc} &= {}_q \mathbf{V}_{\bar{g}\bar{b}}^{\bar{i}\bar{j}} t_{\bar{c}\bar{b}}^{\bar{i}\bar{j}}, & {}^{\mathcal{A}}\bar{\mathbf{F}}_{gc} &= {}_q \mathbf{V}_{\bar{g}\bar{a}}^{\bar{i}\bar{j}} t_{\bar{c}\bar{a}}^{\bar{i}\bar{j}}, \\
{}^{\mathcal{A}}\tilde{\mathbf{R}}_{ae} &= Q_{\bar{a},\bar{e}}^{\bar{g},\bar{c}} {}^{\mathcal{A}}\tilde{\mathbf{F}}_{gc}, & {}^{\mathcal{A}}\bar{\mathbf{R}}_{be} &= Q_{\bar{b},\bar{e}}^{\bar{g},\bar{c}} {}^{\mathcal{A}}\bar{\mathbf{F}}_{gc}, \tag{7.15}
\end{aligned}$$

$$\begin{aligned}
{}^{\mathcal{B}}\tilde{\mathbf{F}}_{km} &= {}_q \mathbf{V}_{\bar{a}\bar{b}}^{\bar{m}\bar{j}} t_{\bar{a}\bar{b}}^{\bar{k}\bar{j}}, & {}^{\mathcal{B}}\bar{\mathbf{F}}_{km} &= {}_q \mathbf{V}_{\bar{a}\bar{b}}^{\bar{m}\bar{i}} t_{\bar{a}\bar{b}}^{\bar{k}\bar{i}}, \\
{}^{\mathcal{B}}\tilde{\mathbf{R}}_{oi} &= \tilde{Q}_{o,i}^{k,m} {}^{\mathcal{B}}\tilde{\mathbf{F}}_{km}, & {}^{\mathcal{B}}\bar{\mathbf{R}}_{oi} &= \bar{Q}_{o,i}^{k,m} {}^{\mathcal{B}}\bar{\mathbf{F}}_{km}, \tag{7.16}
\end{aligned}$$

$$\begin{aligned}
{}^{\mathcal{C}}\mathbf{F}_{\bar{k}\bar{o}}^{\bar{l}\bar{p}} &= {}_q \mathbf{V}_{\bar{a}\bar{b}}^{\bar{o}\bar{p}} t_{\bar{a}\bar{b}}^{\bar{k}\bar{l}}, & {}^{\mathcal{C}}\mathbf{F}_{\bar{k}\bar{o}}^{\bar{l}\bar{p}} &= {}_q \mathbf{V}_{\bar{a}\bar{b}}^{\bar{o}\bar{p}} t_{\bar{a}\bar{b}}^{\bar{k}\bar{l}}, \\
{}^{\mathcal{C}}\mathbf{F}_{\bar{k}\bar{o}}^{\bar{l}\bar{p}} &= {}_q \mathbf{V}_{\bar{a}\bar{b}}^{\bar{o}\bar{p}} t_{\bar{a}\bar{b}}^{\bar{k}\bar{l}}, & {}^{\mathcal{C}}\mathbf{F}_{\bar{k}\bar{o}}^{\bar{l}\bar{p}} &= {}_q \mathbf{V}_{\bar{a}\bar{b}}^{\bar{o}\bar{p}} t_{\bar{a}\bar{b}}^{\bar{k}\bar{l}}, \\
{}^{\mathcal{C}}\mathbf{R}_{i\bar{m}}^{\bar{j}\bar{n}} &= Q_{\bar{i}\bar{j},\bar{m}\bar{n}}^{\bar{k}\bar{l},\bar{o}\bar{p}} {}^{\mathcal{C}}\mathbf{F}_{\bar{k}\bar{o}}^{\bar{l}\bar{p}} + Q_{\bar{i}\bar{j},\bar{m}\bar{n}}^{\bar{k}\bar{l},\bar{o}\bar{p}} {}^{\mathcal{C}}\mathbf{F}_{\bar{k}\bar{o}}^{\bar{l}\bar{p}} + Q_{\bar{i}\bar{j},\bar{m}\bar{n}}^{\bar{k}\bar{l},\bar{o}\bar{p}} {}^{\mathcal{C}}\mathbf{F}_{\bar{k}\bar{o}}^{\bar{l}\bar{p}} + Q_{\bar{i}\bar{j},\bar{m}\bar{n}}^{\bar{k}\bar{l},\bar{o}\bar{p}} {}^{\mathcal{C}}\mathbf{F}_{\bar{k}\bar{o}}^{\bar{l}\bar{p}}, \tag{7.17}
\end{aligned}$$

$$\begin{aligned}
{}^{\mathcal{C}}\mathbf{F}_{\bar{k}\bar{o}}^{\bar{l}\bar{p}} &= {}_q \mathbf{V}_{\bar{a}\bar{b}}^{\bar{o}\bar{p}} t_{\bar{a}\bar{b}}^{\bar{k}\bar{l}}, & {}^{\mathcal{C}}\mathbf{F}_{\bar{k}\bar{o}}^{\bar{l}\bar{p}} &= {}_q \mathbf{V}_{\bar{a}\bar{b}}^{\bar{o}\bar{p}} t_{\bar{a}\bar{b}}^{\bar{k}\bar{l}}, \\
{}^{\mathcal{C}}\mathbf{F}_{\bar{k}\bar{o}}^{\bar{l}\bar{p}} &= {}_q \mathbf{V}_{\bar{a}\bar{b}}^{\bar{o}\bar{p}} t_{\bar{a}\bar{b}}^{\bar{k}\bar{l}}, & {}^{\mathcal{C}}\mathbf{F}_{\bar{k}\bar{o}}^{\bar{l}\bar{p}} &= {}_q \mathbf{V}_{\bar{a}\bar{b}}^{\bar{o}\bar{p}} t_{\bar{a}\bar{b}}^{\bar{k}\bar{l}}, \\
{}^{\mathcal{C}}\mathbf{R}_{i\bar{m}}^{\bar{j}\bar{n}} &= Q_{\bar{i}\bar{j},\bar{m}\bar{n}}^{\bar{k}\bar{l},\bar{o}\bar{p}} {}^{\mathcal{C}}\mathbf{F}_{\bar{k}\bar{o}}^{\bar{l}\bar{p}} + Q_{\bar{i}\bar{j},\bar{m}\bar{n}}^{\bar{k}\bar{l},\bar{o}\bar{p}} {}^{\mathcal{C}}\mathbf{F}_{\bar{k}\bar{o}}^{\bar{l}\bar{p}} + Q_{\bar{i}\bar{j},\bar{m}\bar{n}}^{\bar{k}\bar{l},\bar{o}\bar{p}} {}^{\mathcal{C}}\mathbf{F}_{\bar{k}\bar{o}}^{\bar{l}\bar{p}} + Q_{\bar{i}\bar{j},\bar{m}\bar{n}}^{\bar{k}\bar{l},\bar{o}\bar{p}} {}^{\mathcal{C}}\mathbf{F}_{\bar{k}\bar{o}}^{\bar{l}\bar{p}},
\end{aligned}$$

$$\begin{aligned} \mathcal{D}_q \mathbb{F}_{\bar{e}\bar{c}}^{\bar{m}\bar{k}} &= {}_q V_{\bar{e}\bar{b}}^{\bar{m}\bar{j}} t_{\bar{c}\bar{b}}^{\bar{k}\bar{j}}, & \mathcal{D}_q \mathbb{F}_{\bar{e}\bar{c}}^{\bar{m}\bar{k}} &= {}_q V_{\bar{e}\bar{b}}^{\bar{m}\bar{j}} t_{\bar{c}\bar{b}}^{\bar{k}\bar{j}}, \\ \mathcal{D}_q \mathbb{R}_{\bar{a}\bar{g}}^{\bar{i}\bar{o}} &= Q_{\bar{a}\bar{i},\bar{g}\bar{o}}^{\bar{e}\bar{m},\bar{c}\bar{k}} \mathcal{D}_q \mathbb{F}_{\bar{e}\bar{c}}^{\bar{m}\bar{k}} + Q_{\bar{a}\bar{i},\bar{g}\bar{o}}^{\bar{e}\bar{m},\bar{c}\bar{k}} \mathcal{D}_q \mathbb{F}_{\bar{e}\bar{c}}^{\bar{m}\bar{k}}, \end{aligned}$$

$$\begin{aligned} \mathcal{D}_q \mathbb{F}_{\bar{e}\bar{c}}^{\bar{m}\bar{k}} &= {}_q V_{\bar{e}\bar{b}}^{\bar{m}\bar{j}} t_{\bar{c}\bar{b}}^{\bar{k}\bar{j}}, \\ \mathcal{D}_q \mathbb{R}_{\bar{a}\bar{g}}^{\bar{i}\bar{o}} &= Q_{\bar{a}\bar{i},\bar{g}\bar{o}}^{\bar{e}\bar{m},\bar{c}\bar{k}} \mathcal{D}_q \mathbb{F}_{\bar{e}\bar{c}}^{\bar{m}\bar{k}}, \end{aligned}$$

$$\begin{aligned} \mathcal{D}_q \mathbb{F}_{\bar{e}\bar{c}}^{\bar{m}\bar{k}} &= {}_q V_{\bar{e}\bar{b}}^{\bar{m}\bar{i}} t_{\bar{c}\bar{b}}^{\bar{k}\bar{i}}, \\ \mathcal{D}_q \mathbb{R}_{\bar{a}\bar{g}}^{\bar{j}\bar{o}} &= Q_{\bar{a}\bar{j},\bar{g}\bar{o}}^{\bar{e}\bar{m},\bar{c}\bar{k}} \mathcal{D}_q \mathbb{F}_{\bar{e}\bar{c}}^{\bar{m}\bar{k}}, \end{aligned}$$

(7.18)

$$\begin{aligned} \mathcal{D}_q \mathbb{F}_{\bar{e}\bar{c}}^{\bar{m}\bar{k}} &= {}_q V_{\bar{e}\bar{a}}^{\bar{m}\bar{j}} t_{\bar{c}\bar{a}}^{\bar{k}\bar{j}}, \\ \mathcal{D}_q \mathbb{R}_{\bar{b}\bar{g}}^{\bar{i}\bar{o}} &= Q_{\bar{b}\bar{i},\bar{g}\bar{o}}^{\bar{e}\bar{m},\bar{c}\bar{k}} \mathcal{D}_q \mathbb{F}_{\bar{e}\bar{c}}^{\bar{m}\bar{k}}, \end{aligned}$$

$$\begin{aligned} \mathcal{D}_q \mathbb{F}_{\bar{e}\bar{c}}^{\bar{m}\bar{k}} &= {}_q V_{\bar{e}\bar{a}}^{\bar{m}\bar{i}} t_{\bar{c}\bar{a}}^{\bar{k}\bar{i}}, & \mathcal{D}_q \mathbb{F}_{\bar{e}\bar{c}}^{\bar{m}\bar{k}} &= {}_q V_{\bar{e}\bar{a}}^{\bar{m}\bar{i}} t_{\bar{c}\bar{a}}^{\bar{k}\bar{i}}, \\ \mathcal{D}_q \mathbb{R}_{\bar{b}\bar{g}}^{\bar{j}\bar{o}} &= Q_{\bar{b}\bar{j},\bar{g}\bar{o}}^{\bar{e}\bar{m},\bar{c}\bar{k}} \mathcal{D}_q \mathbb{F}_{\bar{e}\bar{c}}^{\bar{m}\bar{k}} + Q_{\bar{b}\bar{j},\bar{g}\bar{o}}^{\bar{e}\bar{m},\bar{c}\bar{k}} \mathcal{D}_q \mathbb{F}_{\bar{e}\bar{c}}^{\bar{m}\bar{k}}, \end{aligned}$$

$$\begin{aligned} \mathcal{D}_q \mathbb{F}_{\bar{e}\bar{c}}^{\bar{m}\bar{k}} &= {}_q V_{\bar{e}\bar{a}}^{\bar{m}\bar{i}} t_{\bar{c}\bar{a}}^{\bar{k}\bar{i}}, \\ \mathcal{D}_q \mathbb{R}_{\bar{b}\bar{g}}^{\bar{j}\bar{o}} &= Q_{\bar{b}\bar{j},\bar{g}\bar{o}}^{\bar{e}\bar{m},\bar{c}\bar{k}} \mathcal{D}_q \mathbb{F}_{\bar{e}\bar{c}}^{\bar{m}\bar{k}}. \end{aligned}$$

As with the transformed amplitudes equations, there are now six different residual equations that need to be calculated, compared to only two in QVCCD. For the mixed spin case, there are almost twice as many tensor contractions than in the QVCCD residual. It is expected that the evaluation of these residual equations will take nearly four times longer than QVCCD.

All the UQVCCD equations will also have to be solved simultaneously, like UCCSD, due to the coupling terms that appear in the different spin cases.

Chapter 8

Conclusions

A new closed-shell Orbitally Optimised Quasi-Variational Coupled Cluster Doubles (OQVCCD) code has been presented in this thesis. This method is capable of constructing an approximate wavefunction that is a solution to the electronic Schrödinger equation by invoking the Born-Oppenheimer approximation. With this solution, the energy, as well as other molecular properties, can be calculated and investigated.

Transformed amplitude and residual equations have been re-derived and made suitable for efficient computational implementation. This has been achieved by recognising numerous intermediates that are the same and factorising the remaining equations.

Chapter 4 detailed how these equations have been implemented in the Integrated Tensor Framework (ITF). This is a platform within Molpro that allows developers to write fast and efficient code in terms of a domain specific language focused around tensor contractions. Within this context, routines to carry out orbital optimisation and the caching of eigenvectors have also been developed that can be utilised by other methods in the ITF.

Numerical studies were carried out in Chapter 5 with the Quasi-Variational (QV) family of methods to gauge how they perform against more common *ab initio* methods. These include calculating Potential Energy Curves and spectroscopic constants for third-row diatomic molecules with a comparison to Multireference Configuration Interaction (MRCI). The results have shown that the Quasi-Variational (QV) methods are capable of dissociating these systems and producing energy curves that qualitatively match the MRCI results.

Furthermore, the activation and reaction energies of 88 unique reactions have been calculated with several single-reference methods and basis sets. This has allowed an insight into how QVCCD compares to other methods when calculating these important quantities. In general the QV methods predict larger barrier heights than CCSD(T).

From the available CCSDT data, the QV methods appear to correct for the lowering of the barrier height by the perturbative triples correction. For the reaction energies, there appears to be little difference with CCSD(T) due to the small non-dynamic correlation effects in most ground state molecules. However, in general, the QV methods produce larger absolute reaction energies than CCSD(T).

Previous work has developed a renormalised triples correction to replace the standard non-iterative (T) correction in OQVCCD(T). The motivation behind this was to correct the (T) method so it could cope with multireference systems. The derivation of this scheme invoked several approximations to arrive at a numerically robust and computationally competitive correction. A new method, denoted as the asymmetric-renormalised triples correction, AR(T), has been developed from one of these approximations (see Chapter 3), in order to test whether the previous renormalisation scheme is numerically justified in the approximations it makes.

Energy and frequency calculations involving OQVCCDR(T) and OQVCCDAR(T) have been carried out on many different chemical systems (Chapter 5). There appears to be very little difference in the energies and frequencies calculated by both methods. However, at long bond lengths, triply bonded systems like P_2 admit energy differences of around 6 kJ mol^{-1} . For most of the systems examined, there appears to be very little difference in the energies and frequencies calculated by both methods, thereby vindicating the OQVCCDR(T) approximations. Nevertheless, a new method to add to the QV family of methods has been developed which can provide accurate benchmarking values.

Finally, a reason for re-writing the closed-shell QVCCD code was to make it computationally competitive. The old code suffers from poor scaling, long computational times and no parallelisation, which therefore reduced its utility to computational chemists. As previously mentioned, the QVCCD code has been entirely rewritten in the ITF to produce fast, efficient and parallel code. Calculations were carried out in Chapter 5 to compare the old and the new code. Overall, the new code is several times faster; for example, an energy calculation of pentane with a cc-pVTZ basis is over 7 times faster with the new code, representing a time saving of 98 hours.

The QV family of methods represent an alternative to both Traditional Coupled-Cluster (TCC) methods like CCSD and CCSD(T), but also to multireference methods. When TCC is applied to systems with strong non-dynamic correlations the results are not just quantitatively, but can be qualitatively wrong. This means that multireference methods like Multireference Configuration Interaction must be used to produce accurate results. The main problem with these procedures is that an active space must be chosen

by the user. This can be a difficult problem to solve as the molecular orbitals must be explicitly examined to gauge whether they are ‘important’ enough to include into the active space. There is little criteria as to what constitutes as an ‘important’ orbital and so an intelligent guess must be used. The QV methods are inherently single-reference and do not require the user to choose an active space. Yet, it has been shown that they are able to capture non-dynamic correlation effects in a reasonable time frame. With this in mind, the QV methods should certainly be used alongside and instead of the TCC methods when examining multireference systems.

The main focus of this thesis has been the development of an *ab initio* method for approximately solving the Schrödinger equation. Once this has been solved, the question remains: what information can this wavefunction provide? Chapter 6 has attempted to bridge this gap by applying the *on-the-fly* instanton method to calculate reaction rates involving Criegee intermediates.

Criegee reactions occur in the troposphere and are responsible for producing OH radicals in low light environments. [16] The rate determining step for these systems involves a hydrogen transfer processes and so hydrogen tunnelling through the transition state potential barrier is likely to occur. The magnitude of this tunnelling factor has been calculated using different *ab initio* methods to determine the effect each has on the rate.

It was discovered that Density Functional Theory (DFT) performs well compared to CCSD(T) and is therefore recommended to be used. Overall, from these calculations it was discovered that hydrogen tunnelling plays a large role in the rate of the Criegee reaction; at 260 K the rate is nearly 1000 times faster than the classical rate that does not include tunnelling.

Finally, in Chapter 7, ground work was laid out for an Unrestricted QVCCD program. The residual and transformed amplitude equations were explicitly presented in terms of spin orbitals. It is a hope that this work can be used in the future to construct a QVCCD method that can be applied to open-shell systems.

This thesis leaves many options for future work involving QVCCD and the instanton method, some of which are briefly discussed here:

QVCCD and *on-the-fly* instanton calculations

The QV methods were not used with the Criegee systems due to time constraints, however these systems could be ideal for a QV investigation. The main error in the instanton method comes from the calculation of the potential energy surface. It is

possible to use the QV methods to do this and thereby provide accurate answers. It has been observed that OQVCCDR(T) predicts higher barrier heights than CCSD(T) and so the tunnelling factors are likely to be larger.

It would also be interesting to try QV calculations on smaller systems that involve hydrogen tunnelling, for example, $\text{CH}_4 \rightarrow \text{CH}_3 + \text{H}$ and even $\text{H}_2 + \text{H} \rightarrow \text{H} + \text{H}_2$. Highly accurate analytical expressions have been determined for both these reactions and therefore could be used to benchmark the QV methods. The obvious obstacle to this is that both systems are open-shell and therefore an unrestricted code must exist to carry out these calculations.

A wider range of Criegee intermediates

Only two Criegee intermediates were examined with the instanton method. However there are several, larger, Criegee intermediates that are more common in the atmosphere. It would be of great interest to examine how hydrogen tunnelling effects these different systems. It is unlikely that OQVCCDR(T) or even OQVCCD are fast enough to carry out these experiments due to the size of the systems, so DFT methods will have to be used.

Analytical gradients

Currently, if derivatives of the QVCCD are required, then numerical differentiation must be carried out. This can become a problem for even small molecules, as the number of displacements that are calculated grows as $2M$ (for central differences), where M is the number of degrees of freedom. It is this procedure that makes calculating molecular properties and optimising geometries slow for QVCCD. It also prohibits even small molecules being investigated using QVCCD and the instanton method due to the heavy use of first and second derivatives in the program.

Numerical differentiation could be bypassed if analytical formulas for the gradients were developed for QVCCD (a so called Coupled Perturbed-QVCCD method) . Such a set of formulas would be of great utility as molecular properties could be routinely calculated with QVCCD without the prohibitive time cost.

UQVCCD and RQVCCD

As mentioned above, the equations for UQVCCD have been derived, but not implemented within the ITF. This would be a large task as there is no unrestricted infrastructure currently within the ITF. Gathering the different spin parts of the Hamiltonian,

constructing an interface to carry out the integral transformation and designing a new mapping scheme to place the tensors into different class objects are some of the many tasks that will be required. However, an UQVCCD code would be of great benefit and would open up many new areas to investigation.

It is expected that the UQVCCD equations will take around three times as much computational time as QVCCD. Time reductions could be made by constructing an RQVCCD method much like RCCSD. A barrier to this approach would be deriving the equations as they would be more complicated than UQVCCD.

Improvement of qTransform

Usually, a piece of code can always be improved upon. Currently, the OQVCCD(T) code is many times faster than the old code and only 2-3 times slower than CCSD(T). Speed improvements could be derived from making the qTransform function more parallel. Calculations would take less time therefore there would be more incentive to use a single-reference method to model multireference systems.

Transition metals

There is still a large amount of closed-shell chemistry that could be investigated with the QV methods. For example, the transition metal complexes pose a challenging problem for single-reference methods due to non-dynamic correlation effects. This could possibly be overcome by using the QV methods to investigate the properties and kinetics of these systems. Previously, transition metal complexes were out of reach for the old QVCCD code due to slow computational times, however it is now feasible to carry out these kind of calculations with the new code.

Further benchmarking

Comparisons for activation energies and other properties should be made with CCSDT and CCSDT(Q). The challenging part of this task is to find enough systems that are small enough to use the full triples and perturbative quintuples. From some preliminary results (Chapter 5), it appears the QV method predicts barrier heights that are close to the CCSDT values. This was only carried out for two barrier heights and therefore does not constitute a conclusive proof of concept. Further tests should be carried out to test the reliability of the QV methods.

Bibliography

- [1] P. ATKINS and R. FRIEDMAN, *Molecular Quantum Mechanics*, Oxford University Press, 5th edition, 2011.
- [2] E. SCHRÖDINGER, *Collected Papers on Wave Mechanics*, AMS Chelsea Publishing, 2003.
- [3] L. PAULING, *The Nature of the Chemical Bond*, Cornell University Press, 1960.
- [4] M. L. HARRIS, *Stud. Hist. Philos. Sci. Part A* **39**, 78 (2008).
- [5] M. REIHER, *Found. Chem.* **5**, 23 (2003).
- [6] S. G. BRUSH, *Stud. Hist. Philos. Sci. Part A* **30**, 21 (1999).
- [7] I. SHAVITT and R. J. BARTLETT, *Many-Body Methods in Chemistry and Physics*, Cambridge University Press, Cambridge, 1st edition, 2009.
- [8] A. SZABO and N. OSTLUND, *Quantum Chemistry: Introduction to Advanced Electronic Structure Theory*, Dover Publications, 1996.
- [9] P. J. KNOWLES and N. C. HANDY, *Comput. Phys. Commun.* **54**, 75 (1989).
- [10] T. D. CRAWFORD and H. F. SCHAEFER, An Introduction to Coupled Cluster Theory for Computational Chemists, in *Rev. Comput. Chem.*, volume 14, pp. 33–136, 2000.
- [11] D. I. LYAKH, M. MUSIAŁ, V. F. LOTRICH, and R. J. BARTLETT, *Chem. Rev.* **112**, 182 (2012).
- [12] P. G. SZALAY, T. MÜLLER, G. GIDOFALVI, H. LISCHKA, and R. SHEPARD, *Chem. Rev.* **112**, 108 (2012).
- [13] J. B. ROBINSON, *Approximate Variational Coupled Cluster Theories*, PhD thesis, Cardiff University, 2012.

-
- [14] H.-J. WERNER, P. J. KNOWLES, G. KNIZIA, F. R. MANBY, and M. SCHÜTZ, *Wiley Interdiscip. Rev. Comput. Mol. Sci.* **2**, 242 (2012).
- [15] J. B. ROBINSON and P. J. KNOWLES, *J. Chem. Phys.* **138**, 074104 (2013).
- [16] F. LIU, J. M. BEAMES, A. S. PETIT, A. B. MCCOY, and M. I. LESTER, *Science (80-.)*. **304**, 1596 (2014).
- [17] A. N. BEYER, J. O. RICHARDSON, P. J. KNOWLES, J. B. ROMMEL, and S. C. ALTHORPE, *J. Phys. Chem. Lett.* , 4374 (2016).
- [18] D. R. HARTREE, *Math. Proc. Cambridge Philos. Soc.* **24**, 89 (1928).
- [19] R. SHANKAR, *Principles of Quantum Mechanics*, Plenum Press, 2nd edition, 1994.
- [20] S. K. BERBERIAN, *Introduction to Hilbert Space*, AMS Chelsea Publishing, 2nd edition, 1999.
- [21] H. ESSÉN, *Int. J. Quantum Chem.* **12**, 721 (1977).
- [22] H. J. MONKHORST, *Phys. Rev. A* **36**, 1544 (1987).
- [23] P. ATKINS and J. DE PAULA, *Atkins' Physical Chemistry*, Oxford University Press, 9th edition, 2010.
- [24] P.-O. LÖWDIN, *Adv. Chem. Phys.* **2**, 207 (1959).
- [25] F. JENSEN, *Introduction to Computational Chemistry*, John Wiley & Sons, Ltd, 2nd edition, 2007.
- [26] S. S. SHAIK and P. C. HIBERTY, *A Chemist's Guide to Valence Bond Theory*, Wiley-Blackwell, 1st edition, 2007.
- [27] T. H. DUNNING, *J. Chem. Phys.* **90**, 1007 (1989).
- [28] C. C. J. ROOTHAAN, *Rev. Mod. Phys.* **23**, 69 (1951).
- [29] D. P. TEW, W. KLOPPER, and T. HELGAKER, *J. Comput. Chem.* **28**, 1307 (2007).
- [30] S. CARATZOULAS and P. J. KNOWLES, *Mol. Phys.* **98**, 1811 (2000).
- [31] WOLRAM RESEARCH INC, Mathematica 10.2, 2015.
- [32] C. A. COULSON and I. FISCHER, *London, Edinburgh, Dublin Philos. Mag. J. Sci.* **40**, 386 (1949).

-
- [33] A. J. JOHANSSON, *Mol. Phys.* **8976**, 1 (2016).
- [34] P. G. SZALAY, M. NOOIJEN, and R. J. BARTLETT, *J. Chem. Phys.* **103**, 281 (1995).
- [35] R. J. BARTLETT, *Annu. Rev. Phys. Chem.* , 359 (1981).
- [36] J. A. POPLER, M. HEAD-GORDON, and K. RAGHAVACHARI, *J. Chem. Phys.* **87**, 5968 (1987).
- [37] M. W. SCHMIDT and K. RUEDENBERG, *J. Chem. Phys.* **71**, 3951 (1979).
- [38] J. G. SIMMONDS and J. E. M. JR., *A First Look At Perturbation Theory*, Dover Publications, 2nd edition, 1998.
- [39] M. HANRATH, *Chem. Phys.* **356**, 31 (2009).
- [40] M. NOOIJEN, K. R. SHAMASUNDAR, and D. MUKHERJEE, *Mol. Phys.* **103**, 2277 (2005).
- [41] J. A. POPLER, J. S. BINKLEY, and R. SEEGER, *Int. J. Quantum Chem.* **10**, 1 (1976).
- [42] C. HAMPEL and H.-J. WERNER, *J. Chem. Phys.* **104**, 6286 (1996).
- [43] T. HELGAKER, P. JØRGENSEN, and J. OLSEN, *Molecular Electronic-Structure Theory*, John Wiley & Sons, Ltd, 1st edition, 2004.
- [44] A. STONE, *The Theory of Intermolecular Forces*, Oxford University Press, 2nd edition, 2013.
- [45] H. P. KELLY, Applications of Many-Body Diagram Techniques in Atomic Physics, in *Adv. Chem. Phys.*, volume 14, pp. 129–190, John Wiley & Sons, Inc., Hoboken, NJ, USA, 1969.
- [46] D. CREMER and Z. HE, *J. Phys. Chem.* **100**, 6173 (1996).
- [47] N. C. HANDY, P. J. KNOWLES, and K. SOMASUNDRAM, *Theor. Chim. Acta* **68**, 87 (1985).
- [48] J. OLSEN, O. CHRISTIANSEN, H. KOCH, and P. JØRGENSEN, *J. Chem. Phys.* **105**, 5082 (1996).
- [49] S. R. LANGHOFF and E. R. DAVIDSON, *Int. J. Quantum Chem.* **8**, 61 (1974).
- [50] J. PALDUS, *Mol. Phys.* **108**, 2941 (2010).

-
- [51] J. HRUSAK, S. TENNO, and S. IWATA, *J. Chem. Phys.* **106**, 7185 (1997).
- [52] Z. HE and D. CREMER, *Theor. Chim. Acta* **85**, 305 (1993).
- [53] R. AHLRICHS, *Comput. Phys. Commun.* **17**, 31 (1979).
- [54] S. KOCH and W. KUTZELNIGG, *Theor. Chim. Acta* **59**, 387 (1981).
- [55] L. M. J. HUNTINGTON and M. NOOIJEN, *J. Chem. Phys.* **133**, 184109 (2010).
- [56] C. KOLLMAR and F. NEESE, *Mol. Phys.* **108**, 2449 (2010).
- [57] R. AHLRICHS, P. SCHARF, and C. EHRHARDT, *J. Chem. Phys.* **82**, 890 (1985).
- [58] H. J. MONKHORST, *Int. J. Quantum Chem.* **12**, 421 (1977).
- [59] J. ČÍŽEK, *J. Chem. Phys.* **45**, 4256 (1966).
- [60] W. KUTZELNIGG, *Theor. Chim. Acta* **1**, 349 (1991).
- [61] S. PAL, M. D. PRASAD, and D. MUKHERJEE, *Pramana* **18**, 261 (1982).
- [62] W. KUTZELNIGG, *Mol. Phys.* **94**, 65 (1998).
- [63] J. ARPONEN, *Ann. Phys.* **151**, 311 (1983).
- [64] B. COOPER and P. J. KNOWLES, *J. Chem. Phys.* **133**, 234102 (2010).
- [65] K. RAGHAVACHARI, G. W. TRUCKS, J. A. POPLE, and M. HEAD-GORDON, *Chem. Phys. Lett.* **157**, 479 (1989).
- [66] J. F. STANTON, *Chem. Phys. Lett.* **281**, 130 (1997).
- [67] K. RAGHAVACHARI, *Chem. Phys. Lett.* **589**, 35 (2013).
- [68] N. H. MARCH, W. H. YOUNG, and S. SAMPANTHAR, *The Many-Body Problem in Quantum Mechanics*, Dover Publications, New York, N. Y., 1995.
- [69] R. D. MATTUCK, *A Guide to Feynman Diagrams in the Many-Body Problem*, Dover Publications, 2nd edition, 1992.
- [70] D. R. HARTREE, W. HARTREE, and B. SWIRLES, *Philos. Trans. R. Soc. A Math. Phys. Eng. Sci.* **238**, 229 (1939).
- [71] B. O. ROOS, P. R. TAYLOR, and P. E. M. SIGBAHN, *Chem. Phys.* **48**, 157 (1980).

- [72] D. ROCA-SANJUÁN, F. AQUILANTE, and R. LINDH, *Wiley Interdiscip. Rev. Comput. Mol. Sci.* **2**, 585 (2011).
- [73] B. LIU, *J. Chem. Phys.* **58**, 1925 (1973).
- [74] K. R. SHAMASUNDAR, G. KNIZIA, and H.-J. WERNER, *J. Chem. Phys.* **135**, 054101 (2011).
- [75] K. ANDERSSON, P. A. MALMQVIST, B. O. ROOS, A. J. SADLEJ, and K. WOLINSKI, *J. Phys. Chem.* **94**, 5483 (1990).
- [76] G. GHIGO, B. O. ROOS, and P. Å. MALMQVIST, *Chem. Phys. Lett.* **396**, 142 (2004).
- [77] B. O. ROOS and K. ANDERSSON, *Chem. Phys. Lett.* **245**, 215 (1995).
- [78] P. G. SZALAY, *Chem. Phys.* **349**, 121 (2008).
- [79] B. COOPER, *Benchmark Calculations of Projection and Variational Coupled Cluster Methods*, PhD thesis, Cardiff University, 2010.
- [80] A. I. KRYLOV, *Acc. Chem. Res.* **39**, 83 (2006).
- [81] A. I. KRYLOV, *Annu. Rev. Phys. Chem.* **59**, 433 (2008).
- [82] D. LEFRANCOIS, M. WORMIT, and A. DREUW, *J. Chem. Phys.* **143**, 124107 (2015).
- [83] V. RISHI, A. PERERA, and R. J. BARTLETT, *J. Chem. Phys.* **144**, 124117 (2016).
- [84] K. JANKOWSKI and J. PALDUS, *Int. J. Quantum Chem.* **18**, 1243 (1980).
- [85] R. J. BARTLETT and M. MUSIAŁ, *J. Chem. Phys.* **125** (2006).
- [86] D. KATS and F. R. MANBY, *J. Chem. Phys.* **139**, 021102 (2013).
- [87] D. KATS, *J. Chem. Phys.* **144**, 044102 (2016).
- [88] K. CAPELLE, *Brazilian J. Phys.* **36**, 1318 (2006).
- [89] W. KOHN and L. J. SHAM, *Phys. Rev.* **140**, A1133 (1965).
- [90] K. E. RILEY, B. T. OP'T HOLT, and K. M. MERZ, *J. Chem. Theory Comput.* **3**, 407 (2007).

-
- [91] N. MARDIROSSIAN and M. HEAD-GORDON, *J. Chem. Theory Comput.* **12**, 4303 (2016).
- [92] J. P. PERDEW, *AIP Conf. Proc.* **577**, 1 (2001).
- [93] D. CREMER, *Mol. Phys.* **99**, 1899 (2001).
- [94] J. GRÄFENSTEIN and D. CREMER, *Mol. Phys.* **103**, 279 (2005).
- [95] P. J. KNOWLES and B. COOPER, *J. Chem. Phys.* **133**, 224106 (2010).
- [96] J. B. ROBINSON and P. J. KNOWLES, *J. Chem. Phys.* **136**, 054114 (2012).
- [97] H. ANTON and C. RORRES, *Elementary Linear Algebra*, John Wiley & Sons, Inc., 10th edition, 2010.
- [98] F. R. GANTMACHER, *The Theory of Matrices Volume One*, Chelsea Publishing Company, New York, N. Y., 1960.
- [99] D. C. SHERRILL, A. I. KRYLOV, E. F. C. BYRD, and M. HEAD-GORDON, *J. Chem. Phys.* **109**, 4171 (1998).
- [100] N. C. HANDY, J. A. POPLE, M. HEAD-GORDON, K. RAGHAVACHARI, and G. W. TRUCKS, *Chem. Phys. Lett.* **164**, 185 (1989).
- [101] D. THOULESS, *Nucl. Phys.* **21**, 225 (1960).
- [102] C. HAMPEL, K. A. PETERSON, and H.-J. WERNER, *Chem. Phys. Lett.* **190**, 1 (1992).
- [103] C. KOLLMAR and A. HESSELMANN, *Theor. Chem. Acc.* **127**, 311 (2010).
- [104] T. D. CRAWFORD and J. F. STANTON, *J. Chem. Phys.* **112**, 7873 (2000).
- [105] J. F. STANTON, W. N. LIPSCOMB, D. H. MAGERS, and R. J. BARTLETT, *J. Chem. Phys.* **90**, 1077 (1989).
- [106] J. EZÁČ, K. E. RILEY, and P. HOBZA, *J. Chem. Theory Comput.* **7**, 2427 (2011).
- [107] J. B. ROBINSON and P. J. KNOWLES, *J. Chem. Theory Comput.* **8**, 2653 (2012).
- [108] P. PIECUCH and M. WŁOCH, *J. Chem. Phys.* **123** (2005).
- [109] K. KOWALSKI and P. PIECUCH, *J. Chem. Phys.* **122** (2005).
- [110] Y. GE, M. S. GORDON, and P. PIECUCH, *J. Chem. Phys.* **127** (2007).

- [111] M. NOOIJEN and R. J. LE ROY, *J. Mol. Struct. THEOCHEM* **768**, 25 (2006).
- [112] G. E. SCUSERIA, A. C. SCHEINER, T. J. LEE, J. E. RICE, and H. F. SCHAEFER, *J. Chem. Phys.* **86**, 2881 (1987).
- [113] P. PULAY, S. SAEBO, and W. MEYER, *J. Chem. Phys.* **81**, 1901 (1984).
- [114] A. P. RENDELL, T. J. LEE, and A. KOMORNICKI, *Chem. Phys. Lett.* **178**, 462 (1991).
- [115] T. JANOWSKI and P. PULAY, *J. Chem. Theory Comput.* **4**, 1585 (2008).
- [116] J. B. ROBINSON and P. J. KNOWLES, *Phys. Chem. Chem. Phys.* **14**, 6729 (2012).
- [117] J. B. ROBINSON and P. J. KNOWLES, *J. Chem. Phys.* **137**, 054301 (2012).
- [118] K. P. HUBER and G. HERZBERG, Constants of Diatomic Molecules, in *NIST Chem. WebBook, NIST Stand. Ref. Database Number 69*, edited by P. J. LINSTROM and W. G. MALLARD, National Institute of Standards and Technology, Gaithersburg MD, 20899, 2017.
- [119] M. REIHER, *Theor. Chem. Acc.* **116**, 241 (2006).
- [120] <http://doi.org/10.17035/d.2017.0038224345>.
- [121] L.-J. YU, F. SARRAMI, R. J. O'REILLY, and A. KARTON, *Chem. Phys.* **458**, 1 (2015).
- [122] L. GOERIGK and S. GRIMME, *J. Chem. Theory Comput.* **6**, 107 (2010).
- [123] V. GUNER, K. S. KHUONG, A. G. LEACH, P. S. LEE, M. D. BARTBERGER, and K. N. HOUK, *J. Phys. Chem. A* **107**, 11445 (2003).
- [124] D. H. ESS and K. N. HOUK, *J. Phys. Chem. A* **109**, 9542 (2005).
- [125] T. C. DINADAYALANE, R. VIJAYA, A. SMITHA, and G. N. SASTRY, *J. Phys. Chem. A* **106**, 1627 (2002).
- [126] A. KARTON, S. DAON, and J. M. L. MARTIN, *Chem. Phys. Lett.* **510**, 165 (2011).
- [127] E. R. JOHNSON, P. MORI-SANCHEZ, A. J. COHEN, and W. YANG, *J. Chem. Phys.* **129**, 204112 (2008).

-
- [128] Y. ZHAO, O. TISHCHENKO, J. R. GOUR, W. LI, J. J. LUTZ, P. PIECUCH, and D. G. TRUHLAR, *J. Phys. Chem. A* **113**, 5786 (2009).
- [129] <http://doi.org/10.17035/d.2017.0038224181>.
- [130] M. KÁLLAY, Z. ROLIK, I. LADJÁNSZKI, L. SZEGEDY, B. LADÓCZKI, J. CSONTOS, and B. KORNIS, *J. Chem. Phys* **135**, 104111 (2011).
- [131] <http://doi.org/10.17035/d.2017.0038224453>.
- [132] J. I. STEINFELD, *Chemical Kinetics and Dynamics*, Pearson, 2nd edition, 1998.
- [133] H. EYRING, *J. Chem. Phys.* **3**, 107 (1935).
- [134] J. O. RICHARDSON and S. C. ALTHORPE, *J. Chem. Phys.* **131**, 214106 (2009).
- [135] J. O. RICHARDSON, *Ring-polymer approaches to instanton theory*, PhD thesis, Cambridge University, 2012.
- [136] Y. FANG, V. P. BARBER, S. J. KLIPPENSTEIN, A. B. MCCOY, and M. I. LESTER, *J. Chem. Phys.* **146** (2017).
- [137] R. CRIEGEE, *Angew. Chemie Int. Ed. English* **14**, 745 (1975).
- [138] R. P. FEYNMAN and A. R. HIBBS, *Quantum Mechanics and Path Integrals*, Dover Publications, 2nd edition, 2005.
- [139] Y. V. SULEIMANOV, F. J. AOIZ, and H. GUO, *J. Phys. Chem. A* **120**, 8488 (2016).
- [140] S. HABERSHON, D. E. MANOLOPOULOS, T. E. MARKLAND, and T. F. MILLER, *Annu. Rev. Phys. Chem.* **64**, 387 (2013).
- [141] H.-J. WERNER, F. R. MANBY, and P. J. KNOWLES, *J. Chem. Phys.* **118**, 8149 (2003).
- [142] É. BRÉMOND, M. SAVARESE, N. Q. SU, Á. J. PÉREZ-JIMÉNEZ, X. XU, J. C. SANCHO-GARCÍA, and C. ADAMO, *J. Chem. Theory Comput.* **12**, 459 (2016).
- [143] J. TIRADO-RIVES and W. L. JORGENSEN, *J. Chem. Theory Comput.* **4**, 297 (2008).
- [144] Z. C. J. DECKER, K. AU, L. VEREECKEN, and L. SHEPS, *Phys. Chem. Chem. Phys.* , 8541 (2017).
- [145] P. J. KNOWLES and N. C. HANDY, *J. Phys. Chem.* **92**, 3097 (1988).

-
- [146] T. TSUCHIMUCHI and G. E. SCUSERIA, *J. Chem. Phys.* **133**, 141102 (2010).
- [147] C. C. J. ROOTHAAN, *Rev. Mod. Phys.* **32**, 179 (1960).
- [148] P. J. KNOWLES, C. HAMPEL, and H.-J. WERNER, *J. Chem. Phys.* **99**, 5219 (1993).
- [149] G. E. SCUSERIA, *Chem. Phys. Lett.* **176**, 27 (1991).
- [150] J. F. STANTON, *J. Chem. Phys.* **101**, 371 (1994).
- [151] M. RITBY and R. J. BARTLETT, *J. Phys. Chem.* **92**, 3033 (1988).